Quantum mechanics & the big world

Wezel, J. van

Quantum Mechanics is one of the most successful physical theories of the last century. It explains physical phenomena from the smallest to the largest lengthscales. Despite this triumph, quantum mechanics is often perceived as a mysterious theory, involving superposition states that are alien to our everyday Big World.

The construction of a future quantum computer relies on our ability to manipulate quantum superposition states in qubits. In this thesis it is shown that these qubits can be subtly influenced by the physics associated with spontaneous symmetry breaking. This process destroys the quantum nature of the qubit and renders it useless for quantum computation.

An even more fundamental problem with quantum superpositions is that they cannot be reconciled with the theory of general relativity. In the end of this thesis a model is proposed which describes the effective, deteriorating, influence of gravity on quantum states, thus suggesting a path toward the demise of quantum mechanics in the big world.

Jasper van Wezel (The Hague, 1979) started studying physics in 1998 at Leiden University. The research described in this thesis was done at Leiden University between 2003 and 2007.

In 2006 Leiden University has initiated a series *Leiden Dissertations* at Leiden University Press. This series affords an opportunity to those who have recently obtained their doctorate to publish the results of their doctoral research so as to ensure a wide distribution among colleagues and the interested public. The dissertations will become available both in printed and in digital versions. Books from this LUP series can be ordered through www.lup.nl. The large majority of Leiden dissertations from 2005 onwards is available digitally on www.dissertation.leidenuniv.nl.

LUP DISSERTATIONS

Leiden University Press

9 789087 280208

Jasper van Wezel · *Quantum Mechanics & The Big World*

LUP

Jasper van Wezel

Quantum Mechanics & The Big World

ORDER, BROKEN SYMMETRY AND COHERENCE IN QUANTUM MANY-BODY SYSTEMS

LEIDEN UNIVERSITY PRESS

Quantum Mechanics
&
The Big World

order, broken symmetry and coherence in quantum many-body systems

Leiden University Press

Cover illustration: adapted from *Earthrise - Apollo 8*, NASA, 29 dec. 1968
Cover design: Randy Lemaire, Utrecht
Lay out: Jasper van Wezel, Leiden

ISBN 978 90 8728 020 8
NUR 910

Quantum Mechanics
&
The Big World

order, broken symmetry and coherence in quantum many-body systems

PROEFSCHRIFT

TER VERKRIJGING VAN
DE GRAAD VAN DOCTOR AAN DE UNIVERSITEIT LEIDEN,
OP GEZAG VAN RECTOR MAGNIFICUS PROF.MR. P.F. VAN DER HEIJDEN,
VOLGENS BESLUIT VAN HET COLLEGE VOOR PROMOTIES
TE VERDEDIGEN OP WOENSDAG 4 APRIL 2007
KLOKKE 15.00 UUR

DOOR

Jasper van Wezel

GEBOREN TE DEN HAAG
IN 1979

Promotiecommissie:

Promotores:	Prof. dr. J. van den Brink
	Prof. dr. J. Zaanen
Referent:	Prof. dr. C.W.J. Beenakker
Overige leden:	Prof. dr. D. Bouwmeester
	Prof. dr. M.I. Katsnelson (Radboud University of Nijmegen)
	Prof. dr. ir. J.E. Mooij (Delft University of Technology)
	Prof. dr. C. de Morais Smith (University of Utrecht)
	Prof. dr. J.M. van Ruitenbeek

Contents

Part I

Preface

Chapter 1

Introduction

"The more success quantum theory has, the sillier it looks."

This statement made by Albert Einstein in the beginning of the last century nicely illustrates the confusion that the theory of quantum mechanics caused among its inventors [1–9]. Even now, after many decades in which quantum mechanics has proved to be an excellent description of ever growing realms of physics, the confusion still remains [10–13]. All microscopic particles are believed to be quantum mechanical, and the properties of these particles predicted by quantum mechanics have been tested to great accuracy all the way from quarks to collections of billions and billions of atoms and molecules [13]. But therein also lies the problem: if quantum mechanics describes all of the fundamental particles, and if all matter is made out of these quantum mechanical particles, then surely everything we see around us in the everyday world should obey the laws of quantum mechanics as well. Yet we never get to see a coin that shows both heads and tails after a coin toss, or a soccer ball that just manages to tunnel through the goalkeeper's hands to score that last winning point..

The discrepancy between what matter can and cannot do in the everyday "Big World", and what its constituent particles have been proved to be capable of in accordance with quantum mechanics, has lead to a number of extreme proposals for the metaphysical interpretation of the firmly established mathematical framework of quantum mechanics [14–16]. Even though these proposals are usually constructed in such a way that they cannot be proved wrong by any known measurement, the far-stretching implications that they have on our view of the world stops most people from accepting any of them. Instead physicists have adopted a sort of "shut up and calculate" approach to quantum mechanics [17], in which they simply accept that the rules of quantum mechanics will successfully give a statistical description of the outcomes of experiments, even though no one understands exactly how quantum mechanics is reduced to classical physics in each individual measure-

ment [18].

In this thesis I will discuss the role played by quantum mechanics in the everyday, classical Big World. In this first part I will give a short discussion of the interpretational problems posed by quantum mechanics. Apart from the somewhat counter-intuitive features of quantum physics there is also a real, physical shortcoming of the theory, as it turns out not to be able to describe the observed non-unitarity of a single measurement.

In part II of the thesis I will then focus on the typical way that quantum effects show up in macroscopic bodies. The fact that constituent particles are described by a quantum mechanical wavefunction rather than as classical particles influences the thermodynamic properties of the bulk of a piece of matter. As an example of a condensed matter system for which quantum mechanics is essential to understand its collective properties, I will look at the titanium pyroxene compound $NaTiSi_2O_6$ [19, 20]. In this compound there are one dimensional strings of titanium ions that each have a free spin and orbital degree of freedom [21, 22]. The interplay of these degrees of freedom leads to the formation of a novel orbital-assisted Peierls groundstate. As we will see the transition into this Peierls-like state is driven by combined quantum fluctuations of both the spins and the orbitals, and the resulting value of for example the magnetic susceptibility of titanium pyroxene can only be explained by invoking this strongly quantum mechanical behavior of its constituent particles.

The third part of this thesis will be dedicated to the quantum mechanical behavior of macroscopic bodies as a whole. Even though the process of spontaneous symmetry breaking leaves these objects as classical as possible, they are still essentially quantum mechanical. The hidden quantum origin of classical objects can influence them in a very subtle way. One instance in which the illusive quantum influence could in principle be observed is in the operation of mesoscopic, solid-state qubits [23]. Even though these devices are built up out of classical building blocks, they can contain a superposition of two quantum states. This superposition of the system is very sensitive to its surroundings. All interaction with the environment will destroy the superposition through the process of decoherence, and render the qubit in a merely classical state [24]. I will show that the very fact that these qubits are made out of classical, symmetry broken materials already inevitably leads to decoherence. The hidden quantum states of the classical objects are enough to decohere the qubit state within a fundamental timescale that does not depend on the detailed properties of the qubit [23, 25]. This result will be shown to hold for such systems as crystals and antiferromagnets, but also for more robust objects such as superconductors.

Finally, in part IV, I will argue that despite the large extent of its applicability, quantum mechanics must come to an end at some point and make way for purely classical physics. After a brief review of why this must necessarily happen through the wavefunction collapse process, I will focus on one particular idea about the sub-

ject that was recently put forward by Roger Penrose [26,27]. In his proposal Penrose observes that if gravity has anything to do with the reduction of quantum mechanics, then there is a clear timescale at which its influence should start to be visible. This timescale turns out to sit precisely in the experimental gap between microscopic observations and the manipulation of macroscopic bodies [26, 28]. Penrose then writes down an Ansatz-equation to describe the interplay between quantum mechanics and gravitation [29]. I will show that if we take this equation literally it will never be able to fulfill all requirements that observations demand the collapse process to obey. Even an improved version of the equation will turn out to be insufficient, and thus we are forced to leave the collapse process as an unsolved problem.

At the very end of this work though, I will try to argue that perhaps the processes described in this thesis could be combined somehow, and that a dynamical description of the collapse process, in the spirit of Penrose's idea, but based on spontaneous symmetry breaking, might be the most promising way forward for further investigation of the subject.

Chapter 2

The Fundamental Issue

The theory of quantum mechanics as we know it today was formed and slowly given shape by many different physicists throughout the first decades of the previous century. Even though it successfully describes the behavior of microscopic particles in terms of a so-called wavefunction, the metaphysical interpretation of what this wavefunction tells us about the nature of fundamental particles has been a point of fierce discussion ever since its first introduction, and until this very day [11].

There are in fact two sorts of interpretational problems posed by quantum mechanics [12, 13]. The first difficulty concerned with quantum mechanics is the reconciliation of its predictions with the things we already thought to know about nature. Although this level of interpretation has been a real challenge for students of quantum mechanics throughout the last century, it is not really a physical problem. Upon closer inspection of the workings of quantum mechanics it will be seen that the theory is in fact fully consistent with all possible experimental observations, however counter-intuitive these may seem to be at first sight.

Apart from the fact that our intuition is not naturally attuned to the quantum world however, there is also a separate, second issue that has caused much debate. This issue is related to the reduction of quantum mechanics to classical physics during a single measurement, and it is usually referred to as 'the measurement problem', 'quantum state reduction' or 'the collapse of the wavefunction'. The measurement problem is a real, physical problem which states that we do not yet have a description of the dynamical process which reduces a quantum state to a classical object during measurement. Some attempts have been made to construct interpretations of the mathematical framework of quantum mechanics with which the quantum state reduction could be avoided or circumvented. As I will show in this chapter though, none of these interpretations can fully get rid of the measurement problem.

2.1 Intuition

Both interpretational problem posed by quantum mechanics can be discussed most clearly by considering a model experiment. The experiment of choice is the electronic version of the famous experiment proposed by Thomas Young in 1805 [30, 31]. Young suggested to shoot light rays at a screen with two narrow slits in it, so that by looking at the presence or absence of an interference pattern behind the two slits, one could finally reach a conclusion about the nature of light. Of course an interference pattern was seen, and it was consequently concluded that light must consist of waves, and not particles. One could do the same experiment with a beam of electrons, which quantum mechanics tells us are described by a wavefunction as well, and which should thus produce an interference pattern similar to the one observed by Young. This electronic beam experiment was first done in 1961 by Claus Jönsson, and sure enough an interference pattern was observed [32, 33]. With the advance of technology an improved version of the experiment could be done first in 1974 by Pier Giorgio Merli [34], and then more accurately by Tonomura et al. in 1989 [35].

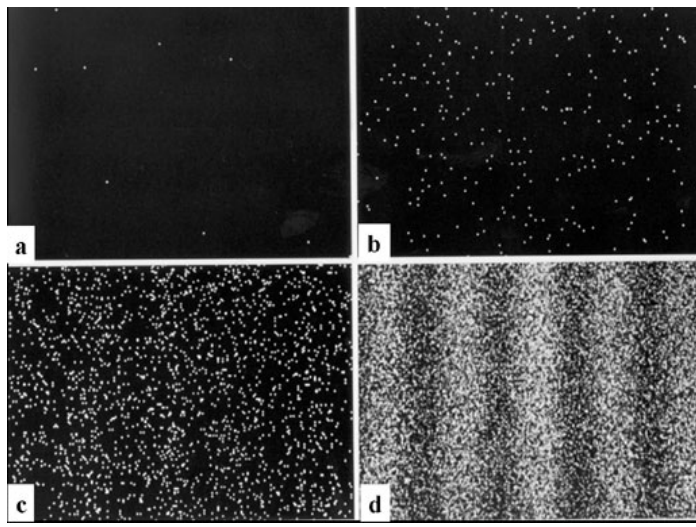

Figure 2.1: A sequence of pictures showing the progress of Young's double slit experiment done with single electrons [35]. In a) there are 8 electron spots, in b) 270, in c) 2000 and in d), after 20 minutes of exposure, there are 6000 electron spots.

In this advanced version, the experimentalists made absolutely sure that there was only one single electron within the setup at any time. Each of these electrons then turned out to produce only a single spot at a seemingly random position on

the measurement screen. Upon combination of all of the spots made during a large ensemble of measurements however, the interference pattern reemerged (see figure 2.1). The experiment can be done routinely nowadays, and can even be reproduced with the electrons replaced by different kinds of particles, ranging from C_{60} molecules to single photons [36, 37].

2.1.1 The Wavefunction

The first problem in interpreting these experiments is the instinctive abhorrence that comes from the realization that in order to produce an interference pattern on the screen, each single electron must have passed through both of the slits. How can one particle possibly be in two positions at the same time? The answer of course is very simple: the electron is not a particle, it is a wave. According to quantum mechanics electrons and all other particles should be described by a wavefunction. The wavefunction is not a literal matter wave such as the one that we could use to describe for example a drop of water spreading out over a table. Instead the quantum wavefunction is a complex valued function which lives in a Hilbert space. Nonetheless it is a wave, and it therefore has all the properties common to waves, as opposed to particles.

The most obvious wave-property is the superposition principle: if a wave has a non-zero amplitude in two places, then one can describe it as a linear superposition of two separate waves, which both have a finite amplitude in only one position. This is the reason that the electron in Young's experiment can pass through two slits at same the time, and interfere with itself afterward. There is no particle being split up, but only a wave passing through two slits simultaneously.

Incidentally, the spreading out of the electron wavefunction over the available space is also an example of the powerful influence that symmetry has on waves. In classical mechanics symmetry already dictates all the conservation laws of a physical system. For example, if space is completely isotropic and homogeneous and thus has translational symmetry, then inevitably momentum is a conserved quantity. After all, if there is a particle with a certain velocity present within such a space, and it would not always retain exactly that velocity, then *where* in space did it change its velocity, and why precisely there[1]?

For waves, the power of symmetry increases even further. If there would be a wave within a completely isotropic and homogeneous space, then *where* would it be? There is no good reason for it to be at any place in particular, and thus the wave must be in all positions at the same time: it must be spread out completely over the

[1] One might think that there is the possibility of changing the particle's velocity with the same amount at every single position, thus still obeying the symmetry of the space. In that case though one could ask in which direction the particle is accelerated at every point in space. That question then cannot be answered, because the space is required to be isotropic.

entire space[2].

The existence and occurrence of superpositions in quantum mechanics thus is a direct result of the combination of the wave nature of microscopic matter with the symmetries that exist in the experimental setup.

2.1.2 Complementarity

The second point which causes confusion when trying to interpret the double slit experiment with our classical intuition, is known as Heisenberg's uncertainty principle. This principle implies that if we would for example try to very gently detect through which of the two slits each single electron passes, then we will be able to retrieve that "which-path information", but the interference pattern on the screen (the "both-paths information") will disappear. Apparently only one of these complementary sets of information can be known to us at any given time. This principle of complementarity not only governs the possible knowledge of which-path and both-paths information, but also the simultaneous knowledge of position and momentum or of orthogonal projections of the spin operator. Indeed, the generic situation in quantum mechanics is that for every observable quantity that one tries to measure there is at least one complementary observable that cannot be accurately measured at the same time.

It becomes even worse if we realize that we can use quantum mechanics to measure both the which-path information and the both-paths information at the same time, store the outcome of the experiment, and then at some later point come back to the experimental setup and choose which of these sets of information to display on our screen. This delayed choice quantum eraser measurement has been performed recently by Marlan O. Scully et al. using pairs of entangled photons [37], as is shown schematically in figure 2.2. The execution of this experiment is of course still in full agreement with quantum mechanics, because in making the delayed choice on what to register, one necessarily needs to quantum-erase the complementary set of information, so that Heisenberg's uncertainty relation is never violated (see figure 2.3).

As a matter of fact, the obedience to Heisenberg's uncertainty relations is another feature that all waves share. A wave by its very nature cannot possibly have both a well defined position in space, and a clearly measurable wavelength (which is set by its momentum). The complementarity of these quantities can already clearly be demonstrated by observing wave patterns on a lake or even in the bath tub. It should therefore be no surprise that only one out of two complementary wave-properties can be detected at any one time. The electron which is allowed to pass through two slits and then to interfere with itself carries only both-paths information and no which-path information. If however one changes the setup in such

[2] Incidentally, a wave can only spread homogeneously over all of space if it has a single, well defined value for its momentum.

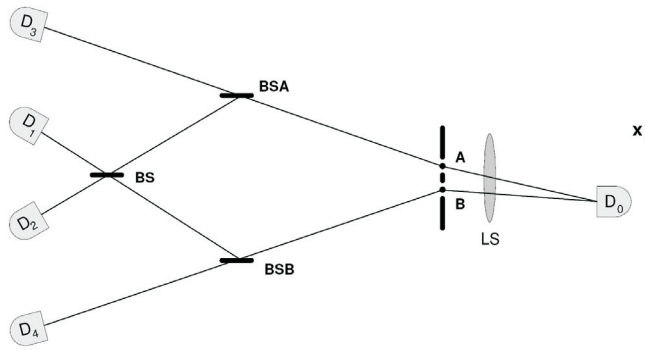

Figure 2.2: A schematic representation of the delayed choice quantum eraser experiment performed by M.O. Scully et al. [37]. At the beginning of the experiment a pair of entangled photons is created either at A or at B (more precisely, the pair is created in a superposition state of being at both A and B). Detector D_0 can be moved along the x-axis to measure the interference of the right moving electron originating from both A and B, while the left moving electron ends up, after encountering two beam splitters, at one of the detectors D_1 through D_4. If the left mover is detected at D_3 or D_4 then which-path information is available, while detection at D_1 or D_2 erases such information. Notice that the detection at D_0 can be performed long before the left moving electron is detected.

a way that the electron will carry which-path information after passing the double slit, then this naturally leads to a corresponding decrease in both-paths information, and thus a disappearance of the interference pattern. This transfer of information is exactly analogous to trying to catch a wave at a particular position in the bathtub, and then afterward not being able to accurately measure its wavelength anymore.

Although the delayed choice quantum eraser experiment may be a bit more elaborate than Young's experiment, the fact that one can look at only one property of the wavefunction at a time still is a direct consequence of Heisenberg's uncertainty principle, and thus of the wave nature of quantum mechanics. In this experiment the which-path or both-paths information is very cleverly separated from the registering device that will show the actual presence or absence of an interference pattern. Only after cross correlating the measurements of this device with the separate measurements that determine which set of information we're looking at, can any pattern be distinguished at all. Because the which-path information, even when separated from the measurement of the interference pattern, remains complementary to the both-paths information, one can only detect one or the other wave property [37].

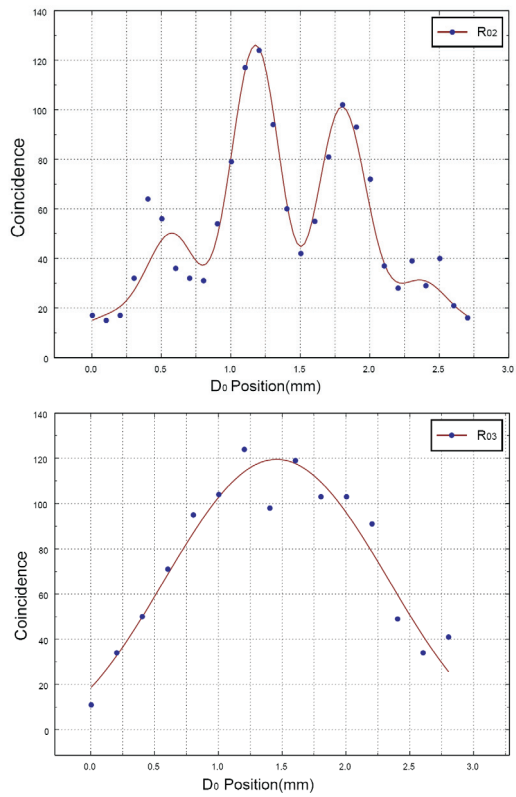

Figure 2.3: The results of the delayed choice quantum eraser experiment of figure 2.2. In the top plot those points from the D_0 detections are selected that coincide with a detection at D_2. Because the which-path information has been erased, an interference pattern can be observed. In the bottom plot the coincidences between D_0 and D_3 are selected. This time which-path information was available, and thus the both-paths information has been lost, in full accordance with Heisenberg's uncertainty principle.

2.2 Interpretations

After accepting all the counter-intuitive features of the double slit experiment as just being due to the wave nature of quantum mechanical objects, there remains one last cause for confusion that needs to be dealt with. The greatest problem posed by the single electron version of Young's experiment is the question of how it is possible that each electron creates only one single spot on the screen [18]. After all, we

know that according to the rules of quantum mechanics the electron must have been spread out in front of the entire screen just before the spot is formed. The emergence of the interference pattern after doing many measurements in fact confirms this. Still what we see on the screen is single well defined position of the electron, and not a superposition of spots all over the screen [35]. If the laws of quantum mechanics were to be followed also by all the individual atoms in the screen then surely a superposition state of the screen with spots on all possible positions would be the required final state of Young's experiment.

More precisely stated, it seems that the measurement of the electron's position (by letting it interact with a screen) breaks the unitarity of the quantum mechanical time evolution. Independent of the number of particles in the system, the defining characteristic of quantum mechanics is its unitarity. After only a single spot has appeared on the screen this unitarity has been broken, as can be clearly seen by realizing that the electron can no longer be propagated back in time to its original state: time inversion symmetry is broken, and thus time evolution can no longer be unitary [18]. The fact that the act of measurement breaks the unitarity of quantum mechanics is the one fundamental, physical problem with the quantum theory.

There have been many attempts to cure this situation, most often through the introduction of 'interpretations' of quantum mechanics in which one tries to avoid the measurement problem altogether.

2.2.1 The Copenhagen Interpretation

The most important of these interpretations has become known as the Copenhagen interpretation of quantum mechanics, and it is based on the ideas of two of the founding fathers of quantum theory: Niels Bohr and Werner Heisenberg [6–8]. Although they disagreed on details, both men advocated the idea that the wavefunction in quantum mechanics should be seen as a probability wave, rather than as a true matter wave. The probabilities described by the wavefunction then represent the possible outcomes of a measurement [38]. Until one has actually performed a measurement, there is no way that one could possibly know anything about the quantum particle in the experimental setup, and thus it is argued that it is useless to discuss or even think about the properties of such a quantum particle before doing a measurement [7]. In particular one is thus not allowed to say that there exists a quantum particle which travels through two slits and is spread out all along the screen just before the spot on the screen has been measured. By selecting which experimental setup to use, the experimentalist in a way *creates* a particle with specific properties. In our case the choice of making the electron visible by using a screen dictated that the electron would show up at a well defined position. The quantum mechanical wavefunction only gives information about the probability of a certain outcome for each possible experimental setup, but not about the actual particle before measurement [7, 8, 38].

John von Neumann has carefully analyzed these ideas and he proposed to describe them formally by the conjunction of two separate processes [39]. In first instance all microscopic systems are described by a wavefunction which evolves precisely according to the rules of quantum mechanics. But at the moment that one performs a measurement on the wavefunction using a classical measurement machine, a second process takes over, which instantaneously collapses the microscopic wavefunction onto one of the experimental outcomes that is allowed by the classical measurement machine. The selection of which state to collapse to is purely probabilistic, with the chance for a certain outcome to appear being determined by the corresponding amplitude of the microscopic wavefunction [38]. This formulation of the measurement process is known as the collapse of the wavefunction, and it is a clearly non-unitary process which formally completes the Copenhagen interpretation.

The problem with this description is that does not solve anything. A rather particular (instantaneous) non-unitary collapse process is introduced and postulated to take place during measurement, which in turn is defined as the interaction with a classical measurement machine. But which objects count as classical measurement machines and which do not? In practice it is often easily decided if something is classical or not. But theoretically a classical table is nothing more than a large collection of quantum mechanical atoms. So the question remains at what point a collection of atoms stops being a complex quantum mechanical wavefunction and begins to be a classical object, which would thus be usable as a measurement machine. The first part of this question can be answered by using the description of spontaneous symmetry breaking, as will be discussed in part III of this thesis. But as I will also argue, an explanation of how such a classical, symmetry broken object could initiate a non-unitary collapse process is still missing.

2.2.2 The Statistical Interpretation

Apart from the Copenhagen interpretation of quantum mechanics, there are two other popular interpretations. The first is the statistical interpretation that was first formulated as such by L.E. Ballentine in 1970 [16], and then used in many different variations [40–45]. The idea behind this interpretation is that quantum mechanics is really complete in itself, as long as one looks only at ensembles of measurements. To describe such ensembles one uses density matrices, which are equivalent to wavefunctions for single measurements, but which have the advantage that they can also be used to describe a statistical mixture of different outcomes within an ensemble of experiments. The disappearance of superpositions of large collections of microscopic particles can be explained in terms of density matrices by the process of decoherence [40, 44, 45]. If an observer looks at the screen in Young's experiment, then he will only register the position of the dark spot on it. He will not know the exact properties of all the individual atoms within the screen. The true superposi-

tion state of the screen having a spot in many different positions at the same time however, does also involve a superposition of these many microscopic degrees of freedom. If one now starts out with a superposition state of all these degrees of freedom, but averages over the unobserved part, then the resulting reduced density matrix will describe a classical, statistical mixture of states and not a quantum mechanical superposition of states. This apparent reduction of a quantum superposition to a statistical mixture is what is usually referred to as decoherence.

The statistical interpretation has the clear advantage that no extra ingredients need to be added to quantum mechanics at all, except for a definition of which degrees of freedom will be measured and which will not. On the other hand it has the great disadvantage that it simply forbids us to discuss or even think about the dynamics of a single act of measurement [16, 43]. According to the statistical interpretation, the non-unitarity of measurement is caused by the averaging over unobserved quantities, which can only be done in the description of an ensemble of measurements. Why the time evolution within a single measurement should be non-unitary remains unclear.

2.2.3 The Many Worlds Interpretation

The second alternative interpretation of quantum mechanics is the many worlds interpretation which was originally proposed by Hugh Everett in 1957 [14]. Instead of introducing an extra distinction between microscopic particles and classical, macroscopic objects, the disciples of this interpretation suggest to take the mathematical formulation of the wavefunction literally [14, 46–48]. One of the fundamental properties of waves in general is that they can occur in superposition with one another. The many worlds interpretation suggests that we should look at the quantum mechanical wavefunction as a literal superposition of infinitely many worlds. There would be one world for each possible outcome of each possible measurement that one could do. Because the human observer of such a measurement is only in one of these many parallel worlds, he can only see one outcome, which then seems to be randomly chosen [14, 46–48]. The probability for a certain outcome to appear is given by the squared amplitude of the wavefunction which must thus represent the percentage of the infinitely many parallel worlds in which that particular outcome is realized (see figure 2.4).

Even though there is no experiment yet that can distinguish between the many worlds interpretation and the Copenhagen interpretation (including collapse of the wavefunction), there is one known experiment with which a truly daring believer of the many worlds interpretation could at least convince oneself of its correctness: the quantum suicide experiment [48, 49]. In this experiment the observer is supposed to set up a device which will kill him as soon as some unstable atom decays. Since the decay process is quantum mechanical there exists at any point in time a superposition of the decayed atom, and the original atom. If indeed this also im-

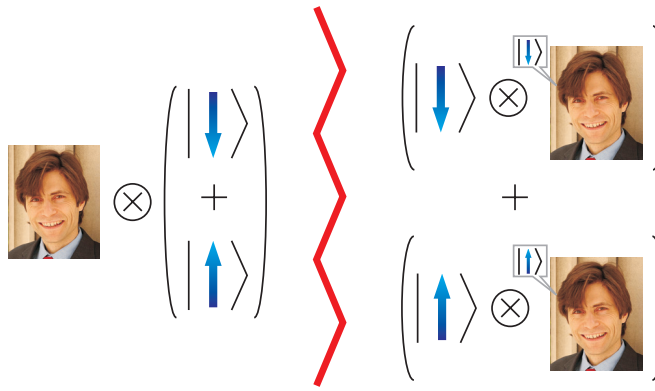

Figure 2.4: A schematic representation of the many worlds interpretation. Initially the observer (represented here by Max Tegmark, the inventor of the quantum suicide experiment [48]) is separated from a quantum system. The quantum system in this case is a spin $1/2$ with its spin polarized in the xy-plane, so that it corresponds to a superposition of states with different z-projection. After the measurement, the observer has found the spin to be either up or down, and the observer and spin therefore form an entangled state. The different parts of the entangled state cannot possibly communicate with each other, and are thus interpreted by the many worlds interpretation as being in two different worlds. The observer is only conscious of one of the outcomes of the experiment, and must therefore live in only one of the worlds.

plies that there exists a superposition of worlds in which the observer ends up dead and alive, then according to the many worlds interpretation one could safely perform such an experiment, since only the living observer is (supposedly) conscious of the outcome of the experiment, and thus the observer will always find himself in a world in which the atom has not decayed yet[3] [48].

2.3 Symmetry Breaking

As we have seen, the quantum mechanical description of microscopic matter in terms of the wavefunction, despite being very powerful and readily explaining the existence of complementary quantities, superpositions, etc., must still come to an

[3]Notice that this last step in the reasoning assumes a sort of free will: it assumes that you have have only one consciousness, and that at the moment of measurement your consciousness can be transferred into either one of the resulting worlds. Taken even more literally, the many worlds interpretation could also mean that we are simply in one part of the universe's wavefunction, with the outcomes of all possible future experiments already decided.

end somewhere. After all, a single measurement of a quantum mechanical property clearly leads to a non-unitary time evolution.

As I will discuss in more detail in part III of this thesis, there is at least one way in which quantum mechanics carries along the means of its own demise. As a collection of quantum particles grows toward an infinite size, it becomes possible for the system as a whole to spontaneously organize into a state which is as classical as possible [50, 51]. That is, after this spontaneous symmetry breaking has occurred, the uncertainties in both momentum and position are as low as can possibly be allowed by Heisenberg's uncertainty relation. Since the uncertainty in position and momentum of the object as a whole is negligible with respect to its size, it can then be ignored in further analyses and for all practical purposes a classical (particle-like) object has been formed. The theory of spontaneous symmetry breaking works very well in explaining the apparent classicality of all sorts of objects, ranging from tables and magnets all the way to superconductors [50, 51]. It is however, only a description of the equilibrium state of matter. In the third part of this thesis I will show that it does have some effects on the dynamics of macroscopic objects (it leads to a fundamental limit of quantum coherence in qubits), but unfortunately spontaneous symmetry breaking cannot be used to formulate a dynamical, non-unitary reduction to classical behavior. In particular, spontaneous symmetry breaking is not a substitute for the collapse process that we need to describe quantum measurement with.

As it is, very little is known about what physical principle could underlie a dynamical description of the wavefunction collapse. Over the past decades many proposals for a possible mechanism have been considered. These range from the introduction of extra nonlinear terms in the time evolution governed by stochastically distributed 'secret parameters' [15], via the description of the time evolution in terms of quantum diffusion equations [52–57] to the introduction of ad hoc localization events [58, 59]. No consensus on any of these theories has been reached, nor is any one of them supported by specific experimental observations.

Recently, there has also been a suggestion by sir Roger Penrose [26, 27], based on earlier ideas [58–60], that the problem may be linked somehow to the problem of the unification of quantum mechanics with gravity. Although I will show in part IV of this thesis that the dynamical description that follows from this proposal cannot fully explain all observed properties of the collapse process, it does have the advantage that it can explain the difference between quantum objects and the classical systems that are to be used as measurement machines by looking at their gravitational self energy.

Despite the huge realm of applicability of the quantum theory, ranging from the quantum mechanics of microscopic particles within larger bodies (see part II of this thesis) to the actual quantum behavior of macroscopic objects as a whole (see part III), it thus is still unclear how to describe a single act of measurement

(as discussed in part IV). The mysterious wavefunction collapse therefore remains a riddle that needs to be solved before one can truly understand the nature of quantum mechanics. With the current rapid advance in the possibilities of manipulating microscopic and mesoscopic quantum objects, it could well be that direct experimental observation of the collapse process is just around the corner. That would then finally liberate the discussion from its metaphysical stronghold and open up a directed experimental and theoretical search for the physical process responsible for the suppression of Quantum Mechanics in the Big World.

Part II

Quantum Mechanics in the Big World

Chapter 1

Introduction

Quantum mechanics dictates the behavior of all physics on microscopic length scales. Consequently it also greatly influences the world at larger distances, because many properties of macroscopic bodies depend on the characteristics of their constituent particles [61, 62]. This is particularly true for the material properties of solid state systems [63, 64]. Many of these material properties can only be explained by considering a quantum mechanical formulation of the underlying microscopic theory. A particularly interesting class of materials to be considered is formed by the transition metal compounds. Because of their strongly interacting electronic structure these materials display an extremely wide range of different types of orderings and excitations, and thus of material properties [65–69]. In this part of the thesis we will study one of these transition metal compounds, $NaTiSi_2O_6$, as an example of how quantum fluctuations on the microscopic level can give rise to ordering and observable thermodynamic effects at the macroscopic level. $NaTiSi_2O_6$ is an interesting example to study here because it turns out to undergo a novel type of orbital-assisted Peierls transition, in which the orbital quantum fluctuations help to stabilize an electronically dimerized phase [19, 20, 70].

1.1 Titanium Pyroxene

The occurrence of an unusually large variety of physical phenomena in the transition metal compounds is mainly due to the fact that the relevant electrons in these systems can be regarded as having separate and independent degrees of freedom related to their charges, spins and orbitals, and to the lattice [67]. Of these the orbital degree of freedom is of particular interest,since it can couple on one hand to the spins via the superexchange interaction, and on the other hand to the lattice via the cooperative Jahn Teller effect [66, 68]. Couplings of this kind are hard to observe in most systems since they can be very easily obscured by more profound magnetic

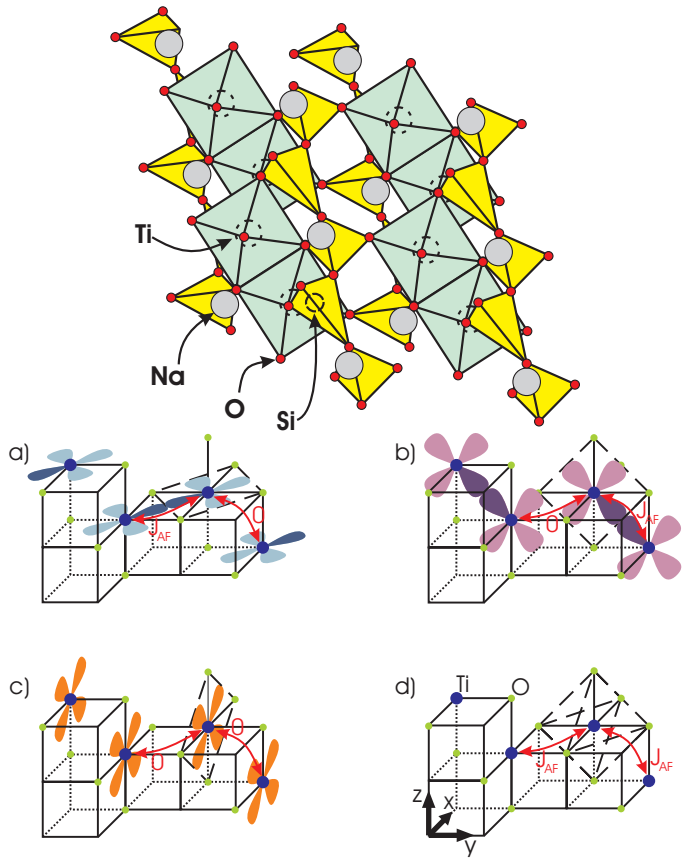

Figure 1.1: Top: A schematic picture of the crystal structure. Bottom: Possible uniform orbital orderings (a-c) and a schematic indication of the orientation of the TiO_6 octahedra (d).

effects. In the pyroxene compound $NaTiSi_2O_6$ however, the coupling of spins and lattice via the orbitals may be visible, and in fact gives rise to a novel kind of phase transition: the orbital Peierls transition.

The crystal structure of titanium pyroxene consists of chains of $Ti^{3+}O_6$ octahedra, separated by SiO_4 tetrahedra and Na^+ ions, as pictured in figure 1.1A [21]. The TiO_6 octahedra are edge-sharing, so that the titanium ions lie on separated zig-zag chains. Since the titanium ions all have one electron in the d-shell, these chains are effectively one dimensional spin $1/2$ chains. The d-orbitals of the titanium atoms are split by the surrounding crystal field into low lying t_{2_g} orbitals,

and energetically less favorable e_g orbitals. For the low energy physics of this system we thus need to consider one dimensional zig-zag chains with on each site a spin $1/2$ occupying one of three possible, degenerate t_{2_g} orbitals [19, 21, 22]. The orientation of the orbitals within the crystal structure is such that there are three different uniform orderings, as shown in figure 1.1B: the orbitals can be oriented completely parallel to both neighbors (d_{zx} orbitals); in this case there is negligible overlap between neighboring orbitals and thus also no exchange coupling between neighboring spins. Another possibility is the d_{xy} orientation. In that case the lobes of the orbitals point directly toward the neighbor on the same xy-plane, but they are exactly parallel to the orbitals on different xy-planes. Consequently there is an exchange coupling present between neighboring spins on the same xy plane, but there is no coupling to the spins on other planes. Finally, in the d_{yz} orientation the situation is just opposite to that of the d_{xy} case; now there is an overlap and an exchange coupling within the yz plane but not within the xy plane [22, 71].

Already at this level of the description it thus becomes clear that the orbital and spin ordering will necessarily be strongly dependent upon each other. We will see that eventually this will give rise to an orbital driven transition in which spin dimers are formed: the orbital Peierls transition.

Chapter 2

The Microscopic Model

Before we turn to the detailed description of our microscopic model for titanium pyroxene, let's first consider what experimental and calculational data that model will have to account for.

2.1 Experimental Data

Powder samples of $NaTiSi_2O_6$ were first studied by Isobe et al. in 2002 [21]. They found that the temperature dependence of the magnetic susceptibility displays a peak at a temperature of 210 K, corresponding to the opening of a spin gap at that temperature (see figure 2.1). This behavior is quite different from what has been found in other pyroxene compounds (for example those containing vanadium or chromium instead of titanium): all of these display low temperature antiferromagnetic order [22]. From the fact that titanium pyroxene consists of one dimensional spin $1/2$ chains, Isobe et al. concluded that instead of the antiferromagnetic ordering, there should be a kind of spin Peierls transition, possibly aided by the appearance of orbital order. The formation of a dimer phase at low temperatures was further supported by their finding a peak in the x-ray diffraction data which splits into two exactly at 210 K. This splitting of the x-ray Bragg peak is indicative of the lowering of the crystallographic symmetry; in this case from a high temperature monoclinic phase to a low temperature triclinic phase.

Raman spectra of $NaTiSi_2O_6$ taken by Konstantinović et al., show that the phonon modes of the crystal are also affected by the transition at 210 Kelvin [22]. A couple of phonon modes shift in energy exactly at this temperature, and almost all modes get broadened above the transition temperature. This broadening of the modes is explained as an indication of having a high temperature dynamical Jahn Teller phase in which orbital fluctuations dominate. The transition at 210K should

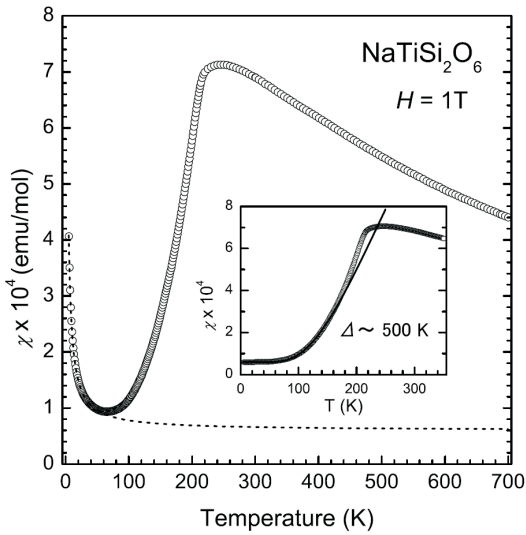

Figure 2.1: The magnetic susceptibility as a function of temperature [21]. The dotted line shows a Curie-law fit, and the inset shows the data with the Curie term subtracted. The solid line in the insert gives a rough estimate of the size of the spin gap.

then correspond to a freezing of the orbitals. Because of the peculiar orientation of the orbitals and their effect on the size of the exchange integral, this in turn will lead to the formation of spin dimers, and thus to the opening of a spin gap. This scenario is further supported by the formulation of a model Hamiltonian for the spin and orbital degrees of freedom in the titanium chains [22].

2.2 Calculational Data

A crystal field analysis of the orbital dimer model however, has lead to a different explanation of the data [72]. In their calculations Bersier et al. find that the t_{2_g} orbitals of the titanium ions are split in energy by the surrounding crystal field to such an extent that they can no longer be considered degenerate. Instead Bersier et al. propose that $NaTiSi_2O_6$ undergoes a structural transition, in which the crystal field produced by the oxygens rotates at 210 K. At high temperatures then, the ground state for the t_{2_g} orbital configuration will be uniform in its overlaps along the chain, whereas at lower temperatures the rotation of the crystal field will induce a rotation of the orbitals, and thus lead to a dimerization of the lattice, and of the spin structure.

Yet another suggestion for explaining the experimental data is made by Popović et al., who used a density functional approach to study the system [73]. After calculating the bandstructure and density of states of the conduction electrons they arrive at the conclusion that the ground state of titanium pyroxene should not be a valence bond state, but rather a Haldane spin one chain: the dimerization of the titanium atoms should then cause the spins to align with their closest neighbor in order to effectively create a spin one, spread out over two neighboring titanium sites. These effective spins in turn tend to align antiferromagnetically, as is depicted in figure 2.2.

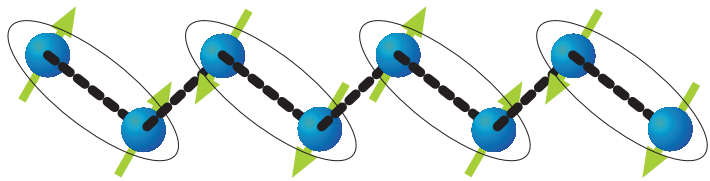

Figure 2.2: The ground state configuration as proposed by Popović et al. Upon inclusion of the quantum fluctuations, the *antiferromagnetic* bonds will turn into spin valence bonds.

In this chapter we argue that all of the above observations, including both the experimental data and the results of the calculational studies, can be explained using the spin orbital model, originally proposed in Konstantinović et al. [19, 22]. We will show that the transition indeed should be considered an orbital-assisted Peierls transition; i.e. an orbital ordering transition which causes both a lattice dimerization and the formation of a spin valence bond state. We will also predict an upper bound for the crystal field splitting of the titanium t_{2_g} orbitals, and we will show that the Haldane chain can be obtained from the same model if we ignore quantum fluctuations.

2.3 The Model

As mentioned before, the $Ti^{3+}O_6$ octahedra in titanium pyroxene form separated, quasi one-dimensional zig-zag chains within the crystal structure. The Coulomb interaction between electrons on the same titanium site is so large that all exchange interactions can be determined by second order perturbation theory in the electron hopping parameter. For a single titanium site, the cubic surrounding formed by the oxygen octahedron splits the $3d$ states into three low lying t_{2_g} states and two e_g states of higher energy. The Ti^{3+} $(3d^1)$ ion then has one electron with spin $1/2$ which can be in any of the three degenerate t_{2_g} orbitals. These orbitals have an overlap, and thus an allowed hopping path and magnetic interaction, with at most

one neighbor (see figure 1.1B). Because the d_{zx} can be considered inert, we will neglect them in the following model description, and only focus on the remaining two t_{2_g} orbitals. If we label these remaining orbitals as the eigenstates of some Ising like operator (say the z-projection of some pseudospin: $T_i^z = 1/2$ corresponds to d_{xy} and $T_i^z = -1/2$ to d_{yz} being occupied on site i), then we can write the effective model Hamiltonian as [19, 22]:

$$H_0 = J \sum_{<i,j>} \vec{S}_i \cdot \vec{S}_j \left[\frac{1}{4} + T_i^z T_j^z + \frac{(-1)^i}{2} \left(T_i^z + T_j^z \right) \right], \tag{2.1}$$

where i and j are on neighboring sites, J is the exchange integral and T^z are the orbital operators. The part between square brackets is such that this Hamiltonian will only give a nonzero result if it acts on a state in which xy (or yz) orbitals are occupied on neighboring sites and these orbitals also are in the same xy (or yz) plane. The ground state of this Hamiltonian will clearly be a state in which the orbitals are all in the same configuration (ferro-orbital order), and in which a spin singlet is formed on all of the bonds on which hopping is allowed by symmetry. The dimerization of the lattice that is seen in x-ray diffraction should then be explained as being due to the Jahn-Teller distortions associated with the orbital ordering. The ordering will in fact tend to lengthen the distance between orbital wavefunctions with lobes pointing toward each other and thus effectively reduce the distance between sites which are not magnetically coupled. At higher temperatures the orbital order will melt, and the spin valence bond pattern will disorder accordingly, thus explaining the disappearance of the spin gap at the transition. The result is a state with large orbital fluctuations which lead to an effective rising of the symmetry of the lattice (since the Jahn Teller distortions are averaged out), and thus a shift in some of the phonon frequencies. The fluctuations at the same time broaden the phonon peaks, and especially those of the modes along the $Ti - O$ bonds.

2.3.1 Crystal Field and Inter Chain Interactions

For the valence bond scenario to be applicable it is clearly important that the two active t_{2_g} orbitals are at least nearly degenerate. To be able to determine the effects of a small crystal field splitting, we will include it in our model Hamiltonian.

On top of this, we will need to raise the dimensionality by introducing some weak inter chain coupling parameter in order to be able to describe a true phase transition with our model. This inter chain coupling will be done in a mean field fashion in our model.

Finally, we will also add an extra "bare" orbital-orbital interaction to the model which has been shown by Hikihara et al. to come directly from the tight binding

perturbation theory, but has been neglected up to this point [71]:

$$H_1 = H_0 + (J_{\rm CF} + J_{\rm IC}) \sum_i T_i^z + \frac{J}{4} \sum_{<i,j>} T_i^z T_j^z, \tag{2.2}$$

where $J_{\rm CF}$ is the size of the crystal field splitting, $J_{\rm IC}$ is the mean orbital field of all neighboring chains, given in terms of the small inter chain coupling parameter J' (which in the present approach is approximated to be of the order of $J/10$), the number of neighboring chains z and the mean value for the orderparameter per site:

$$J_{\rm IC} = \frac{zJ'}{N} \left\langle \sum_i T_i^z \right\rangle. \tag{2.3}$$

2.4 The Analysis

In our analysis of the model Hamiltonian (2.2), we have used three different calculational techniques. First we have neglected all quantum fluctuations by turning all spin operators into Ising operators, so that the Hamiltonian has an exact solution. We have also used a mean field treatment to solve the model including quantum fluctuations, but in doing so we needed to restrict our focus to XY spins. Finally then we have examined the behavior of the full Hamiltonian by doing a Monte Carlo simulation of the system.

2.4.1 Ignoring Quantum Fluctuations

If we turn off quantum fluctuations by projecting all spin operators onto the z-axis, then Hamiltonian (2.2) turns into:

$$\begin{aligned} H_{\rm Ising} &= J \sum_{<i,j>} \left(\frac{1}{4} T_i^z T_j^z + S_i^z S_j^z \left[\frac{1}{4} + T_i^z T_j^z + \frac{(-1)^i}{2} \left(T_i^z + T_j^z \right) \right] \right) \\ &\quad + J_{\rm CF} \sum_i T_i^z, \end{aligned} \tag{2.4}$$

neglecting the inter chain coupling for the moment. It is trivial to see that the groundstate of this (classical) Hamiltonian is given by the configuration in which the orbitals are all aligned, and each spin is anti-aligned with its neighbor along the bond formed by the orbitals. In principle the relative orientation of the spins along the remaining bonds is completely free, giving rise to an infinitely degenerate groundstate. This degeneracy will however be lifted by higher order effects that have been neglected in the approximation so far. As was shown in the work of Hikihara

et al. the Hund's rule coupling will be the dominant higher order effect along the bonds where (2.4) gives no magnetic interaction [71]. The resulting groundstate then is no longer infinitely degenerate but consists of a ferro-orbital state with a chain of alternating ferromagnetically and antiferromagnetically aligned spins on top of it (see figure 2.3). This chain is exactly the ground state found by Popović et al. The fact that ignoring quantum fluctuations leads to the same ground state as the one observed through density functional calculations should come as no surprise: in density functional calculations these quantum fluctuations of the electron spin are neglected as well. Notice that the strongest spin-spin interaction in our model is in fact the antiferromagnetic coupling. The formation of a Haldane-chain like structure will therefore probably not be sustainable if we include quantum fluctuations: in that case the antiferromagnetic bonds will turn into spin valence bonds, and the small residual Hund's rule coupling will play no role in the transition.

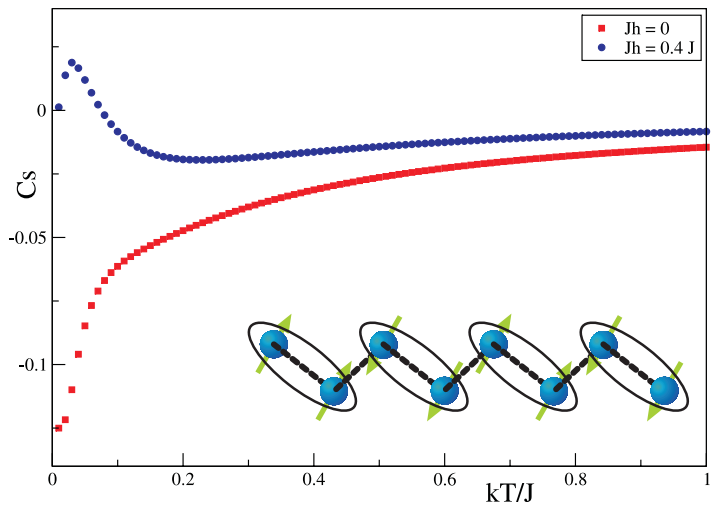

Figure 2.3: The nearest-neighbour spin-spin correlation function Cs for the Ising system of equation (2.4). The lowest line shows the data without any Hund's rule coupling while the line on top shows the data if a small Hund's rule is included. The lowest line converges to a value of $-1/8$ for $T \to 0$, which indicates a random spin ordering on half of the bonds and antiferromagnetic ordering on the other half. The upper line goes to 0 instead and represents the ordering displayed in the inset, which corresponds exactly to the ordering of figure 2.2, found by Popović et al.

2.4.2 Including Quantum Fluctuations

Now that we understand the groundstate of the classical model, let's go back to the full Hamiltonian (2.2), including all of the quantum fluctuations and the inter chain coupling. To get some further analytical understanding of this Hamiltonian we will decouple spin-orbit interaction by introducing mean fields for their respective orderparameters:

$$\begin{aligned} H^S_{\rm MF} &= J \sum_{<i,j>} \left(t + (-)^i \delta t \right) \vec{S}_i \cdot \vec{S}_j \\ H^T_{\rm MF} &= J \sum_{<i,j>} \left(\frac{1}{4} + s + (-)^i \delta s \right) T^z_i T^z_j \\ &\quad + \sum_i \left(\delta s \, J + J_{\rm CF} + J_{\rm IC} \right) T^z_i , \end{aligned} \tag{2.5}$$

where we have recursively defined the mean fields through the equations:

$$\begin{aligned} s + (-)^i \delta s &= \left\langle \vec{S}_i \cdot \vec{S}_j \right\rangle \\ t + (-)^i \delta t &= \left\langle \frac{1}{4} + T^z_i T^z_j + \frac{(-1)^i}{2} \left(T^z_i + T^z_j \right) \right\rangle . \end{aligned}$$

Even after decoupling the spin and orbital part of the Hamiltonian, the spin part still is a bit too involved to be solved head on. Instead we introduce a further approximation by using XY spins instead of full Heisenberg spins (so we project the spin vectors onto the xy plane). This way we do still include spin quantum fluctuations, so we expect the results to be qualitatively correct. Having done the projection, we are now in a position to solve the two parts of the coupled problem independently in terms of the mean fields.

The XY Spins

Let's first consider the spin part of the problem. Since we only have XY-spins left, we can simplify the problem by turning the spins into fermions, using the Jordan-Wigner transformation $S^+_i S^-_{i+1} = a^\dagger_i a_{i+1}$. If we then also switch to Fourier space, we find:

$$H^S_{\rm MF} = J \sum_k \left(t \cos(k) \, a^\dagger_k a_k + i \, \delta t \sin(k) \, a^\dagger_{k+\pi} a_k \right) . \tag{2.6}$$

This fermion Hamiltonian can be forced into the diagonal form $H = \sum_q \epsilon_q c^\dagger_q c_q$ by introducing transformed fermions $c^\dagger$ through $a^\dagger_k = \sum_q c^\dagger_q U_{qk}$. The ϵ_q and U_{qk}

are then simply given by the eigenvalues and eigenvectors of the matrix

$$h_{qk} = t\cos(q)\ \delta_{q,k} + i\ \delta t \sin(q)\ \delta_{q+\pi,k}.$$

Having found this diagonal form it has then become trivial to check that the expressions for the mean spin field and the corresponding susceptibility are given by:

$$\begin{aligned}
s &= \left\langle \frac{1}{N}\sum_i \left(a_i^\dagger a_{i+1} + a_{i+1}^\dagger a_i\right)\right\rangle = \frac{2}{N}\sum_{k,q}\left(\frac{\cos(q)}{1+e^{\beta\epsilon_k}}U_{kq}U_{qk}^\dagger\right)\\
\delta s &= \left\langle \sum_i \frac{(-)^i}{N}\left(a_i^\dagger a_{i+1} + a_{i+1}^\dagger a_i\right)\right\rangle = i\frac{2}{N}\sum_{k,q}\left(\frac{\sin(q)}{1+e^{\beta\epsilon_k}}U_{k,q+\pi}U_{qk}^\dagger\right)\\
\chi_S &= \frac{\beta}{N}\left(\left\langle S^z_{\rm tot}S^z_{\rm tot}\right\rangle - \left\langle S^z_{\rm tot}\right\rangle\left\langle S^z_{\rm tot}\right\rangle\right) = \frac{\beta}{N}\sum_k\left(\frac{e^{\beta\epsilon_k}}{\left(1+e^{\beta\epsilon_k}\right)^2}\right).
\end{aligned} \tag{2.7}$$

Here we have used the Jordan-Wigner transformation to define $S^z = -\frac{1}{2} + a_i^\dagger a_i$.

The Orbitals

Having diagonalized the spin sector, let's turn to the orbital part of the problem (2.5). Since the Hamiltonian involves only Ising operators, it is effectively classical. We can therefore solve this sector by adopting a transfer matrix approach. If we write the classical configuration as a state vector $\prod_i |T_i^z>$, with every $T_i^z = \pm 1/2$, then we can write the partition function for the classical Hamiltonian $H^T_{\rm MF}$ in (2.5) as:

$$Z^T_{\rm MF} = \sum_{T_1^z..T_N^z}\prod_{j=1}^{N/2}\left(\left\langle T^z_{2j}\left|\hat{R}^{\rm even}\right|T^z_{2j+1}\right\rangle\left\langle T^z_{2j+1}\left|\hat{R}^{\rm odd}\right|T^z_{2j+2}\right\rangle\right), \tag{2.8}$$

where the matrices $\hat{R}$, written out in the one particle basis $(+1/2, -1/2)$, are given by:

$$\begin{aligned}
\hat{R}^{\rm even} &= \begin{pmatrix} e^{-\frac{\beta}{4}(J[3\delta s+s+1/4]+2J_{\rm CF}+2J_{\rm IC})} & e^{-\frac{\beta}{4}(J[\delta s-s-1/4]+2J_{\rm CF}+2J_{\rm IC})} \\ e^{\frac{\beta}{4}(J[3\delta s+s+1/4]+2J_{\rm CF}+2J_{\rm IC})} & e^{\frac{\beta}{4}(J[\delta s-s-1/4]+2J_{\rm CF}+2J_{\rm IC})}\end{pmatrix}\\
\hat{R}^{\rm odd} &= \begin{pmatrix} e^{-\frac{\beta}{4}(J[\delta s+s+1/4]+2J_{\rm CF}+2J_{\rm IC})} & e^{-\frac{\beta}{4}(J[3\delta s-s-1/4]+2J_{\rm CF}+2J_{\rm IC})} \\ e^{\frac{\beta}{4}(J[\delta s+s+1/4]+2J_{\rm CF}+2J_{\rm IC})} & e^{\frac{\beta}{4}(J[3\delta s-s-1/4]+2J_{\rm CF}+2J_{\rm IC})}\end{pmatrix}.
\end{aligned}$$

In the form (2.8), we can do the summations over the one particle states, to find that the value for the partition function in terms of the eigenvalues $\lambda_\pm$ of $\hat{R} = \hat{R}^{\rm odd}\hat{R}^{\rm even}$, is simply given by:

$$Z^T_{\rm MF} = \lambda_+^{N/2} + \lambda_-^{N/2}. \tag{2.9}$$

All that remains then, is to relate the quantities of interest to the partition function. This can easily be done if we use the relation $< \partial H/\partial x >= -\beta/Z\ \partial Z/\partial x$:

$$
\begin{aligned}
t &= \frac{1}{N}\left\langle \sum_i \left(\frac{1}{4} + T_i^z T_{i+1}^z + \frac{(-)^i}{2}\left[T_i^z + T_{i+1}^z\right]\right)\right\rangle = \frac{1}{4} - \frac{1}{\beta N Z}\frac{\partial Z}{\partial s} \\
\delta t &= \frac{1}{N}\left\langle \sum_i \left(\frac{(-)^i}{4} + (-)^i T_i^z T_{i+1}^z + \frac{1}{2}\left[T_i^z + T_{i+1}^z\right]\right)\right\rangle = -\frac{1}{\beta N Z}\frac{\partial Z}{\partial \delta s} \\
\chi_T &= \frac{\beta}{N}\left(\left\langle T_{\mathrm{tot}}^z T_{\mathrm{tot}}^z\right\rangle - \left\langle T_{\mathrm{tot}}^z\right\rangle\left\langle T_{\mathrm{tot}}^z\right\rangle\right) = \frac{1}{\beta N}\left(\frac{1}{Z}\frac{\partial^2 Z}{\partial J_{\mathrm{CF}}^2} - \left[\frac{1}{Z}\frac{\partial Z}{\partial J_{\mathrm{CF}}}\right]^2\right) \qquad (2.10)
\end{aligned}
$$

These expressions, combined with the earlier expressions (2.7), enable us to solve for the mean fields self consistently, and in the process find the corresponding values for the mean field susceptibilities as well. Since we can do all of this as a function of temperature, we can then identify magnetic and orbital transition temperatures as being the peaks in the corresponding susceptibilities.

2.4.3 Monte Carlo

Apart from the above analytical considerations, we can also examine the full Hamiltonian (2.2) numerically, without any further approximations. A Monte Carlo treatment of this system turns out to be particularly easy to implement. Because magnetic interactions exist only along the bonds formed by neighboring orbitals, there can be no spin structures that spread beyond two sites: the spatial orientation of the orbitals allows for bonding with one neighbor only. This greatly simplifies the problem, since depending on the orbital configuration, a spin is now either isolated or in a two-spin valence bond state (either singlet or triplet). In both cases we can represent the spin variable by a classical variable, just like the orbitals, and thus we can get away with doing classical Monte Carlo instead of quantum Monte Carlo. We have therefore studied the system (2.2) using a one dimensional, classical Monte Carlo code for a chain of 100 sites, which we then couple to surrounding chains via the mean field inter chain coupling J_{IC}. By varying the external fields in our simulation we were able to extract the spin and orbital susceptibilities as a function of temperature. Again we then identified the top in these susceptibility plots as the transition temperature of the material.

2.5 The Results

As we have seen, the analysis of the model ignoring quantum fluctuations gave us the same groundstate as Popović et al. found in their calculations. However, our system consists of quasi one dimensional spin 1/2 chains, so quantum fluctuations

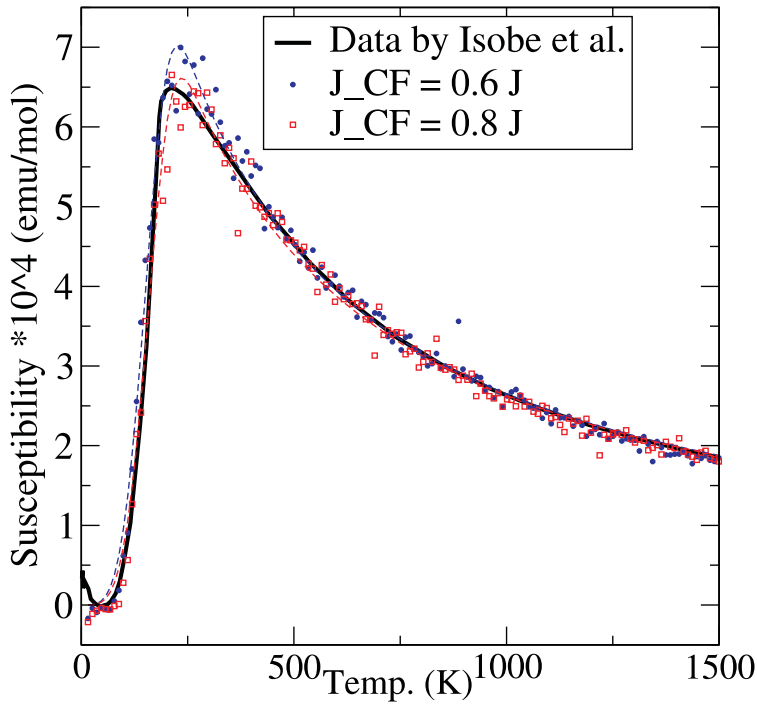

Figure 2.4: A fit of the experimental data using the Monte Carlo results.

can be expected to be important. These quantum fluctuations are taken into account in our mean field approach, as well as in the Monte Carlo simulation. The transition temperatures at which the spin and orbital order emerges in these calculations, are plotted as a function of the crystal field splitting in figure 2.5. In the region below $J_{\mathrm{CF}} \simeq J$ both analyses clearly lead to a coincidence of the transition temperatures. This corresponds nicely to the observed opening of a spin gap combined with phonon shifts at 210 K.

A rough estimate for the crystal field splitting can be found by trying to fit our Monte Carlo data to the experimental data taken by Isobe et al. The results of this fitting procedure are shown on in figure 2.4. The fit captures all qualitative features of the experimental curve, for a value of the crystal field splitting of $J_{\mathrm{CF}} \simeq 0.8J$. Quantitatively it is a little off at the top of the susceptibility curve, but noticing the simplicity of the model, and the fact that we have only one fitting parameter (i.e. J_{CF}), this was to be expected. On the other hand, the crystal field analysis of Bersier et al. lead to a value for the crystal field splitting that was much higher than the exchange coupling [72]. The actual value in titanium pyroxene, is expected to be

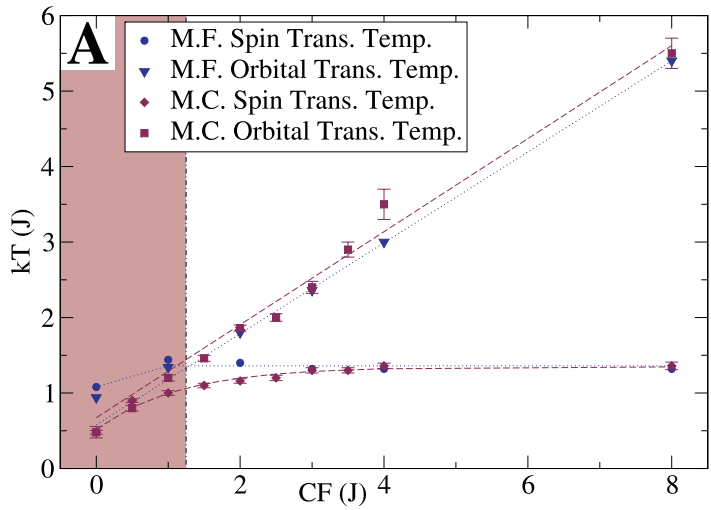

Figure 2.5: The transition temperature as a function of the crystal field splitting, as found in the mean field and Monte Carlo calculations. The mean field data have been adjusted to account for the difference in energy between the excitations for XY spins and full Heisenberg spins.

lower than the value found in their calculations because of the approximations they were forced to make. With our result of figures 2.5 and 2.4, we can now turn around the reasoning, and make a new prediction: assuming that our model captures the correct physics of the transition in $NaTiSi_2O_6$, we can predict that the crystal field splitting J_{CF} will be no larger than the exchange coupling J.

Chapter 3

Conclusions

We have examined the microscopic model Hamiltonian originally proposed by Konstantinović et al. using a Monte Carlo simulation augmented by a mean field treatment and a classical approximation scheme. The model Hamiltonian incorporates both spin and orbital degrees of freedom, and was extended to also include the local crystal field splitting. All treatments of the model have provided strong support for the idea that an orbital-assisted Peierls transition occurs in the titanium chains of $NaTiSi_2O_6$. This transition is characterized by the uniform ordering of the orbitals, accompanied by a lattice dimerization and the formation of spin valence bonds.

Using these calculations we were able to understand all previously published data, including the density functional data which seemed to suggest the formation of a spin one Haldane chain. From the results of our calculations we were furthermore able to abstract a firm upper bound on the size of the crystal field splitting in this material: it should not be larger than the strength of the magnetic exchange interaction. We thus conclude that our microscopic description is consistent with all available data, and that at 210 K, titanium pyroxene undergoes an orbital-assisted Peierls transition.

The occurrence of this orbital-assisted Peierls transition, and the associated effects in the spin susceptibility, the phonon spectrum and so on, are all made possible by the quantum fluctuations of the orbital and spin degrees of freedom. The quantum mechanics of the underlying microscopics thus plays a decisive role in determining the thermodynamic properties of the macroscopic material. This situation is of course not at all unique for titanium pyroxene. In fact most properties of most solid state materials are related to the quantum mechanical bases upon which they are built. As we will see in the next part, this can even extent to properties of the system as a whole: the very rigidity of the solids under consideration is really a quantum effect!

Part III

Quantum Mechanics of the Big World

Chapter 1

Introduction

As we have seen, the quantum mechanical nature of microscopic particles is often a necessary ingredient in understanding the properties of macroscopic materials. Upon realizing this, we could take things one step further, and argue that since all macroscopic objects are ultimately built up from a collection of microscopic parts, they too should obey the laws of quantum mechanics. This simple reasoning immediately leads to a paradox: on the one hand we know from experiment that quantum mechanics is certainly the correct theory to describe atoms, molecules, etc. On the other hand it seems that even though it is constructed from a large number of atoms and molecules, the chair that you are sitting on does not obey quantum mechanics. After all, if the chair had been a quantum mechanical object then it should have respected the translational symmetry of the space around it, and spread throughout the entire room in a wave of quantum superpositions. Clearly this does not happen in the everyday world, and the question thus arises how macroscopic objects can resist their quantum origins.

The way out of this paradox lies in the process of spontaneous symmetry breaking [51, 63]. It turns out that because of their enormous size (as compared to their constituent particles), the wavefunctions of macroscopic objects become extremely unstable, and can easily be molded into as classical a form as possible. In fact, for truly large objects, like tables and chairs, this reduction to a classical form is so easy that it happens spontaneously [50]. And once the translational symmetry of the chair-wavefunction is broken, the shear size of the chair is enough to slow down its delocalization so far that it seems to truly be stuck in place [50, 51].

1.1 Qubits

This process of spontaneous symmetry breaking which enables chairs (and other crystals) to be localized in one position, is also the reason that magnets and anti-

ferromagnets can have their (sublattice) magnetization point in one direction only, that superconductors (and superfluids) can acquire an overall definite phase, and so on [50, 74–77]. It is the reason that the world around us looks classical in the first place. However, it is still a quantum effect, and a very subtle remnant of the quantum nature of macroscopic objects remains, even in the objects of our everyday world [23, 25]. Normally the quantum behavior of macroscopic bodies as a whole is much too delicate to be detected, but if we start to decrease the system size then at some point the quantum origin will start to come into play. In particular, this may lead to unexpected results in the so called solid state qubits: systems designed specifically to be small enough to act quantum mechanically in some ways, but to remain classical in others [24, 78–81]. As we will see in this part of the thesis, the quantum origin of classical objects will inevitably lead to a universal and finite lifetime of solid state qubits [23, 25].

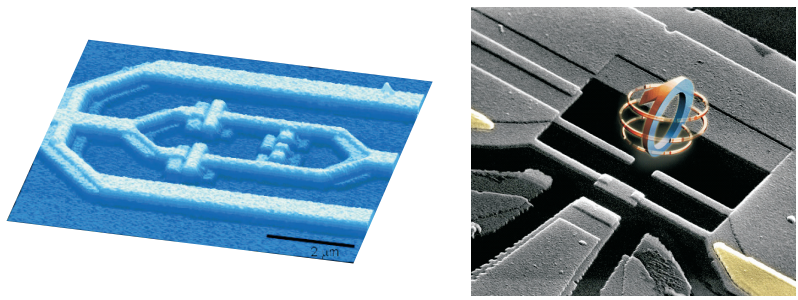

Figure 1.1: Two examples of the many-particle qubits discussed in the text. Left: An STM image of the superconducting flux qubit used in Delft [80]. Supercurrent circulates both clockwise and anti-clockwise through the central ring. The 'obstructions' in the ring are the Josephson junctions. Right: The Cooper-pair box qubit or 'quantronium' studied in Saclay [79, 82]. The actual Cooper-pair box is the small rectangular island in the centre which can hold a superposition of N and $N + 1$ Cooper pairs.

The many-particle qubits that motivate us to study decoherence due to spontaneous symmetry breaking are realized in a number of mesoscopic solid state systems. For instance, by engineering aluminum on a sub-micron length scale, superconducting flux qubits and Cooper pair boxes can be manufactured. The flux qubit is a Josephson device that can be brought into a quantum superposition of two electrical currents: a left and a right circulating current [80, 81]. Typically this current is carried by $N \sim 10^6$ Cooper pairs, where N denotes the number of constituent particles making up the superposition. A Cooper pair box on the other hand is a superconducting island, containing $N \sim 10^8$ electrons, which can be put in a superposition of two states with different average numbers of Cooper

pairs [79,82–84]. Magnetic many-particle qubits are realized for instance in molecular nanomagnets. Molecules with large magnetic moments can be brought into a superposition of directions of magnetization. A well studied example is Mn^{12} acetate, a molecule that contains 12 manganese atoms, coupled together to form a total spin of $S = 10$. The molecule can be brought into a superposition of states with $S^z = +10$ and $S^z = -10$ and coherent Rabi-oscillations of the magnetization have been observed [85]. An even larger molecule is ferritin, which contains about 4500 Fe^{3+} ions [86]. If the total magnetic moment of a ferritin molecule is brought into a coherent superposition, this corresponds to a superposition of $N \sim 10^2$ spins. For these mesoscopic superconducting and magnetic qubits the limit in coherence due to spontaneous symmetry breaking is certainly a relevant process. Even though at present other sources of decoherence form a stricter boundary on the usability of these qubits, the intrinsic limit set by spontaneous symmetry breaking may will be reached within the near future [23].

Chapter 2

The Harmonic Crystal

As mentioned before, one of the most fundamental differences between quantum and classical physics lies in the role of symmetry. Dealing with an exact quantum mechanical eigenstate, all configurations equivalent by symmetry should have exactly the same status in principle, while in a classical state one of them can be singled out. That is, given that space is translationally invariant, a quantum object should be in an eigenstate of total momentum, being spread out with equal probability over all of space. In the classical limit however it takes on a definite locus. The explanation of this 'spontaneous symmetry breaking' as a ramification of the singular nature of the thermodynamic limit is one of the central achievements of quantum condensed matter physics [51, 74]. One imagines a symmetry breaking 'order parameter field' B (e.g., a potential singling out a specific position in space). Upon sending B to zero before taking the thermodynamic limit ($N \to \infty$) one finds the exact quantum groundstate respecting the symmetry. However, taking the opposite order of limits one finds that the classical state becomes fact. Although the concept of spontaneous symmetry breaking was originally introduced in the context of quantum magnetism in solid state physics [51, 74], spontaneous symmetry breaking is a general phenomenon, that is just as relevant in other fields, including elementary particle physics and cosmology [87–92].

2.1 Spontaneous Symmetry Breaking

Let us first consider how spontaneous symmetry breaking arises in a crystalline lattice. Consider the textbook example of a harmonic crystal, with the Hamilto-

nian [64]

$$H = \sum_j \frac{\mathbf{p}_j^2}{2m} + \frac{\kappa}{2} \sum_j \left(\mathbf{x}_j - \mathbf{x}_{j+1}\right)^2, \tag{2.1}$$

where j labels all N atoms in the lattice, which have mass m, momentum $\mathbf{p}_j$ and position $\mathbf{x}_j$. We consider here only a one-dimensional chain of atoms, but all of the following can be straightforwardly generalized to higher dimensions as well. The harmonic potential between neighboring atoms is parametrized by κ; it turns out that the results on spontaneous symmetry breaking that follow are equally valid for an-harmonic potentials. Let us first identify the collective dynamics which describe the spontaneous symmetry breaking of this short-ranged microscopic Hamiltonian.

In the standard treatment of the quantum crystal one begins by introducing new coordinates, which are the displacements of atoms from their equilibrium position. Then, after a Fourier transform the eigenstates of this Hamiltonian are easily found [63, 64]. We take a slightly longer route by introducing bosonic phonon operators from the very beginning and diagonalizing the quadratic part of the Hamiltonian by performing a Bogoliubov transformation at the end. In doing so we do not have to introduce any equilibrium position of the atoms. Instead we can keep track of the center of mass motion of the crystal as a whole, and this brings to the fore the thin spectrum in a natural manner. Moreover, we can use the exact same procedure in the next chapter to find the collective order parameter dynamics for antiferromagnets.

The momentum and position operators are expressed in terms of bosonic operators as

$$p_j = iC\sqrt{\frac{\hbar}{2}}(b_j^\dagger - b_j); \;\; x_j = \frac{1}{C}\sqrt{\frac{\hbar}{2}}(b_j^\dagger + b_j), \tag{2.2}$$

so that the commutation relation $[x_j, p_{j'}] = i\hbar\delta_{j,j'}$ is fulfilled. We choose $C^2 = \sqrt{2m\kappa}$ so that the Hamiltonian reduces to

$$H = \frac{\hbar}{4}\sqrt{\frac{2\kappa}{m}} \sum_j 2(b_j^\dagger b_j + b_j b_j^\dagger) - (b_j^\dagger + b_j)(b_{j+1}^\dagger + b_{j+1}), \tag{2.3}$$

and after a Fourier transformation

$$H \;\; = \;\; \hbar\sqrt{\frac{\kappa}{2m}} \sum_k \left[A_k b_k^\dagger b_k + \frac{B_k}{2}(b_k^\dagger b_{-k}^\dagger + b_k b_{-k}) + 1 \right],$$

where $A_k = 2 - \cos(ka)$, $B_k = -\cos(ka)$ and a is the lattice constant. This Hamiltonian is still not diagonal, since the terms $b_k^\dagger b_{-k}^\dagger$ and $b_k b_{-k}$ create and annihilate

two bosons at the same time. We get rid of these terms by a Bogoliubov transformation (see appendix E). After this the Hamiltonian in terms of transformed boson operators $\beta_k = \cosh(u_k) b_{-k} + \sinh(u_k) b_k^\dagger$ is

$$\begin{aligned} H &= \hbar\sqrt{\frac{\kappa}{m}} \sum_k \left[2 \sin|ka/2| \left(\beta_k^\dagger \beta_k + \frac{1}{2} \right) \right. \\ &+ \left. \frac{1}{4}\sqrt{2}\cos(ka) \right] \\ &= 2\hbar\sqrt{\frac{\kappa}{m}} \sum_k \sin|ka/2| \left[n_k + \frac{1}{2} \right], \end{aligned} \tag{2.4}$$

since $\sum_k \cos k = \frac{N}{2\pi} \int_{-\pi}^{\pi} dk \cos k = 0$.

This result seems to coincide with the textbook Hamiltonian which we would have obtained if we had followed the conventional route of Fourier transforming the Hamiltonian for the displacements, and then quantizing it [64]. However, the Bogoliubov transformation has the advantage that it brings to the fore a rather subtle point. When $k \to 0$ the excitation energy $\omega_k \to 0$ and the two parameters in the Bogoliubov transformation diverge: $\sinh(u_k) \to \infty$ and $\cosh(u_k) \to \infty$. Precisely at $k = 0$ the canonical transformation is no longer well defined. We therefore should investigate the bosonic terms in the Hamiltonian with $k = 0$ separately. This zero momentum part of the Hamiltonian describes the obvious fact that the crystal as a whole carries a kinetic energy associated with the combined mass of all of its constituents, and is given by

$$\begin{aligned} H_{\mathbf{k}=0} &= \hbar\sqrt{\frac{\kappa}{2m}} \left(b_0^\dagger b_0 - \frac{1}{2} \left(b_0^\dagger b_0^\dagger + b_0 b_0 \right) + 1 \right) \\ &= \hbar\sqrt{\frac{\kappa}{2m}} \left[1 - \frac{1}{2} \left(b_0^\dagger - b_0 \right)^2 \right], \end{aligned} \tag{2.5}$$

where $(b_0^\dagger - b_0)^2 = \frac{-2}{\hbar\sqrt{2m\kappa}} \mathbf{p}_0^* \mathbf{p}_0$ so that

$$H_{\mathbf{k}=0} = \frac{p_{\text{tot}}^2}{2Nm} + \text{constant}, \tag{2.6}$$

where $\mathbf{p}_{\text{tot}} \equiv \sum_j \mathbf{p}_j = \sqrt{N}\mathbf{p}_{\mathbf{k}=0}$ is the total momentum of the entire system, or equivalently, its center of mass momentum. When N is large, this Hamiltonian has states that are very low in energy. These states in fact form the thin spectrum of the harmonic crystal. We call this part of the spectrum *thin* because it contains so few states of such low energy that its contribution to the free energy in the thermodynamic limit completely disappears (see appendix B). In turn, this implies that these thin spectrum states do not contribute to any thermodynamically measurable

quantities such as for instance the specific heat of the crystal. Their effect on the properties of the crystal is thus increasingly subtle, but its existence can nonetheless have profound consequences. About a decade ago the deep meaning of the thin spectrum for interacting quantum systems became clear and consequently its explicit mathematical structure was determined [77, 93].

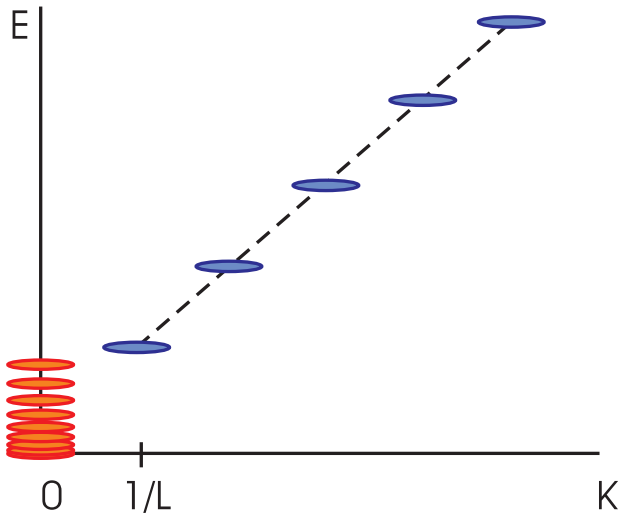

Figure 2.1: A schematic representation of the very longest wavelength excitations of a finite-sized harmonic crystal. The excitations on the right represent the standard phonon modes, which are found at finite wavelengths. The lowest possible wavenumber for a phonon mode is proportional to $1/L$, where L is the linear system size. The thin spectrum on the other hand, which describes the collective dynamics of the crystal as a whole, is found exclusively at $k = 0$. Its excitation energies are lower than even the lowest phonon modes.

The groundstate of the Hamiltonian at $\mathbf{k} = \mathbf{0}$, which governs the collective behavior of the crystal as a whole, obviously has total momentum zero. It thus has no uncertainty in total momentum and maximum uncertainty in total position: translational symmetry is unbroken. Symmetry breaking can occur if we add to the Hamiltonian of equation (2.6) a symmetry breaking field of the form $B\mathbf{x}_{\rm tot}^2/2$, where the center of mass coordinate is $\mathbf{x}_{\rm tot} \equiv \sum_j \mathbf{x}_j$. This yields a harmonic oscillator equation for the collective position coordinate. Its well known groundstate wavefunction is

$$\psi_0(x_{\rm tot}) = \left(\frac{m\omega N}{\pi\hbar}\right)^{1/4} e^{-\frac{m\omega N}{2\hbar}x_{\rm tot}^2}; \quad \omega = \sqrt{\frac{B}{mN}}. \tag{2.7}$$

This state describes a wave-packet for the center of mass coordinate in real space, which of course corresponds to an equivalent superposition of total momentum states: the symmetry breaking field B couples the different thin spectrum states of the crystal. For a vanishing symmetry breaking field B and finite number of atoms we have $\omega N \to 0$ and the collective coordinate is completely delocalized, as before: $\psi_0(x_{\rm tot}) = const.$ But taking the thermodynamic limit ($N \to \infty$) *in presence of a finite symmetry breaking field* gives $\omega N \to \infty$ and the center of mass position becomes completely localized in the center of the potential well ($\psi_0(x_{\rm tot}) = \delta_{\mathbf{x}_{\rm tot},0}$), even if at the end the symmetry breaking field is sent to zero. As we already pointed out, such a singular limit characterizes spontaneous symmetry breaking [51, 77]; in this particular case the translational symmetry of the crystal as a whole is spontaneously broken. The occurrence of a thin spectrum which consists of the states associated with the quantum mechanics of the macroscopic body as a whole is a universal notion. Whenever a system exhibits a continuous symmetry which is broken in the classically realized, macroscopic state, then consequently there must be a spectrum of states associated with the symmetry-restoring fluctuations of the orderparameter as a whole. The smallness of the energy spacing within the thin spectrum warrants the orderparameter dynamics of macroscopic bodies to take place on a time scale much larger than anything observable [50].

2.2 Decoherence

To study the effect of the thin spectrum on the coherence of many particle qubits, let us first investigate the dynamics of such a qubit in the most general terms. Consider a many particle system that is large enough to display a spontaneously broken continuous symmetry, but small enough to be used as a qubit. This qubit will then have a thin spectrum which we can label by the quantum number n. At the same time the system must have two accessible quantum states that can be used as the qubit states, and which can be labeled by the quantum number m. Because we have no experimental control over the thin spectrum states, we will have to start out the experiment with a thermal mixture of those states:

$$\rho_{t<t_0} \quad = \quad \frac{1}{Z} \sum_n e^{-\beta E_0^n} \, |0,n\rangle \, \langle 0,n| \, , \tag{2.8}$$

where ρ_t is the density matrix, E_m^n is the energy of the state $|m,n\rangle$ and where, by definition, the partition function is $Z = \sum_n e^{-\beta E_0^n}$ and $\beta^{-1} = k_B T$. To begin using this qubit in a quantum computation we will typically have to prepare it in some coherent superposition of the states in the two level system. To do this we apply a rotation that takes the state $|0,n\rangle$ into the state $\sqrt{1/2}\,(|0,n\rangle + |1,n\rangle)$ for all values

of n. The resulting density matrix then is given by

$$\begin{aligned}\rho_{t=t_0} &= \frac{1}{2Z}\sum_n e^{-\beta E_0^n}\left(|0,n\rangle\langle 0,n| + |0,n\rangle\langle 1,n|\right.\\ &+ \left.|1,n\rangle\langle 0,n| + |1,n\rangle\langle 1,n|\right). \qquad (2.9)\end{aligned}$$

If we know the Hamiltonian H which governs the dynamics of the qubit, then we can follow the time evolution of this density operator by applying the time evolution operator $U|m,n\rangle \equiv e^{-\frac{i}{\hbar}H(t-t_0)}|m,n\rangle = e^{-\frac{i}{\hbar}E_m^n(t-t_0)}|m,n\rangle$. We then find for the density matrix at $t > t_0$

$$\begin{aligned}\rho_{t>t_0} &= U\rho_{t=t_0}U^\dagger\\ &= \frac{1}{2Z}\sum_n e^{-\beta E_0^n}\left(|0,n\rangle\langle 0,n| + |1,n\rangle\langle 1,n|\right.\\ &+ \left.\left[e^{-\frac{i}{\hbar}(E_0^n-E_1^n)(t-t_0)}|0,n\rangle\langle 1,n| + H.c.\right]\right), \qquad (2.10)\end{aligned}$$

where $H.c.$ denotes the Hermitian conjugate of its preceding term.

Experimentally the thin spectrum is as good as unobservable because of its extremely low energy and its vanishing thermodynamic weight (see appendix B). We therefore have to trace these states out of the density matrix [94, 95]. This will yield a reduced (observable) density matrix, defined by

$$\rho_{t>t_0}^{\rm red} = \sum_j \langle j|\rho_{t>t_0}|j\rangle, \qquad (2.11)$$

where the trace is over thin spectrum states labeled by j and $\langle j|m,n\rangle \equiv |m\rangle\delta_{j,n}$. Performing the trace, we find the following reduced density matrix in the basis of the states $|m\rangle$

$$\rho_{t>t_0}^{\rm red} = \frac{1}{2}\begin{bmatrix} 1 & \rho_{t>t_0}^{\rm OD} \\ \left[\rho_{t>t_0}^{\rm OD}\right]^* & 1 \end{bmatrix}, \qquad (2.12)$$

where the off-diagonal matrix element is defined as

$$\rho_{t>t_0}^{\rm OD} \equiv \frac{1}{Z}\sum_n e^{-\beta E_0^n} e^{-\frac{i}{\hbar}(E_0^n-E_1^n)(t-t_0)}. \qquad (2.13)$$

If this off-diagonal matrix element vanishes at some time, then the qubit will have decohered at that time, due to the presence of the thin spectrum. In general there will be a non-zero $\Delta E_{\rm thin} \equiv E_0^n - E_1^n$, and this shift in energy corresponds to a phase shift of the thin spectrum states. These phases will typically interfere destructively, lowering $\rho_{t>t_0}^{\rm OD}$ and leading to dephasing and decoherence. The timescale for

this decoherence process is set by the inverse of the involved energy scale, and will therefore be proportional to $\hbar/\Delta E_{\text{thin}}$.

For this dephasing to occur however, it is necessary that a finite number of thin spectrum states participates in the dynamics of decoherence. How many states do contribute to the process is governed by the Boltzmann factor $e^{-\beta E_0^n}$, which exponentially suppresses states of energy higher than $\sim k_B T/E_{\text{thin}}$ with E_{thin} the typical level spacing of the thin spectrum states. Putting these arguments together, one finds that the characteristic timescale on which $\rho^{\text{OD}}_{t>t_0}$ will vanish should be proportional to

$$t_{\text{spon}} \propto \frac{\hbar}{k_B T}\frac{E_{\text{thin}}}{\Delta E_{\text{thin}}}. \tag{2.14}$$

In the following sections we will calculate t_{spon} explicitly for a number of realizations of the many particle qubit. We will see that in the generic situation $\Delta E_{\text{thin}} \propto E_{\text{thin}}/N$ so that we find

$$t_{\text{spon}} \propto \frac{N\hbar}{k_B T}, \tag{2.15}$$

which is our main result.

2.2.1 The Interstitial Excitation

As a first example of the influence of the thin spectrum on coherence, let us try to employ the harmonic crystal as a qubit. In order to do so we will have to define a set of two states that are to be used as the calculational states of the qubit. A simple choice for such a set could be to use the presence or absence of an interstitial excitation. This leads to the definition of the state $|m=0\rangle$ describing the crystal with N atoms, and the state $|m=1\rangle$ which has one extra interstitial atom, and is described by the same model, but with $N+1$ atoms in the lattice. The thin spectrum is exactly as described in (2.6), so that the energy can be defined as

$$E_m^n = \frac{n^2}{2M\,(N+m)} + \mu m, \tag{2.16}$$

where M is the mass of an atom, n labels states with different total momentum (which make up the thin spectrum), and μ is the chemical potential associated with adding an extra atom to the lattice.

We are now in the position to simply substitute this information into the general expression for the off-diagonal matrix element of the reduced density matrix (2.13), yielding

$$\rho^{\text{OD}}_{t>t_0} = \frac{1}{Z}\; e^{-\frac{i}{\hbar}\mu(t-t_0)} \sum_n e^{-\beta\frac{n^2}{2MN}} \cdot e^{-\frac{i}{\hbar}\frac{n^2}{2M}\left(\frac{1}{N}-\frac{1}{N+1}\right)(t-t_0)}. \tag{2.17}$$

The constant phase factor $e^{-\frac{i}{\hbar}\mu(t-t_0)}$ does not contribute to the decoherence process, but the terms depending on n introduce phase shifts into the dynamics of the system, which lead to the disappearance of $\rho^{\mathrm{OD}}_{t>t_0}$ over time (see figure 2.2). Upon introduction of $E_{\mathrm{thin}} = 1/(2MN)$ and $\Delta E_{\mathrm{thin}} = 1/(2MN(N+1)) \simeq 1/(2MN^2)$, a straightforward evaluation of the sum over thin spectrum states yields t_{spon}, defined as the half time for $\left|\rho^{\mathrm{OD}}_{t>t_0}\right|$

$$\begin{aligned} t_{\mathrm{spon}} &= \frac{2\pi\hbar}{k_B T}\frac{E_{\mathrm{thin}}}{\Delta E_{\mathrm{thin}}} \\ &= N\frac{2\pi\hbar}{k_B T}. \end{aligned} \tag{2.18}$$

By using the crystal and its interstitial excitation as a qubit we have assumed that we can just ignore the symmetry breaking field as soon as the crystal has been localized in space at some time in the past. In general this may not be true, because the thermodynamic limit and the limit of disappearing localization field do not commute. We should therefore also consider the situation in the presence of a small but finite symmetry breaking field B. In that case the energies of the system will be given by

$$E^n_m = n\sqrt{\frac{B}{2M\,(N+m)}} + \mu m, \tag{2.19}$$

which will again lead to a phase factor which is constant in n, and a sum over phases which can be written as multiples of $E_{\mathrm{thin}} = \sqrt{B/2M\,(N+m)}$ and $\Delta E_{\mathrm{thin}} = E_{\mathrm{thin}}/N$. The summation over thin spectrum states will thus again yield the coherence time $t_{\mathrm{spon}} = N\frac{2\pi\hbar}{k_B T}$.

2.2.2 Goldstone Modes

The interstitial excitation that is used in the previous section to make a qubit state out of the harmonic crystal is a very rough excitation to use for that purpose. The extra atom in the crystal will not only increase the mass of the crystal as a whole but also immediately affect its lattice structure, and thus couple to many phonon-excitations. Because of this, serious decoherence effects are to be expected. In constructing a qubit using the quantum crystal it is therefore better to look for a more 'silent' excitation. These silent excitations are naturally found in the long wavelength Goldstone modes of the crystal, i.e. the low energy phonons [96].

To see what the effect of phonons on the thin spectrum is, we need to consider the symmetry breaking of the crystal more carefully. In the previous section we focused on the collective behavior of the crystal as a whole. Thus we disregarded all internal degrees of freedom. Now we are interested in the localization of

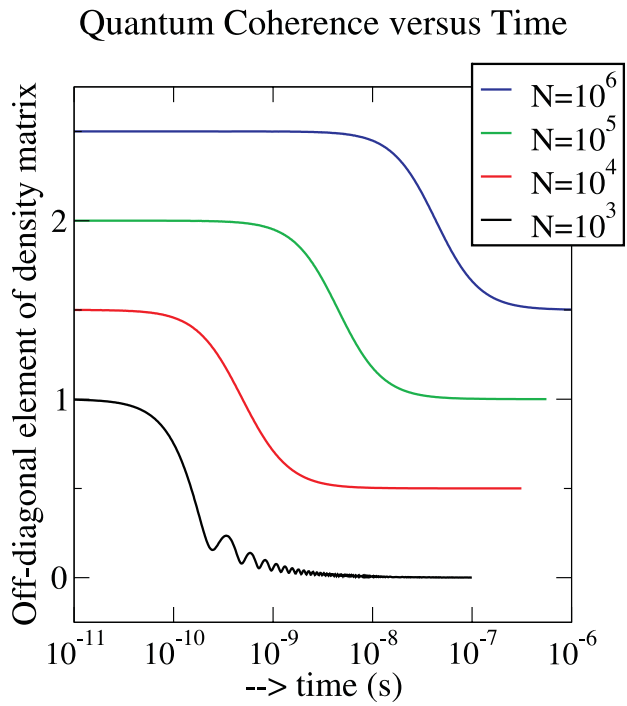

Figure 2.2: The off diagonal element of the reduced density matrix given by equation (2.17) as a function of time. The value 1 implies full coherence, while 0 signifies that the qubit has completely decohered. The curves have been displaced vertically for ease of presentation.

the individual atoms within the crystal structure because the existence of the Goldstone phonons is a manifestation of the internal breaking of translational symmetry within the crystal lattice [96]. For this purpose we introduce a symmetry breaking field V such that it acts as a pinning potential for the individual atoms:

$$\begin{aligned} H &= H_0 + H_{\rm SB} \\ &= \sum_j \frac{\mathbf{p}_j^2}{2m} + \frac{\kappa}{2}\left(\mathbf{x}_j - \mathbf{x}_{j+1}\right)^2 - V\cos\left(2\pi\,\mathbf{x}_j\right). \end{aligned} \tag{2.20}$$

Here the lattice constant a is taken as the unit of length. For small deviations of the atoms from their mean positions, we can expand the symmetry breaking term to

read

$$\begin{aligned} H_{\rm SB} &= V\sum_j 2\pi^2\mathbf{x}_j^2 - \frac{2\pi^4}{3}\mathbf{x}_j^4 \\ &= 2V\pi^2\sum_k \mathbf{x}_k\mathbf{x}_{-k} \\ &\quad -\frac{2V\pi^4}{3N}\sum_{k,K,q}\mathbf{x}_k\mathbf{x}_K\mathbf{x}_q\mathbf{x}_{-k-K-q}, \end{aligned} \tag{2.21}$$

where the last line results from a Fourier transformation of the position operators. The thin spectrum of the crystal is formed by the zero momentum part of the Hamiltonian, while the phonons can be found after the bosonization and Bogoliubov transformation of the finite momentum part. The relation between the phonons and the thin spectrum thus becomes clear if we consider the zero momentum terms of $H_{\rm SB}$ in lowest order given by

$$H_{\rm SB} \approx \frac{2V\pi^2}{N}\mathbf{x}_{\rm tot}^2 - \frac{4V\pi^4}{N^2}\mathbf{x}_{\rm tot}^2\sum_{k\neq 0}\beta_k^\dagger\beta_k + ... \tag{2.22}$$

where higher order collective terms and boson-boson interaction terms are neglected. The first term in this expression is of the form of the symmetry breaking field that we considered before. It contains a factor $1/N$ because of the specific periodic pinning potential that we now consider. The symmetry of the crystal as a whole is still broken by this term, as can be easily checked by comparing the collective fluctuations to the size of the crystal. The energy scale of the thin spectrum is determined by the first term in (2.22) to be $E_{\rm thin} \propto \frac{1}{N}\sqrt{\frac{B}{m}}$. The second term shows how the presence of a phonon excitation will in first order lead to an energy shift in the thin spectrum which sets $\Delta E_{\rm thin} \propto \frac{1}{N^2}\sqrt{\frac{B}{m}}$. Putting these together in the general expression for the decoherence time in Eq. (2.14), we immediately find once again that $t_{\rm spon} \propto N\frac{\hbar}{k_BT}$.

Chapter 3

The Lieb-Mattis model

Let us now turn to the discussion of the antiferromagnetic Lieb-Mattis model [77, 93, 97]. The reason for considering the rather particular, long ranged Lieb-Mattis model is that for a broad class of Heisenberg models with short-ranged interactions it constitutes the effective Hamiltonian for the thin states. Similar collective models underlie the breaking of other continuous symmetries, such as for instance U(1) phase symmetry in a superconductor. In that case the collective Hamiltonian turns out to be very similar to the Lieb-Mattis Hamiltonian as far as the structure of the thin spectrum and the composition of the wavefunction of the symmetry broken state are concerned. To explicitly show how the Lieb-Mattis model arises from a Heisenberg model, let us consider an antiferromagnet on a bipartite lattice with isotropic nearest neighbor interactions between quantum spins of size σ. Its Hamiltonian is [63, 64]

$$H = J \sum_{i,\delta} \mathbf{S}_i \mathbf{S}_{i+\delta}, \tag{3.1}$$

where i labels all the spins on the A sublattice, and the δ are the vectors connecting site i to its neighbors on sublattice B. The generalization to other types of interactions and even other types of lattices is straightforward [98–103]. The magnon spectrum of this Hamiltonian can be found within linear spin wave theory [104]. One approximates the spin operators with Holstein-Primakoff bosons as

$$\begin{aligned} S^z_{i\epsilon A} &\to \quad \sigma - a_i^\dagger a_i, \quad S^z_{i\epsilon B} \to b_i^\dagger b_i - \sigma, \\ S^+_{i\epsilon A} &\to \quad \sqrt{2\sigma}\, a_i, \quad S^+_{i\epsilon B} \to \sqrt{2\sigma}\, b_i^\dagger, \\ S^-_{i\epsilon A} &\to \quad \sqrt{2\sigma}\, a_i^\dagger, \quad S^-_{i\epsilon B} \to \sqrt{2\sigma}\, b_i. \end{aligned} \tag{3.2}$$

To quadratic order in the boson operators the Hamiltonian then becomes, after a Fourier transformation

$$H^{\rm LSW} = \frac{1}{2}JNz\sigma^2 \quad + \quad Jz\sigma\sum_{\mathbf{k}}\Big((a^\dagger_{\mathbf{k}}a_{\mathbf{k}} + b^\dagger_{\mathbf{k}}b_{\mathbf{k}}) \\ + \quad \gamma_{\mathbf{k}}\,(a^\dagger_{\mathbf{k}}b^\dagger_{-\mathbf{k}} + a_{\mathbf{k}}b_{-\mathbf{k}})\Big), \tag{3.3}$$

where z is the coordination number of the lattice, N the number of lattice sites and $\gamma_{\mathbf{k}} \equiv \frac{1}{z}\sum_\delta e^{i\mathbf{k}\delta}$. The last two terms in this expression can be diagonalized by a Bogoliubov transformation (see appendix E). Again the important point is that the Bogoliubov transformation is singular at $\mathbf{k} = \mathbf{0}$ and $\mathbf{k} = \boldsymbol{\pi}$, as in both cases $\gamma^2_{\mathbf{k}} \to 1$. We therefore treat these two k-points separately. Turning back to the notation in terms of spins, using that the Fourier transform of our Hamiltonian is

$$H = J\sum_{\mathbf{k}}\gamma_{\mathbf{k}}\mathbf{S}_{\mathbf{k}}\cdot\mathbf{S}_{-\mathbf{k}} \tag{3.4}$$

and

$$\mathbf{S}_{\mathbf{k}=\mathbf{0}} = \frac{1}{\sqrt{N}}\sum_{i\epsilon A,B}\mathbf{S}_i = \frac{1}{\sqrt{N}}(\mathbf{S}_A + \mathbf{S}_B),$$
$$\mathbf{S}_{\mathbf{k}=\boldsymbol{\pi}} = \frac{1}{\sqrt{N}}(\mathbf{S}_A - \mathbf{S}_B),$$

we find that the singular parts of the spectrum reduce exactly to the Lieb-Mattis Hamiltonian [97, 99, 100]:

$$H = H^{\rm sym}_{\rm LM} + J\sum_{\mathbf{k}\neq\mathbf{0},\boldsymbol{\pi}}\gamma_{\mathbf{k}}\mathbf{S}_{\mathbf{k}}\cdot\mathbf{S}_{-\mathbf{k}}$$
$$H^{\rm sym}_{\rm LM} = \frac{2J}{N}\mathbf{S}_A\cdot\mathbf{S}_B = \frac{J}{N}(\mathbf{S}^2 - \mathbf{S}^2_A - \mathbf{S}^2_B), \tag{3.5}$$

where $\mathbf{S}_A$ and $\mathbf{S}_B$ are the total spins of each sublattice, and $\mathbf{S}$ is the *total* spin of the system. From here on we will focus entirely on this collective Hamiltonian, as it is the only part of the Heisenberg-like Hamiltonians that is relevant for the spontaneous symmetry breaking of the antiferromagnet as a whole. Notice that the *internal* ordering of the individual spins within the antiferromagnet can be destroyed by fluctuations of finite wavelength that we do not consider in this collective, long ranged model [50]. We assign to the Hamiltonian $H^{\rm sym}_{\rm LM}$ the superscript sym because this Hamiltonian, as we will show below, describes the symmetric (symmetry unbroken) state of the antiferromagnet.

In $H^{\rm sym}_{\rm LM}$ each spin on the A sublattice interacts with all spins on the B sublattice and vice versa, thus creating infinite range interactions. The energies of

the Hamiltonian are trivially identified as $\frac{J}{N}[S(S+1) - S_A(S_A+1) - S_B(S_B+1)]$ and the corresponding eigenfunctions are labeled by their quantum numbers $|S_A, S_B, S, M\rangle$. Here the z-component of the total spin $\mathbf{S}$ is denoted by M. Clearly the ground state of $H_{\rm LM}^{\rm sym}$ is a singlet of total spin: the state with lowest energy has $S = 0$. In fact there is an exact proof that the groundstate of any finite spin system of this sort is a total spin zero ($S = 0$) singlet [105]. Notice that all states which differ only in M are degenerate. For simplicity (and without loss of generality) we henceforth take the quantum number M to be zero [97].

The groundstate singlet $|N\sigma/2, N\sigma/2, 0, 0\rangle$, with both S_A and S_B maximal and $S = M = 0$ is separated by energies of order J/N from states with higher S. The set of these extremely low energy states that only differ in their total spin quantum number forms the thin spectrum [51, 74, 93, 97]. Since (3.5) is contained in (3.1) as its $\mathbf{k} = \mathbf{0}$ and $\mathbf{k} = \boldsymbol{\pi}$ components, and since the thin spectrum of the Lieb-Mattis model is formed by the $\mathbf{k} = \mathbf{0}$ component, exactly the same thin spectrum must govern the collective dynamics of other antiferromagnets with short-range interactions [98, 101, 102].

There are also excitations in (3.5) that can be created by lowering S_A or S_B. This costs an energy of order J, and it can easily be shown that these excitations correspond to the elementary excitations, the magnons, of the Lieb-Mattis system [106]. Because of the extremely long ranged interactions the magnons are gapped and dispersionless.

3.1 Breaking the Symmetry

Having defined the Lieb-Mattis model in its symmetric form, we now review how to explicitly break its SU(2) spin rotation symmetry. We will show that in the thermodynamic limit the symmetry breaking occurs spontaneously [51, 74]. Since the groundstate of $H_{\rm LM}^{\rm sym}$ is a singlet of total spin, this state is orthogonal to the Néel state, which is the ground state of a classical antiferromagnet. We should stress here that there is a marked difference between ferro- and antiferromagnets [50]. Even if spontaneous symmetry breaking is very often discussed with the example of a ferromagnet at hand, the spontaneous symmetry breaking in a ferromagnet is not the generic situation for an interacting quantum system. The reason is that the total magnetization (pointing along, e.g., the z-axis), which is the order parameter of a ferromagnet, commutes with the Hamiltonian: it is nothing but the projection of the total spin along that axis, $S_{\rm tot}^z$. So the situation arises that the orderparameter is already a constant of motion of the symmetric Hamiltonian. This is a pathology of the ferromagnet. This same pathology leads to the absence of an interesting thin spectrum, because in the ferromagnet states with different $S_{\rm tot}^z$ are strictly degenerate. Quantum systems in general, however, have non-trivial thin spectra.

Refocusing on antiferromagnets, we need to proof that the Néel state is a stable

groundstate in the thermodynamic limit. In order to do so, an explicit symmetry breaking field B is introduced [77]:

$$H_{\rm LM} = H_{\rm LM}^{\rm sym} - B(S_A^z - S_B^z). \tag{3.6}$$

Clearly the symmetry breaking field induces a finite sublattice magnetization. The field couples the different total spin states of the thin spectrum by the matrix elements

$$\begin{aligned}&\langle S_A, S_B, S, M|S_A^z - S_B^z|S'_A, S'_B, S', M'\rangle \\ &= \delta_{S_A,S'_A}\delta_{S_B,S'_B}\delta_{M,M'}\left[f_{S+1}\delta_{S,S'-1} + g_S\delta_{S,S'} + f_S\delta_{S,S'+1}\right]\end{aligned} \tag{3.7}$$

where

$$f_S \equiv \sqrt{\frac{\left[S^2-(S_A-S_B)^2\right]\left[(S_A+S_B+1)^2-S^2\right]\left[S^2-M^2\right]}{(2S+1)(2S-1)S^2}}$$

and

$$g_S \equiv \frac{(S_A-S_B)(S_A+S_B+1)M}{S(S+1)}. \tag{3.8}$$

These matrix elements are found by performing a rather tedious sum over Clebsch Gordon coefficients in the following expression (see also appendix D):

$$\begin{aligned}&\langle S_A, S_B, S, M|S_A^z - S_B^z|S'_A, S'_B, S', M'\rangle = \\ &\sum_{M_A}\left[C^{S,M}_{S_A,S_B,M_A,M-M_A}C^{S',M}_{S_A,S_B,M_A,M-M_A}(2M_A - M)\right] \\ &\quad \delta_{S_A,S'_A}\delta_{S_B,S'_B}\delta_{M,M'}.\end{aligned} \tag{3.9}$$

The spectrum of eigenstates $|n\rangle$ in the presence of a symmetry breaking field can now be found by expanding these states in the basis of total spin states: $|n\rangle = \sum_S u_S^n|S\rangle$ (for clarity of notation we suppress the dependency of u_S^n and other variables on the quantum numbers S_A, S_B and M). In this basis, Schrödinger's equation becomes [77]

$$\begin{aligned}H_{\rm LM}|n\rangle = E_0^n|n\rangle \Leftrightarrow \\ \textstyle\sum_S\Big[\frac{JS(S+1)}{N}u_S^n + E_{\rm LM}^{\rm sym}u_S^n - Bf_{S+1}u_{S+1}^n \\ -Bf_Su_{S-1}^n\Big]|S\rangle = E_0^n\textstyle\sum_S u_S^n|S\rangle,\end{aligned} \tag{3.10}$$

where $E_{\rm LM}^{\rm sym}$ is the groundstate energy of $H_{\rm LM}^{\rm sym}$ and E_0^n is the energy of eigenstate $|n\rangle$ of the *symmetry broken* Hamiltonian –its thin spectrum. Here we restricted ourselves to the zero-magnon subspace, where $S_A = S_B = N\sigma/2$ (hence the subscript 0 in E_0^n). The generalization to systems with a finite number of magnons will be straightforward.

In the continuum limit where N is large and $0 \ll S \ll N$, the matrix elements due to the symmetry breaking field simplify considerably. It is easy to show that in this case [77]

$$f_S \simeq \frac{N\sigma}{2}\sqrt{1-\left(\frac{S}{N\sigma}\right)^2} \simeq N\sigma/2. \tag{3.11}$$

We will see shortly that only the first $\approx \sqrt{N}$ total spin states contribute to the groundstate wavefunction, so that an expansion in S/N is justified. Notice that when the sublattice spin S_A is reduced by one, i.e. when there is a spin-wave present, the matrix element f_S is reduced: $f_S^1 \approx f_S \frac{N\sigma-1}{N\sigma} = f_S\left(1-\frac{1}{N\sigma}\right)$, for large N. This reflects the fact that a magnon reduces the Néel order parameter (the staggered magnetization) by unity. This effect is small, but turns out to be essential when we shall consider the quantum coherence of magnons: dephasing will occur because magnons give rise to a subtle change in the level splitting of the thin spectrum. This change in level splitting turns out to be inversely proportional to N, the total number of spins in the antiferromagnet.

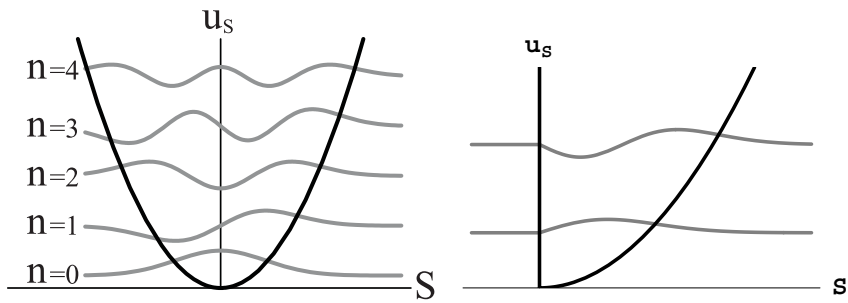

Figure 3.1: Wavefunctions of the thin-spectrum state in presence of a symmetry breaking field, in the continuum limit. The boundary condition $S \geq 0$ implies that of the harmonic oscillator solutions (left) only the odd ones are allowed (right), as these have a node at the origin.

In the continuum limit the Schrödinger's equation (3.10) reduces to [77]

$$-\frac{1}{2}\frac{\partial^2}{\partial S^2}u_S^n + \frac{1}{2}\omega^2 S^2 u_S^n = \nu_n u_S^n, \tag{3.12}$$

where again we have used $0 \ll S \ll N$. In this equation we introduced $\omega = \frac{1}{N}\sqrt{\frac{2J}{B\sigma}}$ and $\nu_n = \frac{E_0^n - E_{\rm LM}^0}{BN\sigma} + 1$. Obviously this is the differential equation of a harmonic oscillator. The eigenstates u_S^n thus are well known and the corresponding eigenvalues

are $\nu_n = (n + 1/2)\omega$, so that

$$E_0^n = E_{\rm LM}^{\rm sym} - BN\sigma + \left(n + \frac{1}{2}\right) E_{\rm thin}, \tag{3.13}$$

where the quantum of energy for the states labeled by n is $E_{\rm thin} = \sqrt{2\sigma JB}$. For the harmonic oscillator n is a non-negative integer. However, in the present situation we have to meet the boundary condition that $S \geq 0$ or, equivalently, that $u_S^n = 0$ if $S < 0$. So u_S^n has to vanish at the origin [50, 77]. This boundary condition is trivially met by eigenfunctions that are odd and have a node at $S = 0$, see Fig. 3.1. Thus solutions to the Schrödinger's equation (3.12) are harmonic oscillator eigenfunctions of order n, where n is an odd positive integer. In Fig. 3.2 the groundstate wavefunction in the continuum limit is compared with the exact wavefunction for large N. It makes clear that the continuum approximation is very good one.

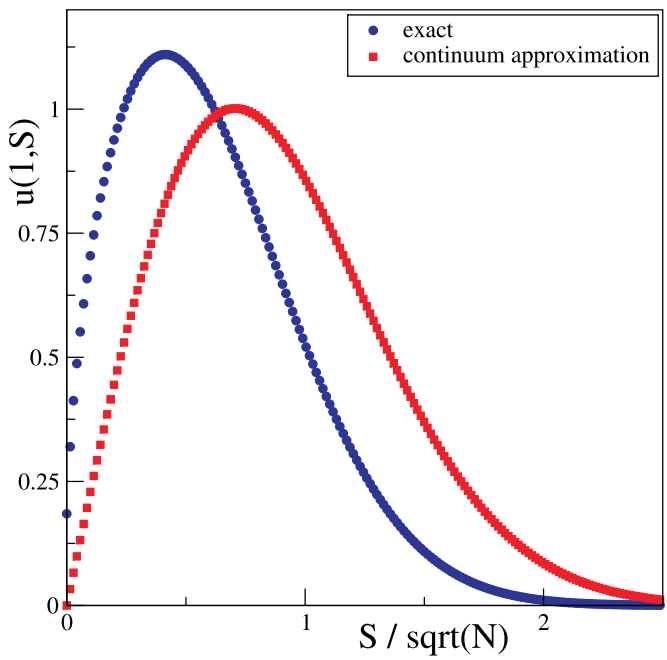

Figure 3.2: Comparison of the exact symmetry broken Néel wavefunction (for $N = 500$ spins) and the Néel wavefunction in the continuum limit (a harmonic oscillator eigenstate). The overlap of the Néel state with the different total spin states is shown as a function of the total spin quantum number. The spin coupling strength is set to $J = 1$ and the symmetry breaking field is $B = 1/10$. The wavefunctions are rescaled such that the maximum of the harmonic oscillator wavefunction is unity.

Let us consider the energy spectrum in Eq. (3.13) in more detail. Clearly if B is zero we recover the groundstate energy $E_{\rm LM}^{\rm sym}$ of the symmetric case that we discussed before. However, if there is a finite staggered field B, there is a gain in groundstate energy proportional to BN, which reveals that the energy spectrum in Eq. (3.13) is the one of a Néel state. The same conclusion is reached by directly calculating the orderparameter (see appendix C). The result is shown in Fig. 3.3. Apparently, for the symmetry broken Néel state to be stable, the symmetry breaking field can be exceedingly small, as long as N is large enough. In other words: in the thermodynamic limit the spin rotation symmetry of $H_{\rm LM}^{\rm sym}$ can be *spontaneously* broken by an infinitesimal field B. Putting it in a more formal manner: spontaneous symmetry breaking is characterized by the singular limit

$$\begin{aligned} \lim_{N\to\infty}\lim_{B\to 0}\left\langle\frac{S_A^z-S_B^z}{N\sigma}\right\rangle &= 0 \quad \text{and} \\ \lim_{B\downarrow 0}\lim_{N\to\infty}\left\langle\frac{S_A^z-S_B^z}{N\sigma}\right\rangle &= 1. \end{aligned} \tag{3.14}$$

This in fact defines spontaneous symmetry breaking, just as it did in the case of the quantum crystal. That for the Lieb-Mattis Hamiltonian this limit is singular is directly clear from Fig. 3.3.

In the symmetry broken Néel state the excitations labeled by n act as a new thin spectrum with excitation energies that are multiples of $E_{\rm thin} = \sqrt{2\sigma JB}$. The magnon excitation energy is still of order J.

3.2 The Many-Spin Qubit

Using the many-body Lieb-Mattis model with N spins and $\sigma = 1/2$, we now study the coherence of the antiferromagnet when it is used as a qubit [23]. Again there are many ways in which one can define a two-level system to be used as the qubit states. The best possible choice in this case is provided by the gapped and dispersionless magnons: we use as a qubit the superposition of a perfectly ordered antiferromagnet and the state of the antiferromagnet with one magnon on each sublattice. Due to the long-range nature of the interaction in the Lieb-Mattis model the gapped magnons themselves are not damped and as such do not decay or decohere. Also, in analogy to the quantum crystal we expect the magnons or Goldstone modes of the antiferromagnet to influence the thin spectrum as little as possible. A magnon has an energy J, which we assume is an energy scale that is available to the (thought-)experimentalist to prepare, manipulate and read out the qubit[1].

[1] Because of a technicality we choose to use a state with two magnons instead of a single one. By doing so we can ensure that our system stays in the subspace of zero total magnetization ($M = 0$), which considerably simplifies the calculations without loss of generality.

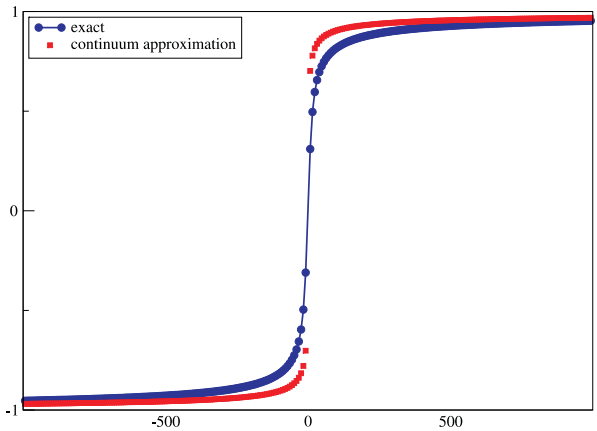

Figure 3.3: Orderparameter as a function of symmetry breaking field. The vertical axis is in units of the normalized order parameter $\langle S_A^z - S_B^z \rangle / N$, while the horizontal axis shows the value of $4N^2B/J$. The exact result is shown for $N = 100$ spins. The continuum expression for the orderparameter depicted here is derived in appendix C.

To find out the precise effect that the presence of a magnon has on the thin spectrum, we can repeat the analysis of the previous section using a Néel state with m excited magnons (by setting $S_A = S_B = N\sigma/2 - m/2$ and using f_S^m instead of f_S). In this case the energy spectrum becomes

$$E_m^n = E_0^n + m(2\sigma J + B) - \frac{m}{2N\sigma}(n + 1/2)E_{\text{thin}}, \tag{3.15}$$

see Fig. 3.4. Note that as we stated before, there is a subtle effect of the magnons on the thin states: m magnons cause a change in energy of the thin spectrum of the order of m/N. This effect turns out to be essential for the decoherence mechanism discussed in this section.

Physically, the change in energy of the thin states due to the presence of a magnon can easily be understood. If there are m magnons present in the antiferromagnet, then the order parameter of the total system is reduced by m. Since the thin spectrum describes the global excitations of the order parameter, its energy is proportional to the order parameter itself. The ratio of the Néel order parameter of the excited state with m magnons and the one of the groundstate with a fully developed order parameter is $(N - m)/N$. Therefore, when there are m magnons present, the relative change of the orderparameter is m/N and the change in energy

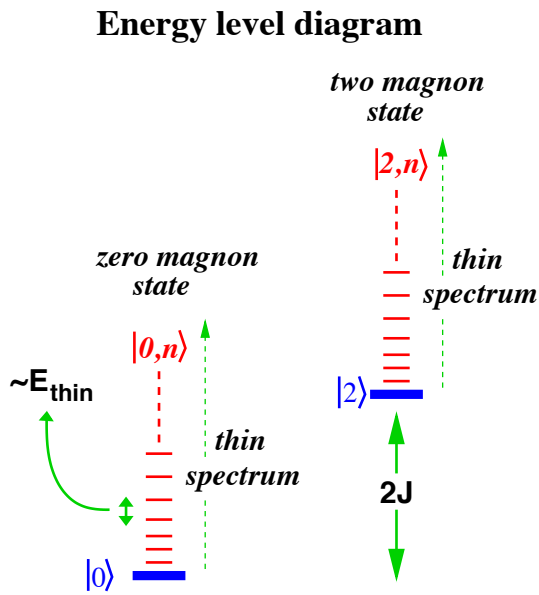

Figure 3.4: Energy level scheme with the zero and two magnon states, each with its tower of thin spectrum states. The level spacing in the thin spectrum is E_{thin}, magnons live on an energy scale J.

of the thin states is therefore of the order mE_{thin}/N which explains the last term in expression (3.15).

3.2.1 Preparing the Initial State

With the exact expressions for all eigenstates and energies of both the symmetric and the symmetry broken Hamiltonian at hand, we are in the position to set up the initial state for our many-particle qubit. Instead of simply assuming that we are in a previously prepared superposition of states with zero and two magnons, we will explicitly construct this initial state. This can be done by coupling at time $t = t_0$ a two spin singlet to the symmetry broken N-spin Lieb-Mattis system, see Fig. 3.5. This will result in the desired superposition state. So for times $t < t_0$, the Lieb-Mattis antiferromagnet is completely decoupled from the two spin singlet and the total wavefunction is thus the direct product of the wavefunctions of the N-spin magnet and the two-spin singlet state:

$$|\psi_{t<t_0}\rangle = |0,n\rangle \otimes \left|singlet\right\rangle. \tag{3.16}$$

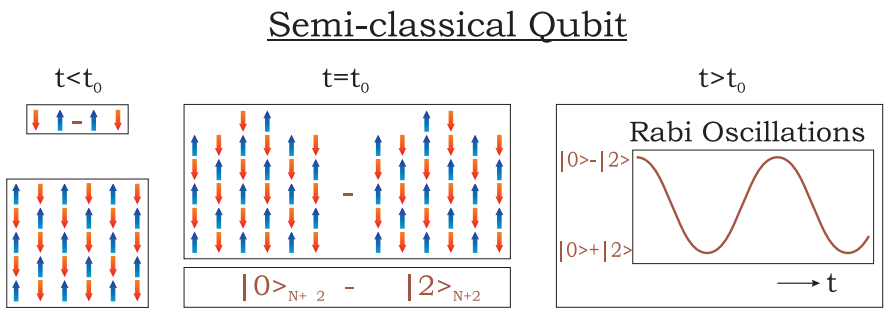

Figure 3.5: Semi-classical time evolution of a two spin qubit that at $t = t_0$ starts interacting with a N-spin Lieb-Mattis magnet, thus forming at $t > t_0$ a many-body qubit made out of $N + 2$ spin. In the semi-classical approximation quantum coherence is preserved at all times, because the thin spectrum is neglected.

Here we denote the Néel state with m magnons and n thin spectrum excitations by $|m, n\rangle$. The state $|singlet\rangle$ is $\frac{1}{\sqrt{2}}\left[|\downarrow_1\uparrow_2\rangle - |\uparrow_1\downarrow_2\rangle\right]$. Upon instantaneous inclusion at $t = t_0$ of the two spin state in the Lieb-Mattis lattice, the groundstate of the decoupled system at $t < t_0$ can be expressed in terms of the eigenstates of the $N + 2$ spin system at $t = t_0$. The exact groundstate wavefunction is then given by the following formidable expression

$$\begin{aligned}
|\psi_{t<t_0}\rangle &= \sum_{S=0}^{N-1} u_S^n \, |S,0\rangle \otimes \big|singlet\big\rangle \\
&= \sum_{S=0}^{N-1} u_S^n \sum C^{S,0}_{N/4,N/4,M_A,-M_A} C^{0,0}_{1/2,1/2,M_1,-M_1} C^{S_{A1},M_A+M_1}_{N/4,1/2,M_A,M_1} \\
&\quad C^{S_{B2},-M_A-M_1}_{N/4,1/2,-M_A,-M_1} C^{S,0}_{S_{A1},S_{B2},M_A+M_1,-M_A-M_1} \delta_{S,S_T} |S_{A1}, S_{B2}, S, 0\rangle, \qquad (3.17)
\end{aligned}$$

where we sum the Clebsch Gordon coefficients over M_A, M_1 and over the total spins S_{A1}, S_{B2} and S, A/B denote the spins on sub-lattices A and B and the spins on sites 1 and 2 make up the singlet. With A1(B2) we denote the set of spins on sublattice A(B) combined with spin 1(2). The sums can be evaluated and we obtain

$$\begin{aligned}
|\psi_{t<t_0}\rangle = \sum_{S=0}^{N-1} u_S^n \Big(& \sqrt{\tfrac{(N-2+2S)(N+4+2S)}{2(N+2)^2}} \big|\tfrac{N+2}{4},\tfrac{N+2}{4},S,0\big\rangle \\
& + \sqrt{\tfrac{2S(S+1)}{(N+2)^2}} \big|\tfrac{N+2}{4},\tfrac{N-2}{4},S,0\big\rangle - \sqrt{\tfrac{2S(S+1)}{(N+2)^2}} \big|\tfrac{N-2}{4},\tfrac{N+2}{4},S,0\big\rangle \\
& + \sqrt{\tfrac{(N-2S)(N+2+2S)}{2(N+2)^2}} \big|\tfrac{N-2}{4},\tfrac{N-2}{4},S,0\big\rangle \Big). \qquad (3.18)
\end{aligned}$$

Again the equations simplify drastically in the continuum limit of large N,

where as before $0 \ll S \ll N$. In this case the wavefunction of the system at $t < t_0$, expressed in the eigenstates of the $N+2$ spin system at $t = t_0$ is

$$|\psi_{t<t_0}\rangle = [|0,n\rangle + |2,n\rangle] / \sqrt{2}. \tag{3.19}$$

Here all states on the right hand side, i.e. all the thin spectrum states labeled by their quantum number n with either zero or two magnons, refer to configurations of $N+2$ spins.

To account for a finite temperature of our many particle qubit, we combine initial states with different n into a thermal mixture before we let it interact with the two spin singlet. We should stress that we only consider temperatures that are much below the magnon energy: $k_B T \ll J$ so that there is no thermal occupation of the magnon states [2]. This implies that the order parameter is not affected by the thermal fluctuations. So, all that we introduce is an incoherent mixture of the low lying thin spectrum states, which all support a finite sublattice magnetization. Still, the implicit assumption is that the thin states are in thermal equilibrium –and it is an important assumption as our final result relies on it. In principle it can of course not be excluded that occupation distribution of the thin spectrum states is far from thermal equilibrium. But as we have not a priori prepared the thin states in some particular way, we assume them to be thermally occupied. The density matrix at times $t < t_0$ is then

$$\begin{aligned} \rho_{t<t_0} &= \frac{1}{Z}\sum_n e^{-\beta E_0^n} |0,n\rangle \otimes |singlet\rangle\langle singlet| \otimes \langle 0,n| \\ &= \frac{1}{2Z}\sum_n e^{-\beta E_0^n} \left(|0,n\rangle\langle 0,n| + |0,n\rangle\langle 2,n| \right. \\ &+ \left. |2,n\rangle\langle 0,n| + |2,n\rangle\langle 2,n|\right), \end{aligned} \tag{3.20}$$

where, by definition, the partition function is $Z = \sum_n e^{-\beta E_0^n}$ and $\beta^{-1} = k_B T$.

3.2.2 Time Evolution and Decoherence

By coupling the symmetry broken Lieb-Mattis model to the two spin singlet, we have created the initial state of our $N+2$ spin qubit. This initial state is precisely equivalent to the initial state (2.9) of the general description, and we can thus follow equations (2.10), (2.11) and (2.12) directly. That way we compute the *exact* time evolution of the initial state density matrix, trace away the thin spectrum states which have vanishing thermodynamic weight, and finally define the off-diagonal element of the reduced density matrix as

[2] Note that in a d-dimensional system the number of spins is $N = L^d$, where L is the linear extent of the system. So the energy scale for the lowest possible spin wave (magnon) excitation is J/L. However the energy scale of the thin spectrum is $J/N = J/L^d$, and is thus –in any dimension higher than one– much lower than the magnon energy scale.

$$\rho^{\rm OD}_{t>t_0} \equiv \frac{1}{Z}\sum_n e^{-\beta E_0^n} e^{-i(E_0^n - E_2^n)(t-t_0)/\hbar}. \tag{3.21}$$

We can then substitute the exact expressions for E_n^m in this matrix element, and perform the summation. We find

$$\rho^{\rm OD}_{t>t_0} = \frac{1-e^{-x}}{1-e^{-Nx}}\,\frac{1-e^{-N(x+i\tau)}}{1-e^{-x-i\tau}}, \tag{3.22}$$

where $x = \frac{E_{\rm thin}}{k_B T}$ and $\tau = \frac{2}{\hbar}\Delta E_{\rm thin}(t-t_0)$, with $E_{\rm thin} = \sqrt{JB}$ and $\Delta E_{\rm thin} = E_{\rm thin}/N$. We again define the coherence time $t_{\rm spon}$ as the half-time of $\left|\rho^{\rm OD}_{t>t_0}\right|$. For $x, \tau \ll 1$, expression (3.22) becomes a Lorentzian, and in that limit one thus finds

$$t_{\rm spon} \simeq \frac{2\pi N\hbar}{k_B T}, \tag{3.23}$$

our main result.

Notice that just as in the case of using a quantum crystal with an interstitial excitation, the coherence time $t_{\rm spon}$ in the end does not depend on any details of the underlying model. The fact that $\Delta E_{\rm thin}$ is proportional to $E_{\rm thin}$ itself removes all dependence of $t_{\rm spon}$ on the model parameters J and B.

3.3 Special Situations

It is remarkable that the coherence time is such a universal time-scale, independent of the detailed form of the thin spectrum –which, after all, is determined by the parameters J and B in the Lieb-Mattis Hamiltonian. Mathematically this is due to the fact that both x and τ are proportional to $E_{\rm thin}$. Physically one can think of this universal time-scale as arising from two separate ingredients. First, the energy of a thin spectrum state $|n\rangle$ changes when magnons appear, as we pointed out above. The change is of the order of $nE_{\rm thin}/N$, where $E_{\rm thin}$ is the characteristic level spacing of the thin spectrum that we happen to be considering. The fact that each thin state shifts its energy somewhat at $t > t_0$ leads to a phase shift of each thin state and in general these phases interfere destructively, leading to dephasing and decoherence. The larger $nE_{\rm thin}/N$, the faster this dynamics.

But from the argument above it is clear that in order for this dephasing to occur, it is necessary for a finite number of thin states to participate in the dynamics of decoherence. Since temperature is finite (but always small compared to the magnon energy) a finite part of the thin spectrum is available for the dynamics. Thin spectrum states with an excitation energy higher than $k_B T$ are suppressed exponentially due to their Boltzmann weights. Therefore the maximum number of thin states

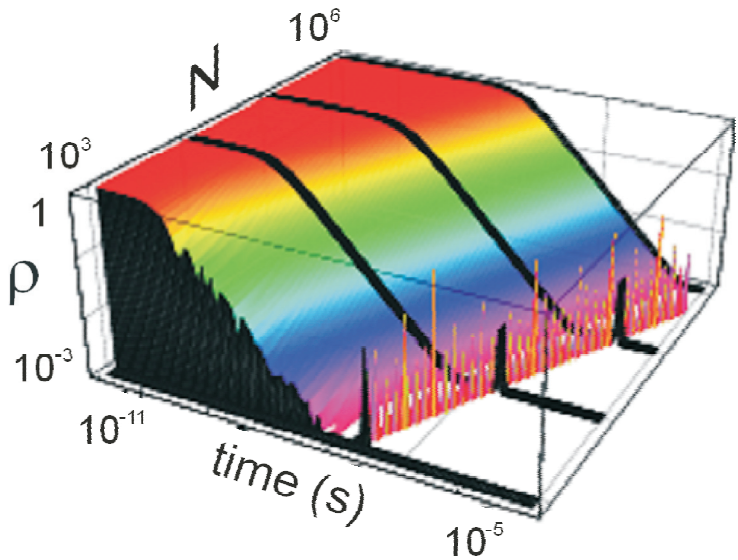

Figure 3.6: Log-log-log plot of the off-diagonal matrix element ρ as a function of time and system size. In this plot the temperature was set to $T = 10$K.

that do contribute is roughly determined by the condition that $n^{\max} \sim k_B T / E_{\text{thin}}$. Putting the ingredients together, we find that the highest energy scale that is available to the system to decohere is approximately $n^{\max} E_{\text{thin}}/N = \frac{k_B T}{E_{\text{thin}}} \frac{E_{\text{thin}}}{N}$. All together, the thin spectrum drops out of the equations. The time scale at which the dynamics take place is determined by the inverse of this energy scale, converted into time. From this argument we immediately find again the coherence time $t_{\text{spon}} \propto \frac{\hbar N}{k_B T}$.

3.3.1 Simulated High Temperature

The physical picture also suggests an alternative way of introducing decoherence into the many particle qubit. Instead of raising the temperature and making an incoherent superposition of more and more thin spectrum states, we could start out at $t < t_0$ with the Lieb-Mattis antiferromagnet in its (zero temperature) symmetric ground state, and then instantaneously turn on the symmetry breaking field B at $t = t_0$. At $t > t_0$ the eigenstates are the Néel-like thin spectrum states $|n\rangle$. No magnons are created by switching on the symmetry breaking field. As we can expand the states $|n\rangle$ in the basis of total spin states as $|n\rangle = \sum_S u_S^n |S\rangle$ we can, by the inverse transformation, expand the total spin singlet state in the basis of the Néel-

like thin spectrum states as $|S = 0\rangle = \sum_n u_n^0 |n\rangle$. We can now use this singlet state as the initial state for our qubit. This singlet state is a superposition of all of the different Néel-like states, which are separated by energies E_{thin}. This procedure thus roughly corresponds to creating a 'maximal temperature' $k_B T \sim N E_{\text{thin}}$. As time evolves, all of these states pick up different phases, which leads to decoherence when we trace over them. The coherence time due to this switching on of the symmetry breaking field is therefore $t_{\text{SB}} = \frac{2\pi\hbar}{\sqrt{JB}}$.

3.3.2 The Symmetric Case

This raises the question what would have happened if we had *not* broken the symmetry in the Lieb-Mattis magnet (by introducing a finite symmetry breaking field B) at all. In the symmetric case S, S_A and S_B are good quantum numbers at all times. It is easy to see that in this situation the thin spectrum, determined by the quantum number S, is independent of the "magnon" states, which are determined by the quantum numbers S_A and S_B. Since in the symmetric Lieb-Mattis Hamiltonian the thin spectrum does not communicate with the magnons and vice versa, we will find $\Delta E_{\text{thin}} = 0$, and accordingly no decoherence.

The fact that S, S_A and S_B are all good quantum numbers, may be regarded as a pathology of the Lieb-Mattis model. In fact, the model is integrable just because there are so many conserved quantities. In a more general, short ranged Heisenberg model the magnons will acquire a finite lifetime and it is expected that they will in general influence the structure of the thin spectrum, even if the symmetry breaking field is absent. In this sense, the Lieb-Mattis model can really be seen as the best case scenario for avoiding decoherence in SU(2) symmetric models. Its infinitely long ranged interactions introduce a large energy gap for all magnons, which thus become extremely 'silent' excitations. On top of that the coupling to the collective dynamics is so subtle that it can only be seen because of the existence of a singular limit: Only because we need to always consider an infinitesimal symmetry breaking field when looking at the thermodynamic limit do we find decoherence at all.

3.3.3 Recurrence

Finally we notice that the off-diagonal elements of the density matrix, given by equation (3.22), are periodic in time, and the initial density matrix recurs when $N\tau = 2\pi$ or, equivalently, $t_{\text{rec}} = \pi\hbar/E_{\text{thin}}$. Such a periodicity is required by the fact that the time evolution is unitary. As the recurrence time is inversely proportional to the level spacing of the thin spectrum, it depends on the microscopic parameters of the model. It becomes infinitely long if the symmetry breaking field vanishes. In the physical limit the recurrence time is always much longer than the decoherence time as $t_{\text{rec}}/t_{\text{spon}} = k_B T/E_{\text{thin}} \gg 1$.

Chapter 4

The Superconductor

It has been proven already three decades ago by Elitzur that local (gauge) symmetries cannot be broken spontaneously without invoking an explicitly asymmetric gauge fix [107]. Also, it has been argued recently that because the local gauge symmetry in superconductors cannot be broken spontaneously, the order should be of a purely topological nature, and that the low energy properties of the superconducting state are determined solely by its topological structure [108]. At first sight then, the claim that a superconductor possesses states related to spontaneous symmetry breaking, which have a vanishing energy gap, might come as a surprise. On the other hand it is well known that the superconducting ground state is characterized by a definite phase and a corresponding uncertainty in the number of Cooper pairs [109]. The underlying Hamiltonian however will be diagonal in the number basis and thus the superconductor will have to spontaneously break its phase symmetry. The breaking of this symmetry in the thermodynamic limit requires the existence of a thin spectrum of total phase states whose energies all collapse onto the groundstate energy in the thermodynamic limit. This result does not disagree with the fact that local symmetry cannot be broken spontaneously. We will show that the symmetry that is broken in a superconductor is a global U(1) phase symmetry. The resulting superconducting state is still manifestly invariant under local gauge transformations.

To clearly illustrate this point we will first discuss the superconducting state of an array of Josephson junctions. In this array the non-commutativity of number and phase variables straightforwardly gives rise to a thin spectrum and to spontaneous symmetry breaking. After that we will switch to a strong coupling model of superconductivity in which the role of gauge symmetry can be more clearly discussed. We will then use this model to describe a Cooper-pair box qubit [79, 83] and show that the presence of the thin spectrum again leads to the maximum coherence time t_{spon} of the qubit, which is of the order of milliseconds. Finally we will

show how the description of the thin spectrum can also be incorporated into the familiar BCS description of superconductivity, and comment on the application of that description to superconducting flux qubits [78, 80, 81].

4.1 The Josephson Junction Array

It is well known that an array of superconducting islands, coupled together by Josephson junctions, can undergo a (quantum) phase transition from an insulating state to a superconducting state [110–116]. Such an array of Josephson junctions occurs naturally in a superconducting granular material in which individual grains of superconducting material are form weak links with neighbouring grains. They can also be made artificially in the lab, so that the number of superconducting islands, the numbers of links with neighbouring islands and the capacities of the Josephson junctions is under full control of the experimentalist (see figure 4.1).The description of a superconductor as an array of Josephson junctions is particularly useful to us here because it naturally focuses the attention on the the conjugate variables number and phase. The description of the symmetry breaking in terms of these variables turns out to be exactly analogous to that of the symmetry breaking in quantum crystals or magnetic systems which we discussed in the previous chapter [25]. The Hamiltonian for the Josephson junction array is given by [112]

$$H^{\mathrm{JJ}} = \sum_{j,\delta} \left[\frac{E_C}{2} n_j^2 - E_J \cos\left(\theta_j - \theta_{j+\delta}\right) \right]. \tag{4.1}$$

Here θ_j represents the phase of the superconducting orderparameter on island j, while n_j gives the number of Cooper pairs above average, and δ connects neighboring sites. The charge or number operator $n_j = -i(\partial/\partial\theta_j)$ is the variable conjugate to the phase, and can be written in terms of the voltage V and the capacitance C of the Josephson junctions as $n_j = (C/2e)V_j$. The coupling constants are the charging energy E_C and the Josephson coupling energy E_J.

The phase θ in this description can be thought of as the phase of the Ginzburg-Landau wavefunction for the superconducting island, or equivalently as the phase describing the perfectly ordered BCS state defined through the wavefunction $|\theta\rangle = \prod_k \left(|u_k| + |v_k| \, e^{i\theta} c_k^\dagger c_{-k}^\dagger \right) |\mathrm{vac}\rangle$ [109]. This phase is not measurable as such, but a difference in phase across a Josephson junction causes a supercurrent given by $J = J_C \sin\left(\theta_j - \theta_{j+\delta}\right)$ to run through the junction, and therefore phase differences are measurable [109]. The condition of measurability implies the gauge independence of these quantities, because a gauge transformation by definition cannot alter the outcome of any experiment. The unmeasurable total phase is in fact not a gauge independent quantity.

If we expand the cosines in the Hamiltonian of equation (4.1) in powers of the phase difference $\theta_j - \theta_{j+\delta}$, then it becomes exactly equal to the description

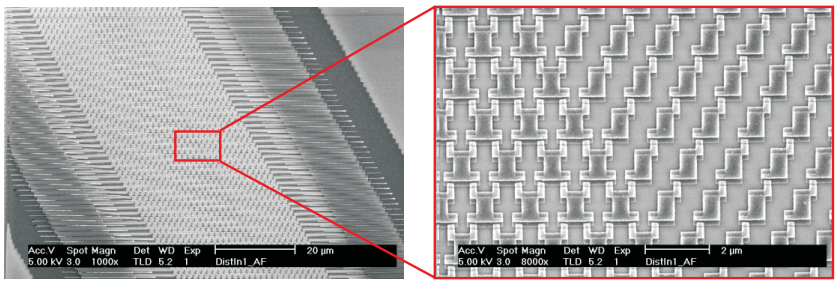

Figure 4.1: An electron microscope image of the Josephson Junction array that is studied in Delft by Mooij et al [117].

of a quantum crystal with (even) anharmonic terms. As we have seen before, the thin spectrum of such a crystal, and thus also the thin spectrum of the Josephson junction array, is given by the infinite wavelength part of the Hamiltonian, because exactly at $k = 0$ the Bogoliubov transformation that would diagonalize the Hamiltonian turns out to be singular [25]. The zero wavenumber part of $H^{\rm JJ}$ is

$$H^{\rm JJ}_{\mathbf{k}=0} = \frac{E_C}{2N} n^2_{\rm tot}, \tag{4.2}$$

where N is the total number of superconducting islands, and $n_{\rm tot} \equiv \sum_j n_j$ is the charge of the total network of Josephson junctions. To see how the array can spontaneously break its total phase symmetry we should add a symmetry breaking field to the collective Hamiltonian. We cannot simply add a term which involves the bare total phase $\theta_{\rm tot}$, because that total phase is not a gauge independent, measurable quantity. Instead we can look at the difference of phase between the Josephson junction array and some given reference superconductor. In the end of course we will let the strength of the symmetry breaking field go to zero, or equivalently move the reference superconductor away to infinity. The collective Hamiltonian including the symmetry breaking field thus becomes

$$H^{\rm JJ}_{\rm SB} = \frac{E_C}{2N} n^2_{\rm tot} - B\cos\left(\theta_{\rm tot} - \theta_{\rm ref}\right). \tag{4.3}$$

For small values of $\Delta\theta_{\rm tot} \equiv \theta_{\rm tot} - \theta_{\rm ref}$ we can expand the cosine to quadratic order and then the Hamiltonian reduces to a harmonic oscillator with well known solutions in terms of Hermite polynomials, in exact analogy to the case of spontaneous symmetry breaking in quantum crystals and antiferromagnets [25]. Using these Hermite polynomials, it is easy to show that indeed the Josephson junction array can spontaneously break the rotational symmetry of its total phase. We do so by looking at the expectation value of the phase fluctuations in the limit of disappear-

ing symmetry breaking field and infinite number of superconducting islands:

$$\begin{aligned} f^2 \equiv \left\langle (\Delta\theta_{\rm tot})^2 \right\rangle - \langle \Delta\theta_{\rm tot} \rangle^2 &\propto \sqrt{\frac{E_C}{NB}} \\ \lim_{N\to\infty}\lim_{B\to 0} f^2 &\to \infty \\ \lim_{B\to 0}\lim_{N\to\infty} f^2 &\to 0. \end{aligned} \tag{4.4}$$

Clearly the fluctuations in the total phase disappear in the thermodynamic limit if only an infinitesimal symmetry breaking field is present. The symmetry broken state that is formed in that limit has a well defined total phase, and must thus be in a superposition of many different total number states. These total number states were precisely the eigenstates of the collective Hamiltonian (4.2), which we identified as being the thin spectrum of the Josephson junction array. The symmetry broken Hamiltonian also has a tower of low lying states that form a sort of dual thin spectrum which consists of all the total phase states necessary to build a state with a fixed total number of Cooper pairs. Notice that the thin spectrum states must be observable states, because the description of the collective dynamics in Hamiltonian (4.3) is still manifestly gauge invariant. This also implies that the symmetry breaking which we have just described is *not* the breaking of a local gauge symmetry. Only the U(1) symmetry of the global total phase is spontaneously broken, and even then only in the sense that its fluctuations disappear in the thermodynamic limit, so that its value relative to that of some other, external superconductor will be fixed[1].

4.2 The Local Pairing Superconductor

Now that we have seen in the previous section that the non-commutativity of number and phase naturally gives rise to the presence of a thin spectrum in a superconducting system, we would like to take a closer look at the process of spontaneous symmetry breaking itself and its relation to gauge symmetry and the superconducting orderparameter. This relation was not visible in the context of a Josephson junction array, because there we started out with islands that were already in a superconducting state. That way we could describe the whole system with an effective Hamiltonian that only consisted of observables related to the macroscopic properties of the superconducting state. For a more general description of superconductivity it would be better to start out with a microscopic Hamiltonian for a single

[1] The fact that we can only define the phase of the superconductor relative to some other, given superconductor is not a problem. Indeed, in the case of the translational symmetry breaking of a crystal which we discussed in the previous chapter, we also silently assumed there was some point in space which we could call the origin of our coordinate system. This given origin of the coordinates corresponds precisely to the given 'origin of phase' defined by the external superconductor in the present discussion.

superconductor that incorporates the effects of the gauge field. The simplest such model is the extensively studied local pairing, negative U Hubbard model [50, 118]

$$\begin{aligned} H &= \frac{1}{2}\sum_{j,\delta,\sigma}\left(t_j^{\delta}c_{j+\delta,\sigma}^{\dagger}c_{j,\sigma}+\left(t_j^{\delta}\right)^{*}c_{j,\sigma}^{\dagger}c_{j+\delta,\sigma}\right) \\ &\quad -|U|\sum_j n_{j,\uparrow}n_{j,\downarrow}. \end{aligned} \tag{4.5}$$

Here $c_j^{\dagger}$ creates an electron on site j, δ connects neighboring sites and n_j counts the number of electrons. The reason to consider this local pairing model rather than for example the BCS model for superconductivity is the fact that this model is explicitly gauge invariant, while the BCS model is not [75]. From the symmetry point of view, the models are the same: there is no phase transition in going form weak to strong coupling superconductivity, only a cross-over [119]. If we parametrize the hopping in terms of a uniform amplitude and a bond dependent phase as $t_j^{\delta}=te^{i\psi_j^{\delta}}$, then minimal coupling allows us to identify the phase of the hopping parameter with the electromagnetic vector potential integrated along the bond under consideration, so that $\psi_j^{\delta}=\frac{e}{\hbar c}\int_j^{j+\delta}A^{\delta}(t)dt$. It is thus clear that the Hamiltonian is manifestly invariant under the gauge transformation [50]

$$\begin{aligned} c_j^{\dagger} &\rightarrow e^{i\frac{e}{\hbar c}f(j)}c_j^{\dagger}, \\ \mathbf{A}(j) &\rightarrow \mathbf{A}(j)+\nabla f(j), \end{aligned} \tag{4.6}$$

which immediately implies

$$\psi_j^{\delta} \rightarrow \psi_j^{\delta}+\frac{e}{\hbar c}\left[f(j+\delta)-f(j)\right]. \tag{4.7}$$

We focus on the strong coupling limit $U \gg t$, so that we only need to consider the physics of the lowest lying Hubbard sector. On each site there will thus be either a pair of electrons or nothing at all. Single electron excitations are only virtually allowed and give rise to pair-pair interactions. The effective low energy theory given by second order perturbation theory can be written in terms of pseudospin operators defined by

$$\begin{aligned} S_j^{+} &= c_{j,\uparrow}^{\dagger}c_{j,\downarrow}^{\dagger} \\ S_j^{z} &= \frac{1}{2}\left(n_{j,\uparrow}+n_{j,\downarrow}-1\right). \end{aligned} \tag{4.8}$$

The z projection of the pseudospin measures the local electron density, while the xy components provide the dynamics of the Cooper pairs. Writing out the Hamiltonian (4.5) to second order in the hopping, and adding a chemical potential μ that

determines the overall electron density and thus explicitly breaks the electron-hole symmetry, we find [50]

$$\begin{aligned} H_{\text{eff}} &= \frac{J}{2}\sum_{j,\delta}\left[e^{i2\psi_j^\delta}S_j^+S_{j+\delta}^- + e^{-i2\psi_j^\delta}S_j^-S_{j+\delta}^+\right] \\ &+ J\sum_{j,\delta}\left[S_j^zS_{j+\delta}^z - \frac{1}{4}\right] - h\sum_j\left[S_j^z + \frac{1}{2}\right]. \end{aligned} \tag{4.9}$$

Here J is defined to be $2t^2/|U|$, and $h \equiv |U| - 2\mu$ determines the overall electron density. Away from half filling (where $h = 0$) the global SU(2) symmetry of the Hamiltonian is broken, and what remains is the U(1) symmetry which describes rotations around the z-axis. Before we discuss the actual spontaneous symmetry breaking and the thin spectrum associated with it, we will show that the emerging classical state which spontaneously breaks the U(1) phase symmetry is in fact a superconducting state.

The state that is classically realized in the thermodynamic limit is not an eigenfunction of the Hamiltonian (4.9), just as the classically realized states of for example crystals, rotors and antiferromagnets are not eigenstates of the underlying Hamiltonians. Instead the classical state can be written as a generalized coherent state. For the $S = 1/2$ pseudospin problem at hand, the coherent state has the form [50]

$$\begin{aligned} |\Psi_{\text{class}}\rangle &= \prod_j\left(e^{-i\frac{\phi_j}{2}}\sin\left(\frac{\theta_j}{2}\right)\right. \\ &\left. + e^{i\frac{\phi_j}{2}}\cos\left(\frac{\theta_j}{2}\right)c_{j,\uparrow}^\dagger c_{j,\downarrow}^\dagger\right)|vac\rangle\,. \end{aligned} \tag{4.10}$$

In this expression the angles ϕ_j and θ_j are the Euler angles which describe the classical vectors that replace the quantum spins in the classical state. To find the ground-state energy of H_{eff} we need to minimize its expectation value in the generalized coherent state with respect to the orientations of the classical spin-vectors. It is easy to check that the classical energy will then be proportional to the difference between neighbouring Euler angles: $E \propto \cos\left(2\psi_j^\delta - \phi_{j+\delta} + \phi_j\right)$. The classical state with lowest energy thus links the orientation of the spin-vectors to the bond variables ψ_j^δ. These variables in turn were connected to the electromagnetic vector potential. In the lowest energy state we find [50]

$$\bar{A}_j^\delta = -\frac{\hbar c}{2e}\frac{\phi_{j+\delta} - \phi_j - \pi}{a}, \tag{4.11}$$

where $\bar{A}_j^\delta$ is the average vector potential along the bond. At distances much larger

than the lattice spacing a this expression becomes

$$\vec{A}\,(\vec{r}) = -\frac{\hbar c}{2e}\vec{\nabla}\phi\,(\vec{r})\,. \tag{4.12}$$

The classical state thus forces the electromagnetic potential to become pure gauge, which of course immediately implies that its rotation will vanish, and thus that the condensate does not allow any magnetic field to penetrate its bulk. This manifestation of the Meissner effect is a direct consequence of the well known Anderson-Higgs mechanism for mass generation [76, 120, 121], and its occurrence is a clear indication that indeed the classical condensate formed by (4.10) describes a superconductor.

4.2.1 The Thin Spectrum

We have seen in the previous section that the tight binding, negative U Hubbard model gives rise to a classical state in the thermodynamic limit which can be identified as a superconductor. Let's now back up a few steps and see if we can describe the symmetry breaking that lead to the formation of this state in a more analytical manner by studying the exact eigenstates of the collective part of the Hamiltonian, just as we did for the Josephson junction array. The difficulty in such a global description will be to correctly account for the gauge field, which can fluctuate locally. To circumvent this problem we introduce transformed pseudospins, analogous to what is done in the weak coupling theory [75, 118]

$$\begin{aligned} \sigma_j^+ &= e^{-2i\sum_{j'=0}^{j}\psi_{j'}^{\delta}} S_j^+ \\ \sigma_j^z &= S_j^z. \end{aligned} \tag{4.13}$$

The summation in the exponent is over some path connecting position j to some origin $j = 0$ (see figure 4.2). For simplicity we will assume the applied external magnetic field to be zero from here on.

Notice that the individual transformed pseudospin operators of equation (4.13) are not by themselves gauge invariant. Their purpose is to transform the local gauge transformations (4.6) of the actual pseudospins $\vec{S}$ into a global transformation of the new pseudospins $\vec{\sigma}$:

$$\begin{aligned} \sigma_j^+ &\rightarrow e^{-2i\sum_{j'=0}^{j}\left[\psi_{j'}^{\delta}+\frac{e}{\hbar c}\left(f(j'+\delta)-f(j')\right)\right]} e^{2i\frac{e}{\hbar c}f(j)} S_j^+ \\ &= e^{2i\frac{e}{\hbar c}f(0)}\sigma_j^+ \equiv e^{i\psi_0}\sigma_j^+ \\ \sigma_j^z &\rightarrow \sigma_j^z. \end{aligned} \tag{4.14}$$

The cancellation of the many exponential factors picked up along the paths connecting $j' = 0$ to $j' = j$ is due to the fact that there is no external magnetic field

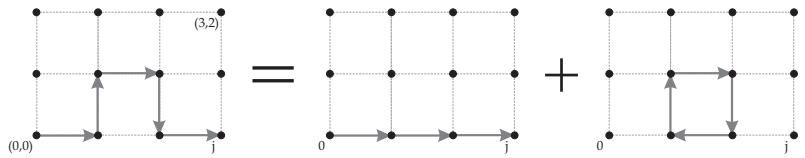

Figure 4.2: Different ways in which the points $(0,0)$ and $(3,0)$ can be connected. The summation over bond variables will in fact be independent of the path chosen, because the difference between two possible paths always consists of a summation around a closed loop. Such a closed-loop summation is sure to give a zero result in the absence of a magnetic field.

present, which guarantees that the sum of the gauge field terms $\psi_{j'}^{\delta}$ around a closed loop is always zero (see figure 4.2). The local gauge transformation of the pseudospins $\vec{S}$ has now been turned into a global transformation of the new pseudospins $\vec{\sigma}$: equation (4.14) describes a global rotation of all pseudospins on the entire lattice around the z-axis. It is the global character of the gauge transformations on the transformed pseudospins that will now allow us to switch to a description of just the collective behavior of the system without invoking any specific gauge choice. In terms of the transformed pseudospins the effective low energy Hamiltonian (4.9) becomes

$$H_{\text{eff}} = J \sum_{j,\delta} \vec{\sigma}_j \cdot \vec{\sigma}_{j+\delta} - h \sum_j \sigma_j^z. \tag{4.15}$$

This Hamiltonian describes an antiferromagnetic interaction between neighboring pseudospins, within an overall uniform magnetic field. Notice that this Hamiltonian is still exactly equal to H_{eff} in equation (4.9), and is thus still gauge invariant. The antiferromagnetic sign of the pseudospin interaction is due to the repulsive effective interaction between Cooper pairs in the local pairing model, and the magnetic field in equation (4.15) is really a pseudomagnetic field, which acts on the pseudospins, and not on the original electrons. The classical state that we expect to find in terms of the pseudospins σ in H_{eff} is a canted antiferromagnet. That is, an antiferromagnet in which all spins are uniformly canted out of the $z = 0$ plane, but in which the xy projections still form an antiferromagnetic pattern. As we noticed before, the canting of the spins which breaks the full SU(2) symmetry is done explicitly by the field h, while the breaking of the in-plane U(1) symmetry into an antiferromagnetic structure will have to be done through spontaneous symmetry breaking.

The thin spectrum of the Hamiltonian H_{eff} consists of the states necessary to construct the symmetry broken classical state. These thin spectrum states describe the dynamics of the superconductor as a whole, and as before they can be found

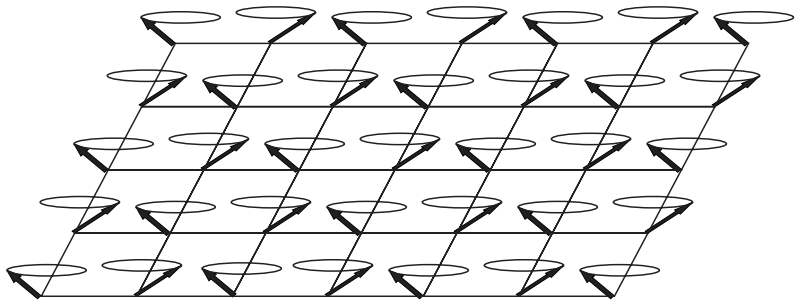

Figure 4.3: A schematic representation of the classically realized state of the tight binding superconductor on a square lattice in which the arrows are a classical cartoon for the transformed pseudospins σ. The circles represent the U(1) symmetry of the Hamiltonian that is spontaneously broken in the superconducting state.

at the singular points of the Bogoliubov transformation which diagonalizes the quadratic part of the Hamiltonian. In the antiferromagnet both the point $\mathbf{k} = \mathbf{0}$ and the point $\mathbf{k} = \boldsymbol{\pi}$ are singular. The resulting collective part of the Hamiltonian is given by

$$H_{\text{coll}} = \frac{4J}{N}\vec{\sigma}_A \cdot \vec{\sigma}_B - h\sigma^z_{\text{tot}}, \tag{4.16}$$

where $\sigma_{A,B}$ denotes all spins on the A, B sublattice and σ_{tot} is the sum of all spins on the entire lattice. This collective Hamiltonian is just a Lieb Mattis model in a uniform magnetic field [25, 77, 93, 97], and the eigenstates are trivially identified as the states labeled by the quantum numbers $\sigma_A, \sigma_B, \sigma_{\text{tot}}$ and σ^z_{tot}. The difference between this collective model and the one describing the spontaneous symmetry breaking in the antiferromagnets discussed before, is the field h. It explicitly reduces the symmetry of the Hamiltonian from SU(2) to U(1). The ground state now has maximum total spin on both the A and B sublattice, and obeys $\sigma_{\text{tot}} = \sigma^z_{\text{tot}} = (hN)/(4J)$. Excitations of the quantum numbers σ_A and σ_B are gapped with an energy J from the groundstate, because of the infinite long range of the interactions in H_{coll}. We will henceforth set these quantum numbers to their maximum value and only consider the low energy excitations which describe the behavior of the entire system as a whole. We can relabel these states by introducing

$$\begin{aligned} \sigma_{\text{tot}} &= \bar{\sigma} + n \\ \sigma^z_{\text{tot}} &= \bar{\sigma} + n - y. \end{aligned} \tag{4.17}$$

Here $\bar{\sigma}$ is the groundstate value for the pseudospin z-projection: $\bar{\sigma} = (hN)/(4J)$. As we will see the excitations labelled by n (which simultaneously increase or decrease σ_{tot} and σ^z_{tot}) form the thin spectrum of the local pairing superconductor.

The excitations y on the other hand (which only decrease $\sigma^z_{\rm tot}$) correspond to a change in the number of Cooper pairs in the superconductor. In terms of the quantum numbers n and y, Schrödinger's equation becomes

$$H_{\rm coll}\left|n,y\right\rangle = \left(E^0_{\rm coll} + hy + \frac{2J}{N}n^2\right)\left|n,y\right\rangle. \tag{4.18}$$

From this equation it is clear that the excitations labeled by n will play the role of the thin spectrum for the local pairing superconductor. It can be easily checked that indeed the contribution of these states to the partition function vanishes in the thermodynamic limit. The excitation labeled by y on the other hand costs an energy proportional to the chemical potential to excite. This is, in other words, the quantum number that determines the average total number of Cooper pairs in the superconductor.

4.2.2 Breaking the Symmetry

To study the spontaneous symmetry breaking of $H_{\rm coll}$ we will have to introduce a symmetry breaking field, which we will send to zero again at the end of the calculation [77]. The field should break the symmetry in the xy plane of the pseudospins and stabilize an antiferromagnetic configuration there. The obvious candidate would be a staggered magnetic field along the x-axis

$$H^{SB}_{\rm coll} = \frac{4J}{N}\vec{\sigma}_A\cdot\vec{\sigma}_B - h\sigma^z_{\rm tot} - B\left(\sigma^x_A - \sigma^x_B\right). \tag{4.19}$$

Notice that this symmetry breaking field is *not* gauge invariant. We can think of this term as arising from the coupling to a different, symmetry broken, external superconductor just as in the case of the Josephson junction array. This form of the symmetry breaking field is then the result of integrating out the second superconductor from an expression which involved the full gauge invariant coupling between the two orderparameters. Alternatively we can see the symmetry breaking field as an implicit gauge fixing term. A gauge transformation corresponds to a uniform rotation of all spins on the entire lattice around the z axis. Every explicit choice for the direction of B along a particular axis in the xy plane is therefore connected to all other directions in the plane by a gauge transformation. This implies that all ordered antiferromagnetic states in the xy plane form a gauge volume of states which are equivalent descriptions of the same physical state. Picking the symmetry breaking field to lie along the x-axis in equation (4.19) thus corresponds to making a gauge choice and we will have to check afterward if the conclusions based on calculations in this particular gauge fix are robust under gauge transformations.

The matrix elements of the symmetry breaking field in the basis $\left|n,y\right\rangle$ can be computed by performing a sum over Clebsch-Gordon coefficients [25]. In the limit

$(n, y) \ll (\bar{\sigma}, N)$, the Hamiltonian can be written in terms of its matrix elements as

$$\begin{aligned} H_{\text{coll}}^{SB} &= \sum_{n,y} |n, y\rangle \left[E_{\text{coll}}^{0} + hy + \frac{2J}{N} n^2 \right] \langle n, y| \\ &\quad - |n \pm 1, y\rangle \left[\frac{B}{4} f(y) \right] \langle n, y| , \end{aligned} \tag{4.20}$$

where $f(y) \equiv \left(2 - \frac{y}{\bar{\sigma}}\right) \sqrt{\left(\frac{N}{2}\right)^2 - \bar{\sigma}^2}$. If we write the eigenfunctions of this equation as $|x, y\rangle = \sum_n \Psi(n, x) |n, y\rangle$ and take the continuum limit, then Schrödinger's equation reduces to the well known harmonic oscillator equation,

$$-\frac{1}{2} \frac{\partial^2}{\partial n^2} \Psi(n, x) + \frac{1}{2} \omega^2 n^2 \Psi(n, x) = \nu \Psi(n, x) , \tag{4.21}$$

with $\omega^2 = \frac{8J}{BNf(y)}$ and $\nu = 1 + 2\frac{E(x,y) - E_{\text{coll}}^0 - hy}{Bf(y)}$. The wavefunctions Ψ are the eigenfunctions of the harmonic oscillator, which can be written explicitly in terms of Hermite polynomials. The corresponding eigenvalues obey $\nu = (x + 1/2)\omega$, and thus we find the energies of the symmetry broken collective Hamiltonian (4.19) to be given by

$$\begin{aligned} E(x, y) &= E_{\text{coll}}^{0} + hy - \frac{1}{2} BNg(y) \\ &\quad + \left(x + \frac{1}{2} \right) \sqrt{2JB} \sqrt{g(y)}, \end{aligned} \tag{4.22}$$

where $g(y) \equiv \left(1 - 2\frac{y}{\bar{\sigma}}\right) \sqrt{1 - \left(\frac{h}{2J}\right)^2}$. The term $\propto BN$ in this expression shows that the symmetry of the system will be spontaneously broken: even if only an infinitesimal symmetry breaking field is present, the pseudospins can gain an infinite amount of energy in the limit of $N \to \infty$ by aligning with that field. In the thermodynamic limit the alignment will thus happen spontaneously and the resulting symmetry broken state is exactly the classically expected canted antiferromagnet.

The z-projection of each pseudospin is just $\bar{\sigma}/N$, while the projections in the xy plane all lie along the x-axis, with signs alternating between nearest neighbors. If we denote the angle in the xy plane of a pseudospin at position j by ϕ_j then the orderparameter equation which describes the anti-alignment of neighboring spins becomes $\phi_{j+\delta} - \phi_j = \pi$. In terms of the angles describing the rotation of the *un*transformed pseudospins S_j around the z-axis, the orderparameter equation directly yields

$$\phi_{j+\delta} - \phi_j = \pi + 2\psi_j^{\delta}. \tag{4.23}$$

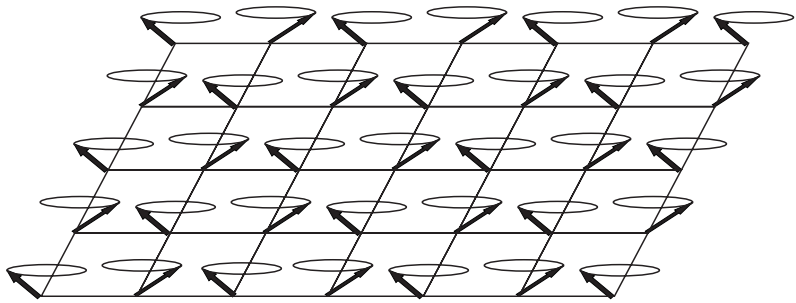

Figure 4.4: A schematic representation of the classically realized state of the tight binding superconductor on a square lattice. The arrows represent a classical cartoon for the transformed pseudospins σ.

This equation is exactly equivalent to equations (4.11) and (4.12) and thus confirms the occurrence of the Meissner effect in the symmetry broken, classically realized state of the local pairing superconductor.

4.2.3 The Gauge Volume

Having found the the eigenfunctions of the collective, symmetry broken Hamiltonian, the question arises what these states represent, and even if they are truly physical states. As mentioned before, the symmetry breaking field in the collective Hamiltonian (4.19) acts as an implicit gauge fix. It is not a priori clear whether or not this (non-physical) gauge fixing introduced any extra unphysical states in the spectrum. If we define the gauge volume of a certain state to be the collection of all possible states that are connected to it by a gauge transformation, then the question is whether the excited states predicted by H^{SB}_{coll} are part of the ground state gauge volume or not.

The ground state of the collective Hamiltonian is a canted antiferromagnet in terms of pseudospins, and we have seen that it corresponds to a superconducting state of Cooper pairs. The excitations labeled by x in the pseudospin picture must involve the superposition of collective excitations with wavenumbers $\mathbf{k} = \mathbf{0}$ and $\mathbf{k} = \boldsymbol{\pi}$. However as mentioned before, the gauge volume of this system is made up of global uniform rotations of all of the pseudospins on the entire lattice around the z-axis. We can thus prove that the excitations labelled by x are not within the gauge volume of the groundstate wavefunction, by showing that the excited states cannot be written as only a global rotation of the groundstate. To do so we will consider one specific thin spectrum state (the state with $x = 0$), and do a gauge transformation on it by rotating it over an angle θ. We will then compare the resulting state with all other thin spectrum states (labelled with $x = X$) of the un-rotated model, and

show that the overlap between the states is smaller than one for all possible choices of X and θ. The thin spectrum with $x \neq 0$ does therefore not contain a states which is merely a rotated version of the state $x = 0$, and thus the thin spectrum states do not coincide with the ground state's gauge volume. Using the explicit formulas for the eigenfunctions of H^{SB}_{coll} it is easy to check that indeed the overlap between the state with $x = X$ and the state with $x = 0$, rotated over an angle θ, is one if and only if both X and θ are zero (see figure 4.5). This shows that indeed the excited state cannot be written only as a global rotation of the groundstate, and thus that the excited state is not within the ground state's gauge volume.

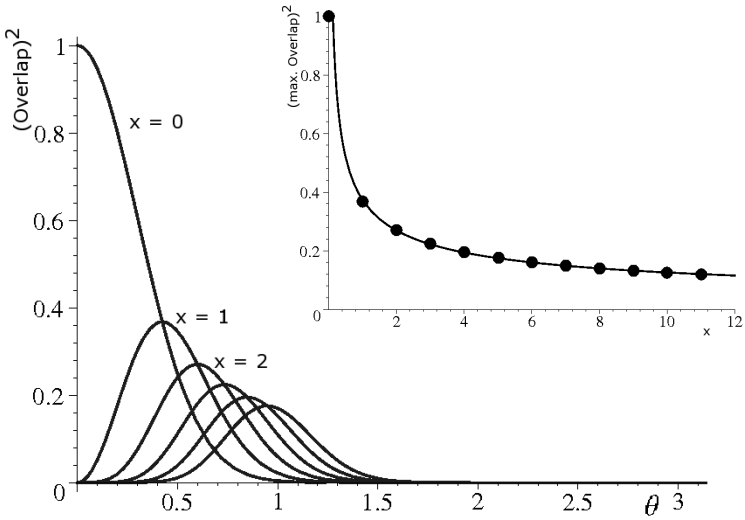

Figure 4.5: The overlap between the thin spectrum state $|x\rangle$ and the rotated ground-state $\hat{R}(\theta)|0\rangle$, as a function of the angle of rotation θ, for different values of x. To make this graph we used the values $J = 10$, $B = h = 1$ and $N = 100$. For higher values of N the graph for each x will be scaled horizontally, but the height of the top remains unaffected. The plot is symmetric under mirroring in the $\theta = 0$ axis. The inset shows the maximum of each curve, plotted as a function of x. The maximum of a curve also corresponds to the maximum overlap that a certain excited thin spectrum state has with (a gauge transformation of) the ground state. The solid line in the inset is included to guide the eye only.

The excitations labeled by y were already identified as corresponding to a change in the average total number of Cooper pairs in the superconductor. They alter the z projection of the pseudospins and thus are trivially seen to be outside of the ground-

state's gauge volume. These excited states are gapped and could thus be used to define an appropriate two-level system for building a qubit out of this local-pairing superconductor. Using that qubit we can then study its decoherence due to the existence of the (dual) thin spectrum formed by the x states.

4.2.4 Decoherence

We would now like to apply the results of the previous section to the description of quantum coherence. In analogy to the result for antiferromagnets [23], we expect the existence of the unobservable thin spectrum to give rise a maximum coherence time $t_{\text{spon}} \propto N\hbar/k_B T$.

Let us define a qubit made of the eigenstates of the collective part of the local pairing superconductor. If temperature is sufficiently low (i.e. $k_B T \ll J, h$) then we can use the states $y = 0$ and $y = 1$ as the computational states of such a qubit. These states correspond to states with a different number of Cooper pairs, and qubits of this type have been made experimentally in the form of Cooper-pair boxes [79, 83, 122]. In these Cooper-pair boxes a superconducting island can be brought into a superposition of having $\bar{N}$ and $\bar{N} + 1$ Cooper-pairs present. Superpositions of this type can reach coherence times of up to 500 ns [84, 123].

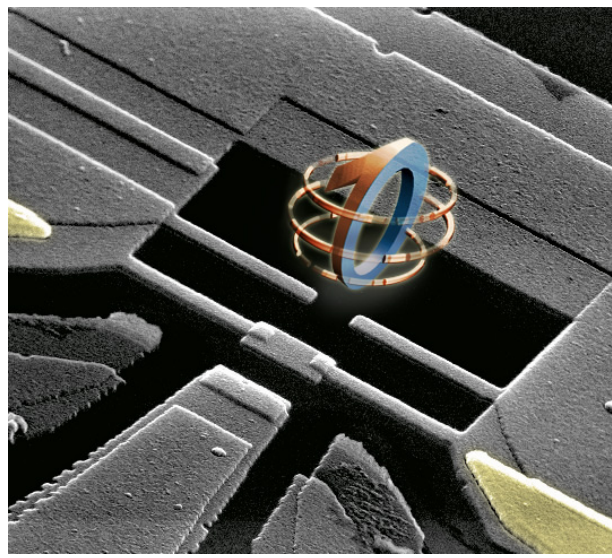

Figure 4.6: The Cooper-pair box qubit or 'quantronium' studied in Saclay [79, 82]. The actual Cooper-pair box is the small rectangular island in the centre which can hold a superposition of N and $N + 1$ Cooper pairs.

In our local pairing description of the qubit, the initial state of the system must be a thermal mixture of thin spectrum states. After all, controlling these states experimentally is practically impossible [51, 63]. The initial state should then be brought into some superposition of the computational states $y = 0$ and $y = 1$, so that it can be used in a quantum computation. Because we know all eigenstates and eigenvalues of the Hamiltonian exactly, we can then explicitly follow the time evolution of the superposition [25]. The complete process is thus described by

$$\begin{aligned}
\rho_{t<0} &= \frac{1}{Z}\sum_x e^{-\beta E(x,0)}\,|x,0\rangle\,\langle x,0| \\
\rho_{t=0} &= \frac{1}{2Z}\sum_x e^{-\beta E(x,0)}\,[|x,0\rangle + |x,1\rangle]\,[\langle x,0| + \langle x,1|] \\
\rho_{t>0} &= \frac{1}{2Z}\sum_x e^{-\beta E(x,0)}\,[|x,0\rangle\,\langle x,0| + |x,1\rangle\,\langle x,1| \\
&\quad + e^{-\frac{i}{\hbar}(E(x,0)-E(x,1))t}\,|x,0\rangle\,\langle x,1| + \text{h.c.}\Big].
\end{aligned} \tag{4.24}$$

where Z is the partition function at $t < 0$. The thin spectrum states labeled by x cannot be observed or controlled experimentally, and they should therefore be traced out of the final density matrix [94, 95]. The remaining reduced density matrix then shows the coherence of only the superposition of y states. The disappearance of the off-diagonal matrix element of the reduced density matrix serves as a measure of the resulting coherence time, and it can easily be checked that this coherence time is given by

$$t_{\text{spon}} = \frac{2\pi\hbar}{k_B T}\frac{\bar{\sigma}}{2}. \tag{4.25}$$

Here $\bar{\sigma}$ signifies, as before, the average number of Cooper pairs on the superconducting island in the groundstate. This coherence time is the maximum coherence time of a superconducting island, which is limited by the existence of a thin spectrum in the superconductor. Just as in the cases of crystals and antiferromagnets, the details of the model (e.g. J or h) do not enter into the expression for the maximum coherence time, which thus looks like a universal timescale [23, 25].

Filling in the values for the constants $\hbar$ and k_B and taking $\bar{\sigma} \simeq 10^6$ and $T \simeq 40$ mK [83], we find a coherence time for the experimentally realized Cooper pair boxes of $\simeq 500$ μs. In fact this is a rather conservative estimate, since the electronic temperature of the Cooper-pair box is probably higher then the environmental temperature of 40 mK. Even so though, the timescale set by the presence of the thin spectrum states which are associated with the spontaneous symmetry breaking, is clearly much larger than the current experimentally seen limit to coherence of the Cooper-pair boxes. This present limit is due to environmental factors, which

induce decoherence in times of the order of microseconds. However, it is well possible that the limit set by the thin states will come within the experimental reach in the near future, either because the isolation from external sources of decoherence will be developed further, or because the size of the Cooper-pair box itself is reduced even more.

4.3 The BCS Superconductor

In the previous sections we have shown that the superconductive groundstate is a state with a spontaneously broken U(1) symmetry. As a consequence the superconductor must have a thin spectrum of states that describe the collective excitations on top of the ground state. In the case of a local pairing model for superconductivity we have found an explicit expression for these thin states and we have shown how they can cause decoherence if we try to use a superconductive island as a qubit.

It could be argued that the local pairing model is somewhat pathological, and not really representative for real-life superconductors, even though from the point of view of symmetry the model is equivalent to a weak coupling model (because there is no phase transition which separates the two [119]). We will therefore also work out the symmetry breaking and decoherence in a BCS description, and show that although the picture changes slightly, the underlying physics is exactly equivalent, and in fact gives rise to the exact same conclusions regarding the thin spectrum and the timescale on which decoherence will set in. The draw-back of doing the calculation in the BCS description is that we cannot do it in a manifestly gauge invariant way, so that the role of the vector potential is obscured.

After creating Cooper pairs, we arrive in the standard BCS theory at the (gauge fixed) effective Hamiltonian [75]

$$\begin{aligned} H_{\mathrm{BCS}} &= \sum_k \epsilon_k \left(c_k^\dagger c_k + c_{-k}^\dagger c_{-k} \right) \\ &\quad -U \sum_{k \neq k'} c_k^\dagger c_{-k}^\dagger c_{-k'} c_{k'}. \end{aligned} \tag{4.26}$$

Here we have adopted the convention to write $(k, \uparrow)$ as k and $(-k, \downarrow)$ as $-k$. The dispersion of the bare Fermi-sea is characterized by ϵ_k while U is the effective pairing interaction due to phonon exchange. U is non-zero and attractive only in a shell around the Fermi energy with a width of about the Debije energy. It is easy to see that extensivity of the model in fact requires U to be inversely proportional to the total number of electrons in the system. We will therefore redefine the pairing potential as $U = V/N$, where N denotes the total number of electrons in the k-space shell in which U is non-zero.

By writing down the Hamiltonian (4.26) we have assumed that there is no external magnetic field and we have fixed the gauge to ensure that the electromagnetic

vector potential vanishes everywhere. Anderson showed that the BCS Hamiltonian in this form can be rewritten as a spin problem by introducing the pseudospins [75]

$$\begin{aligned} S_k^+ &= c_{-k}c_k \\ S_k^z &= \frac{1}{2}\left[1 - c_k^\dagger c_k - c_{-k}^\dagger c_{-k}\right]. \end{aligned} \tag{4.27}$$

In the subspace without any quasiparticles (i.e. $n_k = n_{-k}\ \forall k$), the Hamiltonian up to an overall constant becomes

$$H_{\mathrm{BCS}} = -2\sum_k \epsilon_k S_k^z - \frac{V}{N}\sum_{k\neq k'}\left(S_k^x S_{k'}^x + S_k^y S_{k'}^y\right). \tag{4.28}$$

Interpreted at face value, this Hamiltonian describes pseudo spins on a lattice which has position-label k. On this lattice, three different and independent regions can be identified. In the region $k < k_F - k_D$ (where k_F is the Fermi wavenumber and k_D the Debije wavenumber) we know that the pairing potential vanishes and ϵ_k is negative, so that all pseudospins in that region will point down, which corresponds to completely filled electronic states. In the region $k > k_F + k_D$ the pairing potential is zero as well, but here ϵ_k will be positive, causing all spins to point up, and all electronic states to be empty. In the shell of width k_D around k_F a more interesting situation occurs. There V is nonzero (and approximately constant), while ϵ_k switches sign right at k_F. The pseudo-spin structure that one would classically expect in that region is that of a magnetic domain wall [75]: the pseudospins point up at one end of the region, then continuously fall over until they reach the xy plane exactly at k_F, and then they continue on until they point down at the other end (see figure 4.7). Electronically that structure corresponds to the BCS wavefunction $\prod_k \left(u_k + v_k c_k^\dagger c_{-k}^\dagger\right)|\mathrm{vac}\rangle$ [109].

The Hamiltonian H_{BCS} however is invariant under rotations around the z-axis, and thus the groundstate will also obey this symmetry and have a completely delocalized projection of the pseudospins on the xy plane. To form a true domain wall, and thus the classical superconducting state, this U(1) symmetry will have to be spontaneously broken.

Because the symmetry breaking will only have an effect in the region around k_F and because this region is fully decoupled from the other two regions of k-space, let's focus solely on that shell from now on, and define all sums over k to run from $k_F - k_D$ to $k_F + k_D$. The collective dynamics of the system will again be described by the singular points of the Bogoliubov transformation which diagonalizes the Hamiltonian. Because of the ferromagnetic sign, the collective model in this case consists of only the infinite wavelength part of equation (4.28), which involves

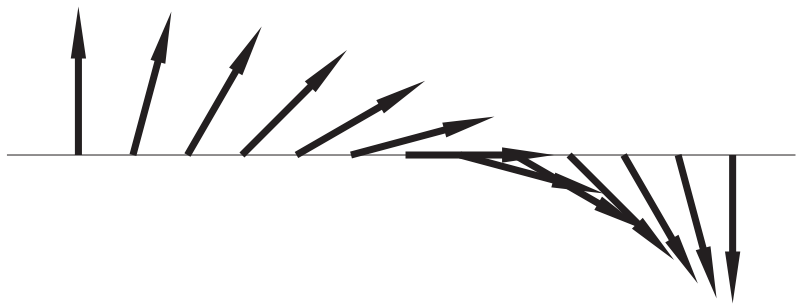

Figure 4.7: A schematic representation of the region of width k_D around k_F. The vectors represent the pseudospins **S**. Spontaneous symmetry breaking causes the projections of the pseudospins in the horizontal plane perpendicular to the paper to align.

only the $q = 0$ part of the Fourier transform $S_q = \sum_k e^{ikq} S_k$:

$$\begin{aligned} H_{\text{coll}} &= -\frac{2}{N}\epsilon_{\text{tot}} S^z_{\text{tot}} - \frac{V(N-1)}{N^2}\left[S^x_{\text{tot}} S^x_{\text{tot}} + S^y_{\text{tot}} S^y_{\text{tot}}\right] \\ &\simeq -\frac{V}{N}\left[\vec{S}_{\text{tot}} \cdot \vec{S}_{\text{tot}} - S^z_{\text{tot}} S^z_{\text{tot}}\right], \end{aligned} \tag{4.29}$$

where $S_{\text{tot}} \equiv \sum_k S_k$ and where we have neglected terms of order $1/N^2$. We have also made a strong coupling approximation by setting $\epsilon_{\text{tot}} = 0$. Other approximations of ϵ_{tot} are possible, but it turns out that after some tedious mathematics these will give the exact same form for the thin spectrum and the maximum coherence time as the simple approximation $\epsilon_{\text{tot}} = 0$. We will discuss two different approximations for ϵ_{tot} at the end of this section. The eigenstates of the collective Hamiltonian are trivially found to be labeled by the total spin quantum number S and its z-projection M, while the corresponding energies are given by $E_{\text{coll}}(S, M) = -V/N\left(S(S+1) - M^2\right)$. The thin spectrum in this case is labeled by M, and describes states with different total electron densities. The total spin excitations labeled by S on the other hand, are gapped with an energy $\sim V$. To break the xy-symmetry of H_{coll} we can add a symmetry breaking field $-BS^x_{\text{tot}}$ along for example the x-axis. After evaluating its matrix elements [25] and taking the continuum limit, Schrödinger's equation can once again be written as a harmonic oscillator equation

$$-\frac{1}{2}\frac{\partial^2}{\partial M^2}\Psi(M,x) + \frac{1}{2}\omega^2 M^2 \Psi(M,x) = \nu\Psi(M,x), \tag{4.30}$$

with $\omega^2 = \frac{2V}{BNS}$ and $\nu = 1 + \frac{E(S,x) - E_{\text{coll}}(S,0)}{BS}$. The symmetry broken wavefunctions

$|S,x\rangle \equiv \sum_M \Psi(M,x)\,|S,M\rangle$ thus have energies

$$E(S,x) = -\frac{V}{N}S(S+1) - BS + \left(x+\frac{1}{2}\right)\sqrt{VB}\sqrt{\frac{2S}{N}}. \tag{4.31}$$

In the ground state S will be maximal (i.e. $N/2$), and then the term $\propto NB$ in the energy signals spontaneous symmetry breaking: in the thermodynamic limit the system can gain an infinite amount of energy by aligning with an infinitesimally small symmetry breaking field. The collective excitations that make up the (dual) thin spectrum on top of the symmetry broken ground state are labeled by x. Their energies are slightly influenced by the remaining collective quantum number S. If we make a superposition of total spin states and trace away the unobservable thin spectrum, then this small shift in the thin spectrum's energy levels will cause the decoherence of the visible, reduced density matrix, in a manner completely analogous to the one described in equation (4.24). The resulting maximum coherence time is given by

$$t_{\text{spon}} = \frac{2\pi\hbar}{k_B T}N, \tag{4.32}$$

where N counts the number of states in the k space volume of k_D around k_F, which is proportional to the number of Cooper pairs in the superconducting condensate. Notice that we find the same universal form for the expression of the coherence time set by spontaneous symmetry breaking as in the case of the local pairing model for superconductivity, as considered in the previous section.

4.3.1 Reintroducing Kinetic Energy

As mentioned before, the collective Hamiltonian (4.29) can be seen as a strong coupling limit, because we require ϵ_{tot} to be much smaller than V. We can drive the system to a somewhat weaker coupling regime by reincluding an approximate form of $\sum_k \epsilon_k S^z_k$ into H_{coll}. One possible choice for such a term would be

$$t\left(S^z_{k_{\min}} - S^z_{k_{\max}}\right), \tag{4.33}$$

which acts as a boundary condition, pulling the pseudospins down at the low k boundary and up at the other end. A second choice could be the inclusion of the term

$$t\left(S^z_A - S^z_B\right), \tag{4.34}$$

where S_A consists of all spins with $k < k_F$ and S_B denotes spins above the Fermi surface. In the latter case we should take care that t cannot be too great, for if it would dominate over V everywhere, then it would transform the domain wall structure of the superconducting state into a trivial Fermi-sphere structure again.

In both of these cases the mathematics of diagonalizing the collective Hamiltonian is complicated by the fact that the kinetic energy term (which is proportional to t) does not commute with the potential energy given by equation (4.29). The potential energy term (proportional to V) is diagonal in a basis labelled by the total spin quantum number S_{tot} and its z-projection S^z_{tot}. If we include a a boundary term such as the one given by equation (4.33) then this can be written as a $4x4$ matrix in the total spin basis (using Clebsch Gordon coefficients to separate the boundary spins from the bulk). This matrix could then be diagonalized numerically. We do not have to go through this diagonalization explicitly though, because we know that the kinetic energy term only couples states with equal z-projection of total spin. The energy spectrum of the Hamiltonian, including the boundary term, can thus be written as $E = (S^z_{\text{tot}})^2 V/N + E(y)$ where $E(y)$ describes the massive excitations which correspond to adding a Cooper pair to the superconductor. The precise form of $E(y)$ depends on t, but for large enough N we can be sure that the minimal value will still be found for the maximal possible value of the quantum number describing total spin in the presence of boundary terms (i.e. $y \propto N/2$). The Hamiltonian in the presence of a symmetry breaking field $-B\sigma^x_{\text{tot}}$ then becomes

$$\begin{aligned} H^{SB}_{\text{coll}} \simeq & \sum_{y,M} |y,M\rangle \left[E(y) + \frac{V}{N} M^2 \right] \langle y,M| \\ & - |y, M \pm 1\rangle \left[\frac{1}{2} By \right] \langle y,M| \,, \end{aligned} \tag{4.35}$$

where the z-projection of total spin is labelled by M. Clearly this Hamiltonian can once again be mapped onto a harmonic oscillator and we can apply again our standard route to finding the maximum coherence time for a superposition of two different y-states. The result is the same as in the earlier case where we just assumed ϵ_{tot} to be zero.

If we choose to include the kinetic energy given by equation (4.34) instead of the boundary term (4.33), then the derivation changes slightly. We will still find the symmetry broken Hamiltonian of equation (4.35) and the corresponding conclusions about the thin spectrum and the decoherence time, but this time the excitations labelled by y are the eigenstates of the 'inverted' harmonic oscillator given

by

$$\begin{aligned} H_{\text{coll}} &= t\left(S_A^z - S_B^z\right) - \frac{V}{N}\left[\vec{S}_{\text{tot}} \cdot \vec{S}_{\text{tot}} - S_{\text{tot}}^z S_{\text{tot}}^z\right] \\ &\simeq \sum_{S,M} |S \pm 1, M\rangle\, t\frac{N}{2}\, \langle S, M| - |S, M\rangle\, \frac{V}{N}\left(M^2 - S^2\right) \langle S, M| \,. \end{aligned} \tag{4.36}$$

The eigenstates of this Hamiltonian can be written out explicitly in terms of Hermite polynomials, but the facts that the ground states has $y \propto N/2$ and that the kinetic energy does not couple terms with different M is enough to deduce equation (4.35) from it.

We thus find that for all the approximations of the kinetic energy term, the thin spectrum is described as the spectrum of a harmonic oscillator with level spacing $E_{\text{thin}} = \sqrt{VBy/N}$, which always leads to a maximum coherence time for the superconducting qubit given by the universal form

$$t_{\text{spon}} = \frac{2\pi\hbar}{k_B T} N. \tag{4.37}$$

Chapter 5

Conclusions

All many-body qubits have an intrinsic limit to their maximum coherence times. This limit to coherence is caused by the thin spectrum. In quantum systems a continuous symmetry can spontaneously be broken in the thermodynamic limit due to the thin states, which can be identified with the collective, zero momentum, excitations of the orderparameter. In this part of the thesis I have outlined a general procedure for finding the thin spectrum states in a quantum system. The states within the thin spectrum are extremely low in energy and at the same time they are so few that their contribution to the thermodynamic partition function vanishes.

After introducting a symmetry breaking field, the resulting symmetry broken groundstate is a superposition of (only) the thin spectrum states. The fact that the formation of the symmetry broken state occurs spontaneously in the thermodynamic limit can then easily be checked by considering the non-commuting limits of disappearing field and sending the number of involved particles to infinity.

This has important consequences for a many-body quantum system which is brought into a superposition of two different internal states. We have shown that in that case the thin states will in general participate in the time evolution of the full many-body system, even if their effect on any thermodynamic quantity vanishes. This leads to dephasing and therefore decoherence when the thin states are integrated out. We have found that the time-scale corresponding to the dephasing process depends only on the energy scale of the thin spectrum and the energy shifts induced in the thin spectrum by the superposed initial states. Because the shifts in energy generally are proportional to the level spacing itself, the decoherence time in the end depends only on the temperature and size of the system, and not on the underlying details of the model.

We have shown how such superpositions can be defined and studied in a quantum crystal, in the Lieb-Mattis antiferromagnet, and in different models for superconductivity. In all of these cases we have shown that the presence of the thin

spectrum states associated with spontaneous symmetry breaking, will lead to decoherence of the qubit within the time $t_{\text{spon}} = 2\pi\hbar N/k_B T$, where N counts the number of microscopic constituent particles involved in the superposition state. This timescale is universal in the sense that it does not depend on the underlying model parameters.

In the relevant experimental systems, the decoherence caused by the thin spectrum is at the moment much weaker than that caused by other sources. However it may well come within experimental reach within the near future, and we thus present it as a challenge to the experimental community to actually measure the maximum coherence time that the thin spectrum states give rise to.

The very existence of the thin spectrum and the fact that it can cause the decoherence of mesoscopic systems with a broken symmetry shows that even objects in our everyday world, which we consider for all practical purposes to be classical objects, can be subtly influenced by their quantum origin. Spontaneous symmetry breaking provides us with an explanation of why the classical world can look classical in the first place, but it does not completely rule out the possibility of observing Quantum Mechanical effects *of* the Big World.

Part IV

Quantum Mechanics or the Big World

Chapter 1

Introduction

Now that we have seen that quantum mechanics can automatically reduce to classicality through the process of spontaneous symmetry breaking [25,124], why should we still set out to find an additional way of restricting its influence in the everyday world? Why do we even need a collapse process?

To answer this question we again consider the canonical double-slit experiment for single electrons which we discussed in the introduction of this thesis [30, 31]. In that experiment each electron produces only one single spot on the screen, even though the interference pattern formed by a large collection of these spots shows that just before the electrons hit the screen, their wavefunctions must have been spread out all over space [35]. The fact that only one spot is produced in a single experiment, and not a superposition of spots cannot be due to spontaneous symmetry breaking. In fact we have already seen a worked out example of such a situation in the previous part. In equations (3.17) – (3.19) of part III we described the process of a two-spin singlet state being instantaneously included into the lattice of an N-spin antiferromagnet. The result was a superposition of zero and two magnon states. It can straightforwardly be checked that this result holds even in the thermodynamic limit and in the presence of a non-zero symmetry breaking field. Thus the symmetry breaking field can never force the antiferromagnet to choose between having either zero or two magnons, just like it could never make the screen choose to show one particular spot rather than another. The fact that we do observe only a single spot in experiment demands another explanation: the collapse of the wavefunction.

1.1 The Collapse Process

An adherent of the statistical interpretation of quantum mechanics might step forward at this point and argue that the appearance of only a single spot on the screen

is really due to our inability to monitor exactly what is going on in detail within the microscopic environment of the screen. The fact that we see only a single spot and not a superposition is then attributed to the decohering effect of the environment which can diagonalize the reduced density matrix description of the combined system of screen and electron [24, 40, 125–128]. The fact remains though that this diagonal density matrix can only describe an ensemble of measurements, and that there seems to be no valid description for the behavior of a single electron [18].

A more precise way of formulating the need for a collapse process is to say that quantum mechanical time evolution is always unitary. In experiments this unitarity is manifestly broken, as can be easily seen by realizing that the measurement process does not have time-inversion symmetry. Starting from a single spot on a screen and letting time run backward it is impossible to find a single electron in front of the double slits of the exemplary experiment[1]. So what we need is the introduction of an extra non-unitary process into the time evolution of quantum mechanics, and this process we will call the collapse process [39]. By including such a non-unitary process into the microscopic quantum mechanical theory we should eventually find a description of the dynamics which define measurement.

The collapse has to possess three defining characteristics. First of all it must be non-unitary and lead to evolution of quantum states into everyday states, like the ones that can be observed all around us. In particular the final states of the collapse process must not include macroscopic superpositions. The proper way to formalize this requirement is by the introduction of a pointer basis, as was first pointed out by Zurek [127,130]. The second requirement is that quantum mechanics must survive unharmed for microscopic particles. In that regime quantum mechanics has been very thoroughly tested and is certainly correct. One way to effectively make the collapse process act on macroscopic bodies, but not on microscopic particles would be to make it act on both, but to let the timescale over which it becomes noticeable depend on the number of constituent particles or, equivalently, on the total mass of an object. That way the process would take too long to notice for small systems, but would be almost instantaneous for classical objects. The final requirement on the collapse process is that it must reproduce Born's rule [38]. The probability for ending up in a certain macroscopic state after doing a measurement must be equal to the squared amplitude of that part of the microscopic wavefunction that corresponded to the measured value. This implies the introduction of uncertainty and stochasticity into the time evolution in one way or another.

[1] In classical mechanics the fact that measurement can break time inversion symmetry while Newtonian mechanics is invariant under time inversion, is solved by introducing the concept of entropy, and thus defining an arrow of time [129]. In quantum mechanics this is not sufficient, because one can easily check, using the density matrix language, that one would still be left with macroscopic superpositions that are not observed in nature [18].

Chapter 2

Penrose's Observation

Many proposals exist for the way that quantum collapse could work in practice [8, 14–16, 26, 27, 40, 46–48, 52–60]. Some of these proposals are really alternative interpretations of the mathematics of quantum mechanics rather than actual new physical processes [8, 14–16, 40, 46–48], but even discounting those, many other proposals remain. Most of these introduce some form of a randomly fluctuating non-unitary term into Schrödinger's equation in order to make the theory collapse onto the pointer basis, but still obey Born's rule [52–59]. In some cases the fluctuating term is linked to gravity, so that the mass of a state can be used to discriminate the microscopic particles from the macroscopic objects [58–60]. Building on these ideas, sir Roger Penrose has made a very simple, yet important observation: the necessary mass at which gravity could begin to have an effect on quantum mechanics lies in a regime that has been out of reach for almost all possible experiments up to now. With only very few exceptions [28, 131], all experiments have been targeted at either much lower masses, displaying only quantum behavior, or at much larger masses, which always behave classically [26, 27].

2.1 Superposed Gravitational Fields

The core of the argument lies in the incompatibility of quantum mechanics and general relativity. Quantum mechanics is a strictly unitary theory while general relativity is characterized by the covariance of physics under general coordinate transformations (the theory is diffeomorphism invariant). These two properties cannot be reconciled with one another. A simple way of seeing this is to consider some lump of mass in a (deep) double well potential [26]. A state in which the lump is stationary in one of the wells can be labeled $|L\rangle$, and analogously the state with the lump in a neighboring well can be labeled $|R\rangle$. The states $|L\rangle$ and $|R\rangle$ are stable states in the quantum mechanical description because they are eigenstates of

the Hamiltonian. Because both states have the same energy quantum mechanics dictates that the superposition state

$$|\psi\rangle = \alpha\,|L\rangle + \beta\,|R\rangle\,, \tag{2.1}$$

is also a stable eigenstate of the Hamiltonian, carrying the same total energy. Gravitationally, each of the states $|R\rangle$ and $|L\rangle$ individually is also a stable state because they are eigenstates of their associated time translations as given by the Killing vector fields (i.e. the states are eigenvectors of the operator $\partial/\partial t$). In general relativity however, there is a problem with deciding whether or not the superposition state is a stable state. First of all the principle of general covariance forbids us to assign a coordinate to each individual point in spacetime, and thus there is no meaningful way of distinguishing between states $|L\rangle$ and $|R\rangle$. As far as gravity is concerned there really is only one state. This technicality can be circumvented by introducing some massive object (say, the earth) at a reasonable distance from the periodic potential so that $|L\rangle$ and $|R\rangle$ can be distinguished even in a covariant way by their distance to the earth. But then the second and more serious problem arises: even if the two states can be distinguished, then still the gauge freedom of general relativity forbids a global pointwise identification of the two different, superposed spacetimes. The only allowed thing to do is to match the superposed geodesics locally. Without a global pointwise identification though, it becomes impossible to discuss the direction of the Killing vector at a specific point in spacetime, and thus it becomes impossible to define the time evolution of the superposed states [26, 27].

2.1.1 Approximate Pointwise Identification

The best thing that can be done to describe the superposition of the two states is to identify the points of one spacetime as closely as possible with the points of the other, and to use the ill-definedness of the identification as a measure of the corresponding uncertainty in total energy [26]. The 'fuzziness' in the concept of energy for the superposed state can be interpreted as an indication that we are dealing with an unstable configuration, and in accordance with Heisenberg's uncertainty principle we can then postulate that an uncertainty in energy ΔE of this unstable superposed state should correspond to a lifetime $\tau = \hbar/\Delta E$ of the state $|\psi\rangle$. In other words, the uncertainty in energy (or time translation) introduced by general relativity will lead to the collapse of $|\psi\rangle$ into either the stable state $|L\rangle$ or $|R\rangle$, within a collapse time τ.

One way to give a mathematical description of the mismatch between two spacetimes is to do the best possible pointwise identification and then to look at the difference between the force that a free-falling observer feels at a certain point in one state and the force at the same point in the other state. This basically is a measure of how well one has succeeded in matching the geodesics of one spacetime to those

of the other. The definition of the mismatch in terms of these forces is coordinate independent and invariant under accelerations of the coordinate frame [26].

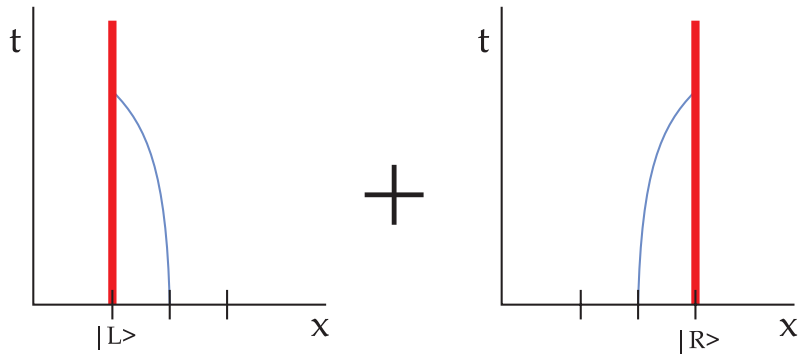

Figure 2.1: A spacetime diagram in one spatial dimension depicting the mismatch in geodesics between the two superposed spacetimes. A free falling observer starting out from a position exactly between $|L\rangle$ and $|R\rangle$ will trace out the thin geodesic, while the mass at $|L\rangle$ or $|R\rangle$ will follow the thick world line. The uncertainty in energy of the superposition of spacetimes follows from comparing the thin geodesics in the two superposed states.

The uncertainty in energy corresponding to the mismatch in forces is easily found by integrating the size of the force difference over the space coordinates in a single time slice [27]:

$$\begin{aligned} \Delta E &= \int \left(\mathbf{F}-\mathbf{F}'\right)\cdot\left(\mathbf{F}-\mathbf{F}'\right) d\mathbf{x} \\ &= \int \left(\nabla\Phi-\nabla\Phi'\right)\cdot\left(\nabla\Phi-\nabla\Phi'\right) d\mathbf{x} \\ &= -\int \left(\Phi-\Phi'\right)\left(\nabla^2\Phi-\nabla^2\Phi'\right) d\mathbf{x}. \end{aligned} \tag{2.2}$$

Here $\mathbf{F}$ is the force on a freely falling observer, Φ is the gravitational potential and the integration is done over all of space within a single time slice. Unprimed quantities refer to the state $|L\rangle$, while primed quantities are to be evaluated in state $|R\rangle$. By using Poisson's formula and the integral equation for the gravitational potential, this expression reduces further to

$$\begin{aligned} \Delta E &= 4\pi G \int \left(\Phi-\Phi'\right)\left(\rho-\rho'\right) d\mathbf{x} \\ &= -4\pi G \int\int \frac{\left(\rho(\mathbf{x})-\rho'(\mathbf{x})\right)\left(\rho(\mathbf{y})-\rho'(\mathbf{y})\right)}{|\mathbf{x}-\mathbf{y}|}\, d\mathbf{x}d\mathbf{y}, \end{aligned} \tag{2.3}$$

which is just the gravitational self energy of the difference between the two mass distributions[1] [27].

2.1.2 The Collapse Time

The fact that it is impossible to define a Killing vector field for a superposition of two different spacetimes, makes it plausible that the superposition state is in fact unstable. In that case an estimate for its mean lifetime is given by Heisenberg's uncertainty relation to be

$$\tau_{\text{coll}} = \frac{\hbar}{\Delta E}. \tag{2.4}$$

This time can then be interpreted as an effective collapse time. At times greater then the mean lifetime the superposition state typically will have decayed into one of the two gravitationally stable component states.

None of the above considerations give us any clue as to how the collapse process would work in practice, nor do they give us any indication of which direction to take to even begin looking for a theory that might unite quantum mechanical and gravitational time evolution. However, if we assume for the moment that such a collapse process exists, and that it is caused by the incompatibility of superpositions and general covariance giving rise to an uncertainty in energy, then it is clear that the timescale at which the collapse should take place is of the order of τ_{coll}.

The main point in Penrose's observation is that the size of this timescale is rather special. For microscopic particles it is enormously large. A simple estimate shows that a single proton can be expected to stay in a superposition state for at least a few million years, and thus its decay will never be observed. On the other hand the timescale becomes short for macroscopic bodies. Even a drop of water with a diameter of only a hundredth of a millimeter will not sustain a superposition for more than a millionth of a second, and it will thus for all practical purposes always seem to be in a classical state. The surprising observation is that the regime in between, where the mass is such that the collapse time becomes measurable, has not been experimentally explored at all yet and in fact seems to be just beyond the reach of what can currently be experimentally tested [28, 131]. That region though is the place to look if one wants to establish whether gravity has anything to do with wavefunction collapse.

2.2 The Schrödinger-Newton Equation

To theoretically study the possibility of gravitationally induced quantum collapse any further, one will need to introduce a specific model, which describes exactly

[1] Notice that this expression also includes an infinite self energy term that comes from the interaction of each point with itself. This part of the energy ΔE is neglected in the calculations that follow.

how gravity alters the usual quantum mechanics. In particular, the model will have to provide a time evolution for the actual collapse process, and it will have to single out one specific basis into which classical (or macroscopic) bodies will collapse. In order to provide just such a basis, Penrose introduced the so called Schrödinger-Newton equation [26, 27, 29]

$$\begin{aligned} -\frac{\hbar^2}{2m}\nabla^2\psi + U\psi &= E\psi \\ \nabla^2 U &= 4\pi G m^2 |\psi|^2 , \end{aligned} \tag{2.5}$$

where ψ is the quantum mechanical wavefunction, U is the gravitational self energy which acts as a potential energy, and E is the total energy eigenvalue.

The Schrödinger-Newton equation is a non-linear eigenvalue equation in which the expectation value of the wavefunction itself serves to generate the potential energy which helps determine the eigenfunctions of the equation, and thus the stable wavefunctions of the system. This extended form of the Schrödinger equation has been studied in the spherically symmetric limit and a set of "bound state" solutions has been found [29]. What has not been considered yet is what this form of the total energy operator would imply for the actual time evolution of a microscopic system.

Different forms of a time evolution operator involving gravity have been introduced by others [58–60]. Most of these approaches have the disadvantage that they need to introduce either a large number of randomly fluctuating fields or, equivalently, a random localization process. Since none of these randomly fluctuating fields has actually been observed, it is difficult to experimentally test or distinguish these different theories.

Before we turn to a discussion of the time evolution implied by the Schrödinger-Newton equation, we will first show in the following chapter that it is possible to make an experimental prediction based on Penrose's ideas without invoking any specific scheme for the description of the exact time evolution.

Chapter 3

An Experimental Test

Assuming that gravity has something to do with the quantum collapse process, and assuming that this leads to a timescale τ_{coll}, as proposed by Penrose, it is possible to make at least some experimental predictions without referring to any underlying description of the collapse process. In particular, we will consider in this chapter what the idea of having a gravitationally induced collapse would imply for the superposition state of counter rotating supercurrents in a flux-qubit.

3.1 The Flux Qubit

In recent years there has been an enormous experimental effort to create and control quantum superposition states [36, 79, 80]. The pursuit is fueled by the hope that one day we'll be able to control the quantum world with such accuracy that we could build a quantum computer. The concept of the quantum computer was conceived by various people already in the 1970's, and popularized in 1981 by Richard Feynman [132]. After Peter Shor showed in 1994 that a quantum computer could be used to factorize large integers and thus potentially break encryption codes used by conventional computers [133], the race for creating a quantum computer in the lab broke loose. Many different proposals and realizations of single qubit systems have been studied since. One of the proposed setups for creating a qubit (i.e. a controllable quantum superposition) is to take a superconducting loop which contains a Josephson junction, and use a magnetic flux to put it into a superposition of a clockwise and a counterclockwise rotating supercurrent [78, 80, 81].

Because a supercurrent is a collective, coherent current of a macroscopic number of electrons, the superposition state that is achieved in the flux qubit is a sort of macroscopic Schrödinger cat like state [78]. The combined weight of all the electrons in the supercurrent can in principle be made so large that gravitational effects

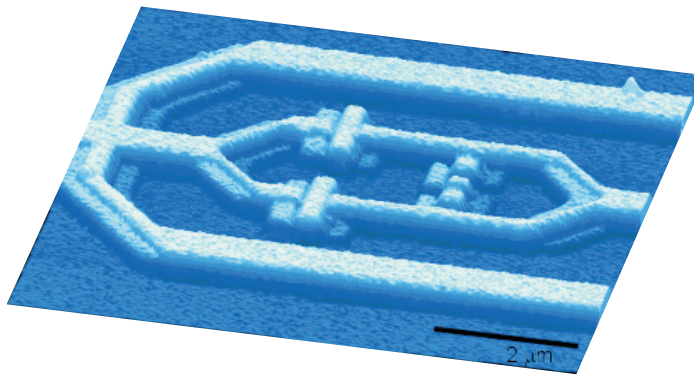

Figure 3.1: An STM image of the superconducting flux qubit used in Delft [80]. Supercurrent circulates both clockwise and anti-clockwise through the central ring. The 'obstructions' in the ring are the Josephson junctions.

of the type envisioned by Penrose might become observable. If we have an indication of the timescale on which to expect the onset of gravitational collapse, and a way to distinguish gravitational collapse from the usual processes of decoherence, then the flux qubit could prove to be a window through which we can study the quantum collapse process.

3.1.1 Trains and Wagons

In the proposal by Penrose the uncertainty in energy due to gravity equals the self energy of the difference of the mass distributions of the superposed states. If we were to apply that principle blindly to our scenario, then we would immediately be faced by an infinite lifetime of the superposition state in the flux qubit. After all, there may be a macroscopic current which is moving both clockwise and counterclockwise, but the mass distribution associated with that current is the same for both directions, and constant in time[1]. Thus, a uniform current would be allowed to flow in superposition forever. This certainly is not a property that we want to have in a quantum collapse theory. After all, the exact same reasoning could be used to argue that a sufficiently smooth soccer ball could be shot at the goal in a superposition of top and bottom spin, or that a sufficiently densely packed passenger train could ride a circular track in opposite directions at the same time.

The way out of this dilemma is in fact a very simple one: the supercurrents as a whole may have a vanishing difference of mass distributions, but if we consider

[1] There may be a relativistic correction to the uniform mass distributions associated with the different framedraggings induced by the current but since this effect has a prefactor of order v/c, it is neglected in the present discussion.

only a part of the current, then the individual part certainly does have a non-zero gravitational self energy. The reasoning thus comes down to saying that a train can be brought into a superposition state if and only if all of its wagons individually could be brought into a superposition state of their own. In other words, if a single wagon were to collapse under its own gravitational influence then the entire train must follow, even if the mass distribution of the train as a whole does not necessarily call for a cessation of the superposed state.

In our case we are allowed to discuss the supercurrent in a flux qubit as if it were a quantum train built up out of different wagons, as long as we represent the wagons by large enough patches of supercurrent. If we only consider patches of supercurrent that are at least large enough for Heisenberg's uncertainty relation to allow a relatively well defined local phase (by using $\Delta\varphi\,\Delta N > \hbar$ and $\Delta\varphi \propto 1/\sqrt{N}$) and thus a well defined local orderparameter, then we can identify a particular spatial region using its local phase and follow it in time as if it were a colored wagon riding along in a train of patches of supercurrent. To see whether the whole of the supercurrent can be in a superposition of counter rotating states, we will have to consider the spatial superpositions of all possible sizes of patches of supercurrent large enough to be individually identified, and then ensure that none of them will individually collapse.

3.2 Self Energy

Consider a piece of the superconducting ring which is short enough to approximate it, for the time being, by a straight strip. At time $t = 0$ we can identify a piece of supercurrent of length L, and then follow it along as it starts to flow both to the left and to the right. In the beginning the two superposed copies of the original piece will still overlap, and the gravitational self energy of their difference in mass distribution will be due only to the non-overlapping flanks. At a time $t = t_1$, the two copies will just touch each other, and then start to move apart, thus increasing their gravitational energy because of a growing distance, rather than because of a growing amount of non-overlapping mass. The gravitational self energy in both cases $t < t_1$ and $t > t_1$, is easily calculated by evaluating the integral for ΔE (equation (2.3)), while keeping in mind that we should throw out the (infinite) contribution to the self energy caused by the interaction of each flank with itself. In the calculation we can assume all the mass of the non-overlapping part of the superposed pieces of supercurrent to be concentrated in their respective centers of mass, so that we can write the density distribution as $|\psi(x)|^2 = \frac{1}{2}\left(\delta\left(x - L/2\right) + \delta\left(x + L/2\right)\right)$ (see figure 3.2). The remaining gravitational "interaction" energy between the flanks then

becomes

$$\begin{aligned} \Delta E &= 2G \int\int \frac{\frac{1}{2}M_1\delta\,(x - L/2)\;\frac{1}{2}M_2\delta\left(y + L/2\right)}{\left|x - y\right|}\,dx\,dy \\ &= \frac{1}{2}\,G\frac{M_1 M_2}{L}. \end{aligned} \tag{3.1}$$

Here M_1 and M_2 are the masses of the non-overlapping pieces on the left and right,

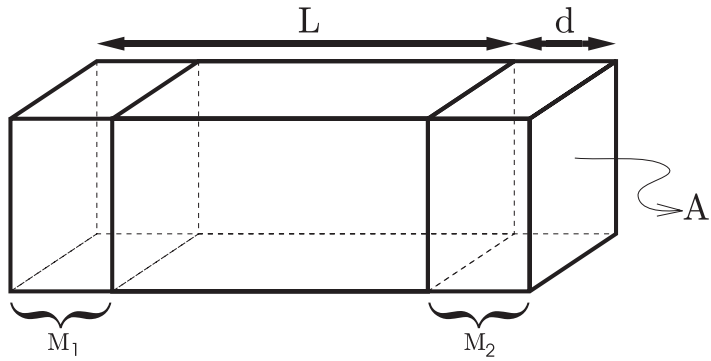

Figure 3.2: Schematic depiction of the superposition of two blocks of supercurrent. Both blocks have length L, and have moved $d/2$ from their coincidence position.

while L is the distance between them, as in figure 3.2. Clearly the energy ΔE is just the usual Newtonian gravitational energy of the masses M_1 and M_2. If the width of the non-overlapping piece is d then $M_1 = M_2 = \frac{d}{L}M$, with M the mass of the total piece of supercurrent under consideration. The gravitational self energy then becomes

$$\Delta E = \frac{1}{2}GM^2\frac{d^2}{L^3}. \tag{3.2}$$

3.2.1 Alternative Approaches

Although the calculation of the self energy using the integral equation (3.1) is very straightforward in the case of straight strip of material, it can become rather cumbersome if we consider different geometries for the superconducting device, especially in the regime where there still is a finite overlap between the superposed copies. It will therefore be good to consider two alternative ways of identifying the gravitational self energy in that regime. Of course both of these alternative methods will in the end be precisely equivalent to the formal integration of equation (3.1).

The Gravitational Plasmon

One possible approach is to see the current setup as a gravitational analogue of the $k = 0$ plasmon. In electrodynamics such a plasmon is formed by displacing the negatively charged particles in a piece of material while keeping the compensating positively charged background fixed [64]. The two oppositely charged surfaces at the flanks of the material then create a constant electrical field throughout the material. All charges within the material consequently feel a constant force which pulls the displaced piece back in line with the background. The acceleration caused by these forces is exactly that of a harmonic oscillator, and thus the piece of displaced material starts to oscillate with a finite frequency (and a finite energy) [64].

Our case is a bit different because gravity is uniformly attractive, and because we would like to consider only the centers of mass of the non overlapping pieces instead of an infinitely wide surface charge. Nevertheless the moral of the story remains unchanged. The two displaced pieces of mass (as depicted in figure 3.2) act on each other via a gravitational force between the flanks. This force field does not have any effect on the overlapping pieces of mass, because of the symmetry of the setup. However the motion that results from the applied force on the flank influences the whole of the displaced mass, since it does form a rigid body. Thus the mass that is accelerated by the force on the left flank is M, and not just M_1. Putting all of these ingredients together, it is clear that the force which M_2 exerts on a (test)mass m_1 located at the center of mass of M_1 will be

$$F_{m_1} = G\frac{m_1 M_2}{L^2}. \tag{3.3}$$

The resulting acceleration is independent of the mass of m_1, and given by

$$a_1 = G\frac{M_2}{L^2}. \tag{3.4}$$

This acceleration is shared by the entire left block of mass M. After parametrization of the position of the leftmost side of that block with x_0, the mass of the right flank becomes $M_2 = 2\rho A x_0$, with ρ the mass density and A the area of the strip perpendicular to its length L (see figure 3.2). We can then write

$$\begin{aligned} \ddot{x_0} &= a_1 \\ &= -G\rho A\frac{2x_0}{L^2} \\ \Rightarrow x_0 &= -\frac{d}{2}\cos\left(\sqrt{G\rho A\frac{2}{L^2}}\,t\right), \end{aligned} \tag{3.5}$$

where in the last line we have used the boundary conditions $x_0(0) = -\frac{d}{2}$ and $\dot{x_0}(0) = 0$. The gravitational self energy that we are after is the same as the potential energy of the gravitational plasmon, which in turn equals the total kinetic

energy of both of the superposed pieces at the moment that $x_0 = 0$. This energy is now easily found to be

$$\begin{aligned} E_{\text{kin}} &= 2\frac{1}{2}M\left(\dot{x_0}|_{x_0=0}\right)^2 \\ &= \frac{1}{2}G\left(\rho A\right)^2\frac{d^2}{L} \\ &= \frac{1}{2}GM^2\frac{d^2}{L^3}, \end{aligned} \tag{3.6}$$

which equals (3.2), as anticipated.

The Work of Separation

The second possible way to arrive at the same result is to consider the work done in pulling apart the two copies of our piece of supercurrent. If we always pull with equal force to the left and to the right, then at each point along the way the force to be overcome on, say, the left piece is

$$F_{M_1} = G\frac{M_1 M_2}{L^2}. \tag{3.7}$$

However, the mass that we are moving is not only M_1, but in fact the full mass M of the entire piece of current under consideration[2]. The work done on the left piece of supercurrent is thus

$$W_1 = G\int \frac{MM_2}{L^2}dx. \tag{3.8}$$

Writing everything again in terms of d and x_0, the total work done on both copies of the supercurrent during the separation process turns out to be

$$\begin{aligned} W &= 2G\frac{M^2}{L^3}\int_{\frac{L+d}{2}}^{\frac{L}{2}}\left(2x_0 - L\right)dx_0 \\ &= \frac{1}{2}GM^2\frac{d^2}{L^3}. \end{aligned} \tag{3.9}$$

Again of course this equals the result (3.2). In more complicated situations calculating the work done will turn out be easier than evaluating the formal integral (3.1).

[2]This situation is precisely analogous to the one for the gravitational plasmon, where $\ddot{x_0}$ was proportional to M_2, while the kinetic energy was written as $1/2M\dot{x_0}^2$.

3.2.2 The Collapse Time

Having found the gravitational self energy of the superposition state of a linear piece of current within a string of superconducting material, we can now evaluate the time at which that superposition must collapse because of the instability induced by gravity. If the current velocity is v, and the two copies start moving apart at $t = 0$, then the gravitational self energy can be written as

$$\begin{aligned}
\Delta E &= \begin{cases} \frac{1}{2} G M^2 \frac{(2vt)^2}{L^3} & \text{if } vt \leq \frac{L}{2} \\ G M^2 \left(\frac{1}{L} - \frac{1}{4vt} \right) & \text{if } vt \geq \frac{L}{2} \end{cases} \\
\Delta E &= \begin{cases} \frac{1}{2} G (\rho A)^2 \frac{(2vt)^2}{L} & \text{if } vt \leq \frac{L}{2} \\ G (\rho A)^2 \left(L - \frac{L^2}{4vt} \right) & \text{if } vt \geq \frac{L}{2} \end{cases} .
\end{aligned} \tag{3.10}$$

In the last line we have used $M = \rho A L$ to write everything in terms of the length of the piece of current under consideration. Notice that the velocity v of the patch of current is directly proportional to the strength of the current I. The initial increase of the gravitational self energy (3.10) is caused by the increasing amount of non-overlapping mass at the flanks, while after $t = L/2v$ the growth in energy is purely due to the growing distance between the superposed copies. A sketch of the function ΔE is given in figure 3.3.

The timescale τ associated with the uncertainty in energy due to gravity is given by Heisenberg's uncertainty relation (2.4). The collapse of the separating pieces of supercurrent can be expected to occur as soon as the lifetime according to Heisenberg's uncertainty relation equals the actual time that the superposition has existed. For the case of the linear strip of supercurrent this amounts to

$$\begin{aligned}
t_{\text{coll}} &= \tau (t_{\text{coll}}) = \frac{\hbar}{\Delta E (t_{\text{coll}})} \\
t_{\text{coll}} &= \begin{cases} \frac{\hbar L}{2G(\rho A v t_{\text{coll}})^2} & \text{if } vt_{\text{coll}} \leq \frac{L}{2} \\ \frac{4\hbar v t_{\text{coll}}}{G(\rho A)^2 L (4vt_{\text{coll}} - L)} & \text{if } vt_{\text{coll}} \geq \frac{L}{2} \end{cases} \\
\Rightarrow t_{\text{coll}} &= \begin{cases} \sqrt[3]{\frac{\hbar L}{2G(\rho A v)^2}} & \text{if } t_{\text{coll}} \leq \frac{L}{2v} \\ \frac{\hbar}{G(\rho A)^2 L} + \frac{L}{4v} & \text{if } t_{\text{coll}} \geq \frac{L}{2v} \end{cases} .
\end{aligned} \tag{3.11}$$

For large enough L the collapse time in fact increases with increasing size of the piece of current under consideration. This may seem rather counter-intuitive at first sight, but it is simply due to the form of the self energy (3.2). The self energy for

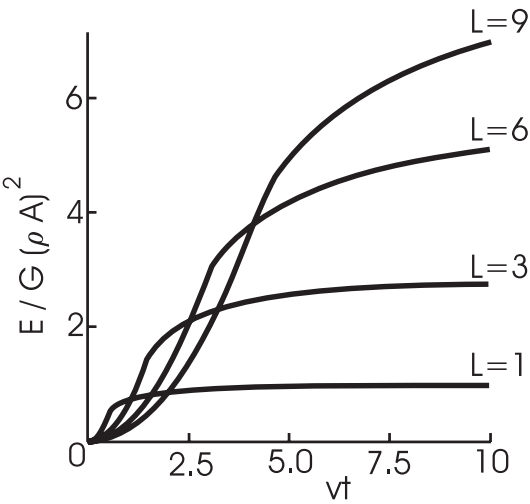

Figure 3.3: Sketch of the gravitational self energy of the difference in mass distribution of two separating copies of a block of supercurrent in a linear chain. The different curves represent different sizes of the block of supercurrent under consideration. The line with the lowest final energy describes the smallest block of current.

a large block displaced over a distance $d = vt$ is less then the self energy of a smaller block displaced by the same amount. This can easily be understood by considering the work done in creating the superposition. Only the non-overlapping flanks exert a force on each other (see figure 3.2). The force depends on the masses of the non-overlapping parts, which is always just $\rho A d$, and on the distance between them. Because the separation of the flanks is larger for a larger piece of current, the self energy stored in the superposition is smaller. If we compare a small and larger block displaced over their respective body sizes however, then of course the energy in the larger piece is higher.

To now find the actual collapse time of the entire flow through a linear superconducting strip, we apply the train-and-wagon reasoning discussed in the beginning of this chapter, and consider all possible sizes of separating blocks of current. We should then find out which of these collapses first, and conclude that that collapsing piece of current will cause the entire flow to come to a halt. The minimum collapse time with respect to the block size L, streaming at a given velocity v, is easily found to be

$$t_{\text{coll}}^{\min} = \sqrt{\frac{\hbar}{G\,(\rho A)^2\, v}}. \tag{3.12}$$

So we conclude that even though an infinitely long strip of supercurrent flowing both left and right represents a superposition state involving an infinite amount of superposed mass, it does not collapse within an infinitely short time. In fact, it can remain in that superposition state for the finite time $t_{\text{coll}}^{\min}$. On the other hand, even though the mass distribution of the superposed states as a whole is exactly the same, the superposition state will also not be able to exist for an infinitely long amount of time. Indeed, it will have to collapse after the finite lifetime given by $t_{\text{coll}}^{\min}$.

If one could actually construct an infinitely long superconducting wire with a cross section comparable to those used in the flux qubits, and one could then somehow create a current of, say, about 1 μA running both up and down the wire, then this superposed current could exist according to (3.12) for just about one hour. In comparison, a human moving into a superposition state with a speed of 1 m/s would collapse after 10^{-14} seconds, and reach a maximum separation of superposed copies of only 10^{-14} m.

3.3 The Flux Qubit Collapse

Having worked out the simple case for a straight, infinitely long superconductor, we can now turn to the actual flux qubit. In the end the main experimental difficulty will be to distinguish the gravitationally induced collapse from the different environmental decoherence processes [24]. One possible way to shed light on that matter would be to see if the collapse time depends on the exact geometry of the qubit, since decoherence effects in general do not [134]. Let's therefore consider a superconducting ring that consists of two parts with different cross sections, as shown in 3.4. By independently varying the areas of the two regions we can then study the dependence of the collapse time on the geometry of the qubit. To simplify the calculation we will assume that the volumes of both parts are equal, and we will only consider a superposed flow of blocks of supercurrent which start at $t = 0$ with their centers of mass exactly at the transition point between large and small cross sections.

3.3.1 The Gravitational Self Energy

In analogy with the previous section we will first consider the self energy due to the non-overlapping flanks of the superposed pieces of supercurrent. The distance between the center of mass coordinates of the two copies, measured along the perimeter of the circularly shaped qubit depicted in 3.4 and 3.5, can straightforwardly be written as

$$L_{\text{arc}} = \frac{1}{2}\left[\left(\frac{A_1}{A_2} - 1\right) x_1 + \left(1 - \frac{A_2}{A_1}\right) x_2 + \frac{A_1 + A_2}{A_1 A_2}\frac{M}{\rho}\right], \tag{3.13}$$

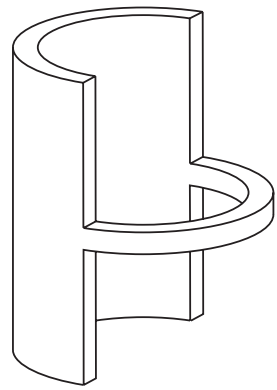

Figure 3.4: Schematic picture of the proposed flux qubit geometry. By independently varying the areas of the two regions it is possible to study the dependence of the collapse time on the geometry of the qubit.

where M is the mass of the block that is to be superposed, and A_1 and A_2 are the cross sections perpendicular to the current flow in the different parts of the qubit. The gravitational force between the two flanks does not act along the perimeter

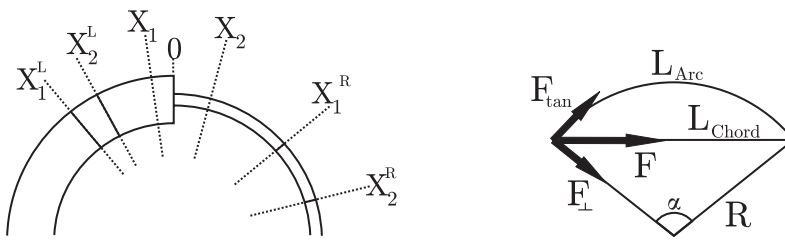

Figure 3.5: Left: schematic representation of the separating blocks of current. The left and right side of block 1 are X_1^L and X_1^R respectively, and its centre of mass is at X_1. Right: diagram showing the orientation of forces in the flanks of the block of current.

of the circle, but rather along the chord connecting the centers of the flanks. The part of the force along the tangent to the circle will contribute to the work done in creating the superposition state, while the part of the force perpendicular to the circle will not contribute anything and can be discarded (see figure 3.5). These quantities can be expressed in terms of the arc length L_{arc} and the (mean) radius of

the flux qubit R as

$$\begin{aligned} L_{\text{chord}} &= 2R\sin\left(\frac{L_{\text{arc}}}{2R}\right) \\ F_{\tan} &= F\cos\left(\frac{L_{\text{arc}}}{2R}\right). \end{aligned} \tag{3.14}$$

From geometric considerations it is clear that if the strengths of the currents moving in opposite directions are equal, then so are the masses of the flanks. Additionally, the centers of mass of the superposed blocks of current must then obey the relation $x_1 = -\frac{A_2}{A_1}x_2$. We can now simply calculate the work done on for example block 1 in creating the superposition state, and find it to be

$$\begin{aligned} W_1 &= \int_0^{v_1 t} GM\rho\,(A_2x_2 - A_1x_1)\cos\left(\frac{L_{\text{arc}}}{2R}\right)/L_{\text{chord}}^2\,dx_1 \\ &= GM\frac{\rho A_1}{4R^2}\frac{\cos\left(\frac{L_{\text{arc}}}{2R}\right)}{\sin^2\left(\frac{L_{\text{arc}}}{2R}\right)}(v_1 t)^2\,. \end{aligned} \tag{3.15}$$

If we combine the work done on both of the copies and write everything in terms of dimensionless quantities then the total gravitational self energy of the superposition reduces to

$$Y = \frac{1}{4\pi N}\frac{\cos\left(\frac{\pi}{N}\right)}{\sin^2\left(\frac{\pi}{N}\right)}X^2 \qquad \text{for } 0 \le X \le \frac{\pi}{N}, \tag{3.16}$$

where we have defined $X \equiv t\frac{I}{\rho_e R}\frac{A_1+A_2}{2A_1A_2}$ and $Y \equiv E\frac{R}{GM_{\text{tot}}^2}\frac{A_1+A_2}{2A_1A_2}$, with ρ_e the charge density of the supercurrent, M_{tot} the total mass of the supercurrent around the full ring and $N \equiv M_{\text{tot}}/M$ the number of patches of supercurrent needed to cover the whole ring.

After the two copies of the block of current have been completely detached from one another, the energy added to them during further separation is just the normal Newtonian self energy of two separated masses $E = GM^2\,(1/L_0 - 1/L)$. Expressing this in terms of dimensionless units as well, and realizing that after the blocks have rounded a quarter of the ring they will start coming together again, we can

write the full expression for the self energy during half a revolution as

$$\begin{aligned} Y &= \frac{1}{4\pi N}\frac{\cos\left(\frac{\pi}{N}\right)}{\sin^2\left(\frac{\pi}{N}\right)}X^2 \qquad \text{for } 0 \le X \le \frac{\pi}{N} \\ Y &= \frac{\pi}{4N^3}\frac{\cos\left(\frac{\pi}{N}\right)}{\sin^2\left(\frac{\pi}{N}\right)} \\ &\quad + \frac{1}{2N^2}\left[\frac{1}{\sin\left(\frac{\pi}{N}\right)} - \frac{1}{\sin(X)}\right] \text{ for } \frac{\pi}{N} \le X \le \frac{\pi}{2} \\ Y(X) &= Y(\pi - X) \qquad \text{for } \frac{\pi}{2} \le X \le \pi. \end{aligned} \tag{3.17}$$

This form of the gravitational self energy has been plotted in figure 3.6 for different values of N.

If the current has not collapsed after half a revolution then the superposed blocks will be exactly on top of each other again, and thus stable with respect to gravity. We therefore only need to consider the current up to $X = \pi$, because if it has not collapsed by then, the supercurrent will be able to outrun the gravitational collapse process forever.

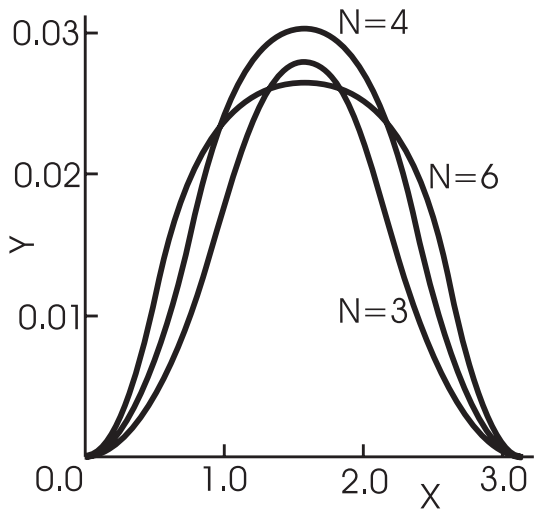

Figure 3.6: The dimensionless energy $Y \equiv E\frac{R}{GM_{\rm tot}^2}\frac{A_1+A_2}{2A_1A_2}$ as a function of the dimensionless time $X \equiv t\frac{I}{\rho_e R}\frac{A_1+A_2}{2A_1A_2}$. As in figure 3.3, the different curves represent different sizes of the block of supercurrent under consideration (parametrized by N). The curve with the lowest maximum has the highest value for N.

3.3.2 The Qubit Collapse Time

Having found the gravitational self energy of a piece of current within the flux qubit, we can again use Heisenberg's uncertainty relation to construct the maximum lifetime for that piece. The collapse time of the counter rotating currents as a whole must then correspond to the shortest possible collapse time of any of the current's building blocks.

Using the definition for the gravitational self energy (3.17), we can define $Y^{\max}$ as the maximum Y with respect to N for a given X. The condition for the collapse time to equal the inverse of the gravitational energy then becomes, in dimensionless units

$$XY = Z, \tag{3.18}$$

with $Z \equiv I\frac{\hbar}{GM_{\rm tot}^2\rho_e}\frac{A_1+A_2}{2A_1A_2}$. We can then use a simple computer program to trace out the collapse 'time' $X_{\rm coll}$ as a function of the 'current' Z. The curve thus found is depicted in figure 3.7. As it turns out there is a very good and simple fit of the curve, given by

$$Z = b\left[1-\cos\left(\frac{\pi}{a}X_{\rm coll}\right)\right]. \tag{3.19}$$

with the fitting parameters $a = 2.17$ and $b = 0.029$.

To come to the final expression for the collapse time in terms of the applied current and the geometrical parameters of the flux qubit, we reinsert dimensionful units, and invert the expression for Z ($X_{\rm coll}$) to find

$$t_{\rm coll} = \frac{a}{\pi}\frac{\rho_e}{I}\frac{2A_1A_2}{A_1+A_2}R\cdot \arccos\left[1-\frac{1}{b}\frac{\hbar}{Gm_e^2}\left(\frac{q_e}{2\pi\rho_e}\right)^2\frac{I}{\rho_e}\left(\frac{A_1+A_2}{2A_1A_2}\right)^3\frac{1}{R^2}\right]. \tag{3.20}$$

Here q_e and m_e are the charge and mass of an electron. Notice that in the limit $R\to\infty$ the functional form of this expression reduces to that of equation (3.12)[3]. From this expression it is immediately clear that if the current becomes large enough to make the argument of the arccosine smaller than -1, then there will be no collapse time. This signifies the point at which the current moves so fast that it can move a block of current of any size all the way around the (half) loop of the qubit before its gravitationally induced energy uncertainty has had a chance to collapse it. If I is smaller than that, then collapse is inevitable, and the collapse time is given by $t_{\rm coll}$.

[3]To be precise, the limit $R\to\infty$ yields $t_{\rm coll} = a/(\sqrt{2b}\,\pi^2\sqrt{\hbar/G(\rho A)^2\nu} = 0.91\sqrt{\hbar/G(\rho A)^2\nu}$. The difference in the prefactor from the earlier result is due to the fact that in the ring the collapse can also occur as the two copies of a piece of supercurrent are moving toward each other. If we consider only the self energy for pieces of supercurrent in one half of the ring, then the prefactor would indeed come out to be one.

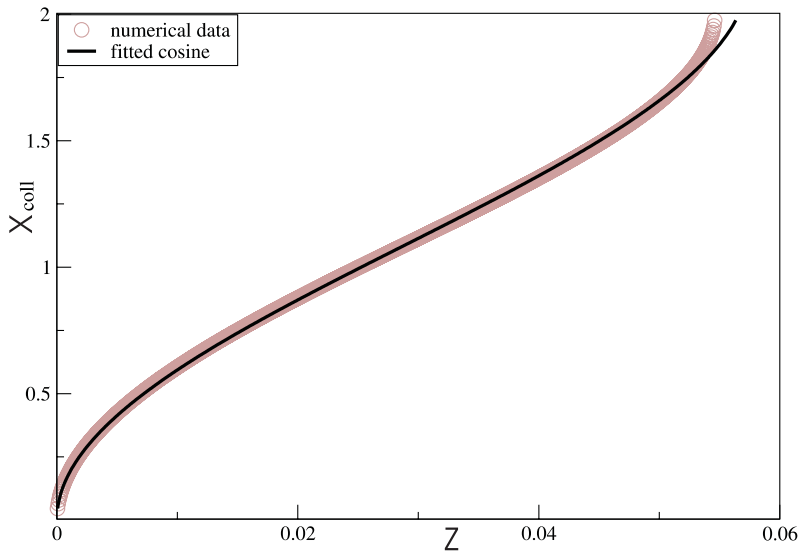

Figure 3.7: The dimensionless collapse time X_{coll} as a function of the dimensionless current Z. The fit is the line defined by equation (3.19).

Practical Implications

In order to be able to measure the collapse time t_{coll} in the lab, we'll need to make it as small as possible. After all, the gravitational collapse must occur before any of the normal processes of decoherence has had a chance to destroy the superposition state. The difference between A_1 and A_2 does not seem very useful in that regard. We might as well have taken just a uniform cross section. However, the dependence of t_{coll} on $(A_1 + A_2)\,/2A_1A_2$ does provide an additional test to see if we really are dealing with gravitationally induced collapse. To make the lifetime t_{coll} as small as possible, one should stick with just one cross section A, make the current as large as allowed, and then further tune the system by making A larger while keeping RA fixed. In the end this will lead to a very narrow, very long cylinder of superconducting material, with a slit etched out along its length to allow for the placement of a Josephson junction. The superposition state is the created by piercing exactly half a flux quantum through the inside of the superconducting tube.

Looking at state of the art experimental setups like the ones used in the flux qubit experiments in Delft [80, 81], the maximum possible current in a qubit turns out to be of the order of a microamp with a qubit radius of around a micrometer. Using these values, the condition for the current not to outrun its own collapse

process reduces to

$$\begin{aligned} \frac{I}{R^2 A^3} &\leq 10^{27} \\ A &\geq 10^{-7}, \end{aligned} \tag{3.21}$$

satisfying this condition with A as small as possible, the collapse time becomes approximately

$$\begin{aligned} t_{\text{coll}} &\simeq 10^8 \frac{AR}{I} \\ t_{\text{coll}} &\simeq 10 \text{ sec.} \end{aligned} \tag{3.22}$$

So, in the end we need to create a flux tube with a cross section of its wall of about 10^{-7} m^2, and then still the collapse time is of the order of 10 seconds. Measuring the gravitationally induced collapse in a flux qubit thus seems to be a rather tough experimental challenge indeed! Especially since normal environmental sources of decoherence tend to increase with system size [134].

But with the present sharp rise in experimental know-how regarding the manipulation of nano-sized objects and the fabrication of this kind of flux tube, the experimental test of the idea that gravity might lead to the instability of quantum superpositions and consequently to quantum collapse, may come within reach in the future.

Chapter 4

Time Evolution

As we have seen in the previous chapter, the assumption that gravity induces some uncertainty in the total energy of a quantum superposition state and thus allows quantum superpositions only a finite lifetime given by the inverse of that energy uncertainty can in principle lead to testable predictions about the timescale at which collapse is expected to occur. On the other hand, it does not tell us anything about the dynamics of the collapse process itself [26]. The equations that are supposed to lead from a well defined microscopic superposition state to a collapsed macroscopic measuring apparatus remain completely unknown.

In addition to describing the incompatibility of quantum mechanics' unitarity and gravity's general covariance, Penrose also proposed to use the so called Schrödinger-Newton equation as the defining equation for which states could be stable under gravitationally induced collapse, and which could not [29]. This Schrödinger-Newton equation is a non linear set of equation defined as

$$\begin{aligned} -\frac{\hbar^2}{2m}\nabla^2\psi + U\psi &= E\psi \\ \nabla^2 U &= 4\pi G m^2 |\psi|^2 . \end{aligned} \tag{4.1}$$

Because the total energy operator is the generator for time translations, we should in principle also be able to use these equations to describe the dynamical collapse of a quantum superposition. In this chapter we will take the Schrödinger-Newton equation (4.1) not as a simple Ansatz which is meant to hint at the final shape of gravitationally collapsed states, but rather as a literal replacement for the Hamiltonian which can give us both the total energy and the time evolution of a quantum mechanical superposition state.

4.1 A Two State Measurement

The very simplest possible experiment that any description of a collapse process should be able to describe is the reduction of a macroscopic superposition over two distinct states to just one of these states. One can imagine the macroscopic superposition to be formed in a process akin to the one used in the previous part to describe the interaction between a two spin singlet and an antiferromagnet (3.17)-(3.19). The general idea is thus that we start out with some microscopic superposition of two different quantum states. The difference between these states might give rise to a gravitational self energy, but the mass involved is supposed to be so small that the microscopic matter will not collapse by itself. At some point in time a coupling between the microscopic state and a macroscopic measuring machine will be instantaneously turned on. In general this will yield a macroscopic superposition and the difference between the superposed states will in general also have a finite gravitational self energy. Now the macroscopic mass involved in this self energy is expected to make the collapse process very fast, and as a result it will seem as if an instantaneous measurement has yielded only one of the two possible outcomes. Optimally the distribution between the two outcomes found in many repetitions of the experiment would mirror the squared wavefunction of the microscopic superposition that we started out with, in accordance with Born's rule [38].

4.1.1 The General Two State Time Evolution

To see whether the Schrödinger-Newton equation can indeed lead to the collapse of a two state measurement, we will first write down the generic time evolution of a superposition of two states. The most general superposition state over a basis with two elements is given by

$$|\psi_0\rangle = ne^{i\frac{\chi}{2}}\left[e^{i\frac{\varphi}{2}}\cos(\theta/2)\,|0\rangle + e^{-i\frac{\varphi}{2}}\sin(\theta/2)\,|1\rangle\right], \tag{4.2}$$

where n is the norm of the wavefunction, which is usually set to 1, and where χ is the total phase which is usually ignored because it cannot be measured by any quantum mechanical process. To define the time evolution of this wavefunction we introduce a generator for time translations G [62]. In its most general form, this generator is just a complex 2x2 matrix in the basis $\{|0\rangle, |1\rangle\}$, with eight independent real entries:

$$G = \begin{pmatrix} \alpha_R + i\alpha_I & \beta_R + i\beta_I \\ \gamma_R + i\gamma_I & \delta_R + i\delta_I \end{pmatrix}. \tag{4.3}$$

The Hermitian part of this generator will coincide with the usual Hermitian quantum mechanical Hamiltonian H, while the remaining non-Hermitian (and possibly even non-linear) part should lead to the non-unitary collapse dynamics. The time

evolution of the wavefunction can be generated from the definition of G by looking at the infinitesimal time translation of $|\psi_0\rangle$

$$\begin{aligned} |\psi_\epsilon\rangle &= e^{i\epsilon G}|\psi_0\rangle \\ &= \left(1 + i\epsilon G + O\left(\epsilon^2\right)\right)|\psi_0\rangle \\ &\equiv Ne^{i\frac{X}{2}}\left[e^{i\frac{\Phi}{2}}\cos\left(\Theta/2\right)|0\rangle + e^{-i\frac{\Phi}{2}}\sin\left(\Theta/2\right)|0\rangle\right]. \end{aligned} \tag{4.4}$$

Here ϵ is an infinitesimally small parameter that measures time. The parameters N, X, Φ and Θ defining the new wavefunction at time $t = \epsilon$ are written in terms of the old parameters n, χ, φ and θ at time $t = 0$, and are defined to first order in ϵ. It is now easy to extract the time evolution of these parameters using the definition of the time derivative. The time derivative of for example n is given by the limit $\epsilon \to 0$ of $(N - n)/\epsilon$. After some algebra this implies that

$$\begin{aligned} \dot{\theta} &= (\alpha_I - \delta_I)\sin(\theta) + 2\left(\beta_I\cos(\varphi) - \beta_R\sin(\varphi)\right)\sin^2(\theta/2) \\ &\quad -2\left(\gamma_I\cos(\varphi) + \gamma_R\sin(\varphi)\right)\cos^2(\theta/2) \\ \dot{\varphi} &= (\alpha_R - \delta_R) + \left(\beta_R\cos(\varphi) + \beta_I\sin(\varphi)\right)\tan(\theta/2) \\ &\quad -\left(\gamma_R\cos(\varphi) - \gamma_I\sin(\varphi)\right)\cot(\theta/2) \\ \dot{\chi} &= (\alpha_R + \delta_R) + \left(\beta_R\cos(\varphi) + \beta_I\sin(\varphi)\right)\tan(\theta/2) \\ &\quad +\left(\gamma_R\cos(\varphi) - \gamma_I\sin(\varphi)\right)\cot(\theta/2) \\ \dot{n} &= -\alpha_I\cos^2(\theta/2) - \delta_I\sin^2(\theta/2) + 1/2\left(\beta_R - \gamma_R\right)\sin(\varphi)\sin(\theta) \\ &\quad -1/2\left(\beta_I + \gamma_I\right)\cos(\varphi)\sin(\theta). \end{aligned} \tag{4.5}$$

Notice that in the case of purely unitary time evolution, generated by a purely Hermitian generator G, the derivatives simplify considerably, and become identical to the usual quantum mechanical time evolution

$$\begin{aligned} \dot{\theta} &= 2\left(\beta_I\cos(\varphi) - \beta_R\sin(\varphi)\right) \\ \dot{\varphi} &= (\alpha_R - \delta_R) - 2\left(\beta_R\cos(\varphi) + \beta_I\sin(\varphi)\right)/\tan(\theta) \\ \dot{\chi} &= (\alpha_R + \delta_R) + 2\left(\beta_R\cos(\varphi) + \beta_I\sin(\varphi)\right)/\sin(\theta) \\ \dot{n} &= 0. \end{aligned} \tag{4.6}$$

4.1.2 Specific Time Evolutions

It is clear from the time derivatives (4.5) that the total phase and norm variables do not influence the time evolution of the superposition state as long as the generator G does not explicitly depend on them. We can thus study the time evolution by considering only the variables φ and θ. Their time evolution can be visualized as a flow on the Bloch sphere (see figure 4.1). Each flowline on the sphere then represents the path traced out by the time evolution of an initial state somewhere along

the path. As long as the time evolution is purely unitary, and the generator G thus purely Hermitian, the flow pattern is in fact always the same: it consists of rotations around an axis spanned by the two eigenstates of the Hamiltonian, as depicted in figure 4.2. These eigenstates are always on opposite poles, and their rotation away from the north and south pole depends on the rotation of the Hamiltonian away from being a diagonal operator.

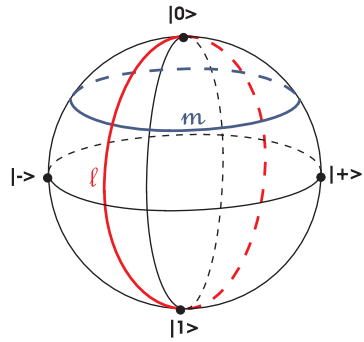

Figure 4.1: The Bloch sphere. The line m is a line of constant θ, while l has constant φ. The states $|\pm\rangle$ are defined as $\sqrt{1/2}\,[|0\rangle \pm |1\rangle]$.

Hamiltonian Flow

As an example, let's consider the Hamiltonian with $\beta_R = \gamma_R = t$ and all other entries zero. Notice that t represents a mixing parameter here, not time. The time derivatives (4.5) in this case reduce to

$$\begin{aligned} \dot{\theta} &= -2t \sin(\varphi) \\ \dot{\varphi} &= -2t \cos(\varphi) / \tan(\theta) \\ \dot{\chi} &= 2t \cos(\varphi) / \sin(\theta) \\ \dot{n} &= 0. \end{aligned} \tag{4.7}$$

As mentioned before, we are really only interested in the explicit time evolution of φ and θ. To find a closed form for the description of the flowlines it is useful to notice that $\partial_\theta \left[\dot{\theta} \sin(\theta)\right] = -\partial_\varphi \left[\dot{\varphi} \sin(\theta)\right]$. This implies that the set of differential equations that we're trying to solve is a so called exact set of ordinary differential equations [135], and that we can solve it by looking for a potential V which obeys

$$\begin{aligned} -\partial_\theta V &= \dot{\varphi} \sin(\theta) \\ \partial_\varphi V &= \dot{\theta} \sin(\theta)\,. \end{aligned} \tag{4.8}$$

This set of equations is easily solved, and yields the potential $V = 2t\cos(\varphi)\sin(\theta)$. The streamlines describing the flow on the Bloch sphere are lines of constant potential V, which are given by

$$\cos(\varphi)\sin(\theta) = \text{ constant.} \tag{4.9}$$

The flow therefore is a rotation around the axis through the north and south poles at $\sqrt{1/2}\,[|0\rangle \pm |1\rangle]$, as seen in figure 4.2. These are of course also precisely the eigenstates of the Hamiltonian. The flow in circles around the poles (for example the one starting out at $|0\rangle$) is what we usually refer to as Rabbi oscillations.

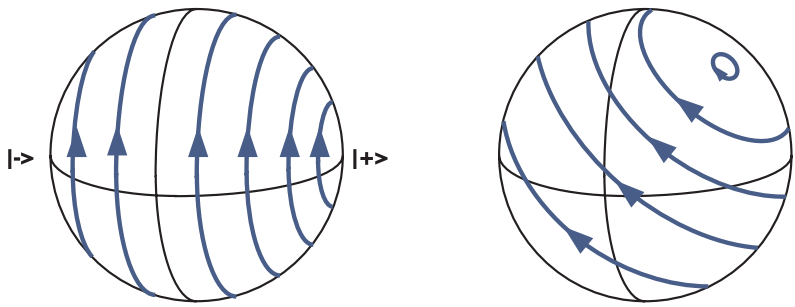

Figure 4.2: Left: the flow as described by equations (4.7). Right: the flow pattern of some general Hamiltonian generator of time evolution.

General Non-Hermitian Terms

In addition to the Hamiltonian part of G we could also include non-Hermitian terms in the definition of the generator of time evolution. In general these terms can lead to many different possible flow patterns on the Bloch sphere. However, if we leave out the Hamiltonian part of G and only consider the non-unitary time evolution for a moment, then we can identify three main types of behavior for simple non-Hermitian terms in the time evolution generator.

Terms of the type $\alpha_I = \delta_I \neq 0$, add nothing to the time evolution of the superposed state, and only influence the norm of the wavefunction. Terms of the type $\alpha_I = -\delta_I \neq 0$ and rotations thereof (like $\beta_R = -\gamma_R$ or $\beta_I = \gamma_I$) cause a flow from one pole to the opposite pole. That is, one the poles becomes a source and the opposite a sink for the flowlines. Finally, asymmetric terms like $\beta_R \neq 0$, $\gamma_R = 0$, give rise to asymmetric flows through a saddle point with flowlines both emerging from them and disappearing into them, as shown in figure 4.3.

All of these types of flow can of course be combined with one another, and with the usual Hermitian flow patterns. We find that usually a simple addition of the involved velocity vectors tangent to the Bloch sphere gives a good indication of

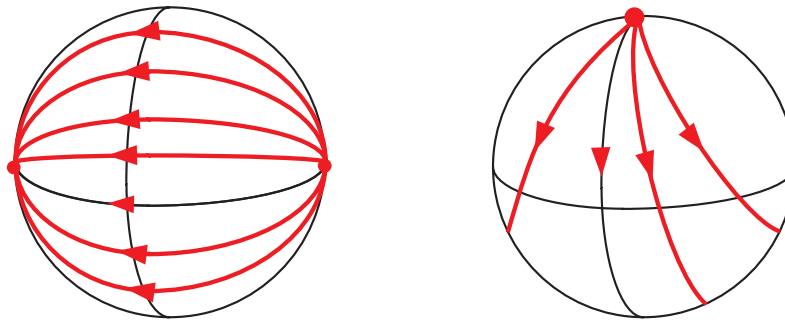

Figure 4.3: Left: the flow of the type $\alpha_I = -\delta_I \neq 0$. Right: the flow of the type $\beta_R \neq 0$, $\gamma_R = 0$.

what the flow will then look like. Many much more complicated flow patterns can be formed if we allow the matrix elements of G to be non-linear as well as non-Hermitian.

Schrödinger-Newton

One such a non-linear term which we would like to consider is the one given by the Schrödinger-Newton equation (4.1) [29]. The total energy operator introduced in the Schrödinger-Newton equation for a superposition of mass over two distinct positions $|x = 0\rangle$ and $|x = 1\rangle$ is

$$G = \begin{pmatrix} U\,(x=0) & t \\ t & U\,(x=1) \end{pmatrix}, \tag{4.10}$$

where the gravitational potential $U(x)$ is given by $\nabla^2 U(x) = \gamma\,|\langle\psi\ |x\rangle|^2$. For simplicity we will absorb the constant γ into the norm of the wavefunction, and again ignore the dynamics of that norm. We will also take out the normal Hamiltonian part of G by setting $t = 0$. After all, the collapse process should be caused by the non-unitary part of the time evolution.

To solve for the gravitational potential while avoiding the infinite self energy of a point particle, we will consider the states labeled by x to represent a mass distribution stretched out over an infinite sheet in the y, z-plane, but completely localized in the x-direction[1]. The superposition thus achieved should be a good description of for example a large block of mass which is superposed over a distance small compared to its own length, such as the one shown in figure 3.2. Using appropriate boundary conditions for the gravitational potential and completely ignoring

[1] For a description of the spacetime metric associated with such an infinite plane, see the Appendix F.

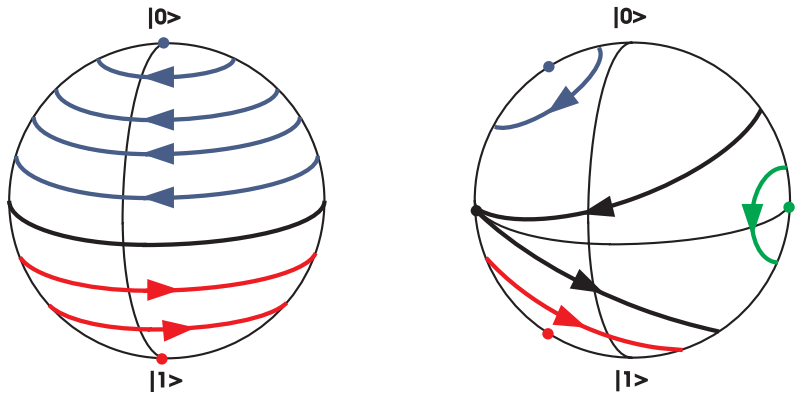

Figure 4.4: Left: the flow as defined by the generator G of equation (4.10), with t set to zero. Right: the flow defined by the Schrödinger-Newton equation, including the kinetic energy.

the norm of the wavefunction, the essential part of the time evolution generator reduces to

$$G = \begin{pmatrix} -\cos(\theta) & 0 \\ 0 & \cos(\theta) \end{pmatrix}. \tag{4.11}$$

Clearly the matrix G is a non-linear operator, because it depends on the value of the parameter θ which defines the state on which G acts. On the other hand G is still akin to a Hermitian matrix in the sense that its transpose equals its complex conjugate. The flow pattern associated with this generator is easily found to consist of circular flowlines around the north and south pole. In contrast with the usual Hamiltonian flow though, the circulation on the northern hemisphere is in the opposite direction of its southern counterpart (see figure 4.4). The gravitational term has thus introduced a division between the northern and the southern hemisphere, but it has not caused any sinks or sources to appear on the Bloch sphere, and it is thus inadequate as a dynamical description of the quantum collapse model. Even if we reintroduce the mixing parameter t, this will only distort the flow lines from their perfectly circular orbits and produce some sort of a tennis ball flow pattern as depicted in figure 4.4. However, it does not introduce any sources or sinks that would represent the final states in a collapse process.

Alternative Gravitational Terms

The lack of sources and, more importantly, sinks in the flow pattern associated with the Schrödinger-Newton equation implies that it cannot be used as a description of

the dynamical process of wavefunction collapse. We can however, use the knowledge of the types of patterns caused by non-Hermitian terms to try and introduce sinks into the dynamics by slightly altering the Schrödinger-Newton equation. The simplest way to do so would be to turn the gravitational self energy term into an imaginary energy. What the exact physical meaning of such a term would be is unclear at the moment, but its form suggests that it could be a dissipation term induced into quantum mechanics by gravity. For now we will not consider the justification of the non-unitary dynamics, but merely study the implications of having a generator of time evolution given by

$$G' = \begin{pmatrix} -i\cos(\theta) & 0 \\ 0 & i\cos(\theta) \end{pmatrix}. \tag{4.12}$$

The flowlines generated by this matrix all lie along the meridian and the flow goes north on the northern hemisphere, while it goes south on the southern hemisphere (see figure 4.5). Thus all states starting out above the equator will eventually collapse onto the north pole, and all states south of the equator find their destination on the south pole. If we introduce a normal, real quantum mechanical energy into the dynamics as well, then these straight flowlines will turn into spirals which flow around the north-south axis as well as toward one of the poles. The dynamics thus has two of the three properties expected of a working model for the quantum collapse process. It identifies the states into which a superposition can collapse (the poles) by making sure that spatial superpositions disappear. At the same time it explains why microscopic superpositions can exist while macroscopic superpositions are never seen: the spiraling motion for microscopic particles is extremely close to perfect circular motion because the mass of the particles is small compared to their usual quantum mechanical potential and kinetic energy. On the other hand the gravitational term dominates for macroscopic objects, and thus their superposition states will be destroyed in a very short time.

As it is, the time evolution defined by G' cannot be used to reproduce Born's rule. A state on the northern hemisphere will always collapse onto the north pole and never onto the south pole. The only way to cure this problem is to introduce a random variable into the dynamics. Because the total phase of a quantum mechanical state can never be measured it seems natural to take its value as a random variable. We introduce it into the altered Schrödinger-Newton equation so that the time evolution generator becomes

$$G'' = \begin{pmatrix} -i\left[\cos(\theta) + f(\chi)\right] & 0 \\ 0 & i\left[\cos(\theta) + f(\chi)\right] \end{pmatrix}. \tag{4.13}$$

Here $f(\chi)$ is some function of the total phase that will be chosen to make the dynamics agree with Born's rule. The flow pattern of this adjusted G'' is the same as the flow pattern we found before for G', only now the seperatrix between streaming northward and streaming southward lies not at the equator but at the line

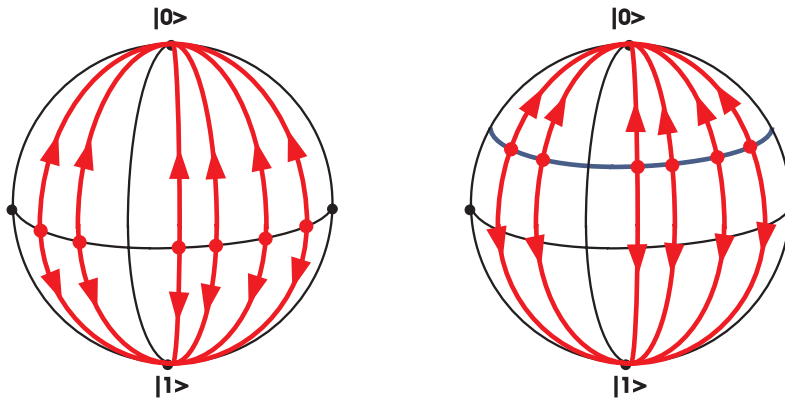

Figure 4.5: Left: the flow as defined by the generator G' of equation (4.12). Right: the flow defined by the adjusted generator G'' of equation (4.13).

$\cos(\theta) = -f(\chi)$ (see figure 4.5). If we assume χ to be taken at random from a flat distribution between 0 and 2π, then it is easily checked that the dynamics agrees perfectly with Born's rule if we set $f(\chi) = \chi/\pi - 1$.

We have thus found a model that describes the collapse of a quantum mechanical superposition over two different states; that distinguishes between microscopic and macroscopic superpositions; and that results in the emergence of Born's rule if it is repeated many times with the same initial conditions, but a random total phase variable.

4.2 A Three State Measurement

Although the model seems to work very well for describing the collapse of a two-state measurement, it cannot truly be adopted as a possible scenario for the solution of the measurement problem unless it also works for general superpositions. The first step toward testing the model for such a general quantum collapse is to ensure that it works for a wavefunction superposed over three states instead of just two. To do so we can simply repeat the analysis of the previous section, but now use the initial state

$$\begin{aligned} |\psi_0\rangle \;=\; & n e^{i\frac{\chi}{2}} \Big[e^{i\frac{\varphi+\phi}{2}} \cos(\theta/2)\cos(\eta/2)\,|0\rangle + e^{i\frac{\varphi-\phi}{2}} \cos(\theta/2)\sin(\eta/2)\,|1\rangle \\ & + e^{-i\frac{\phi-\varphi}{2}} \sin(\theta/2)\,|2\rangle \Big]. \end{aligned} \tag{4.14}$$

If we also use a 3x3 matrix for the time evolution generator, then the computation of the time derivatives of θ, η and so on is exactly analogous to the two state case.

To see what the effect of our modified Schrödinger-Newton time evolution G'' is in this case, we consider the states $|0\rangle$, $|1\rangle$ and $|2\rangle$ to represent infinitely high columns of mass, positioned on the vertices of an equilateral triangle in the x, y-plane. That way we find that the gravitational potential, up to constant prefactor, is given by

$$\begin{aligned} \nabla^2 U\left(|x\rangle\right) &\propto |\langle\psi|\, x\rangle|^2 \\ \Rightarrow U\left(|0\rangle\right) &\propto 1 - 3\cos^2\left(\theta/2\right)\cos^2\left(\eta/2\right) \\ U\left(|1\rangle\right) &\propto 1 - 3\cos^2\left(\theta/2\right)\sin^2\left(\eta/2\right) \\ U\left(|2\rangle\right) &\propto 1 - 3\sin^2\left(\theta/2\right). \end{aligned} \tag{4.15}$$

Using these values we can then define the 3x3 generator of time evolution G'' in analogy with equation (4.13) by setting $\langle x|\, G''\, |x\rangle = i\left(U\left(|x\rangle\right) + f_x\left(\chi\right)\right)$. In analogy to the two state time evolution, we have introduced a function f which depends on the total phase variable and which is designed to generate the randomness we need to be able to agree with Born's rule. The time derivatives which describe the flow of the state vector through configuration space during the time evolution defined by this G'' turn out to be

$$\begin{aligned} \dot{\theta} &= \sin\left(\theta\right)\left[a\cos^2\left(\eta/2\right) + b - \cos\left(\theta\right) + \frac{1}{2}\cos^2\left(\theta/2\right)\sin^2\left(\eta\right)\right] \\ \dot{\eta} &= \sin\left(\eta\right)\left[a - \cos^2\left(\theta/2\right)\cos\left(\eta\right)\right], \end{aligned} \tag{4.16}$$

with $a \equiv f_0 - f_1$ and $b \equiv f_1 - f_2$. The total phase and norm of the wavefunction cannot be measured and we will thus ignore their time evolutions. The relative phases φ and ϕ turn out to be constant in time, and are therefore irrelevant for the collapse process. To visualize the flow we can use the surface of one octant of a sphere on which θ measures altitude and η latitude, so that the states $|0\rangle$, $|1\rangle$ and $|2\rangle$ are at the vertices of the surface, as shown in figure 4.6. The generic flow diagram of the equations (4.16) has a central source from which all flowlines emanate. The flowlines end either at the sinks located at the vertices of the octant or at a saddle point on one of the edges of the surface. From the saddle point the flow continues to the vertices again (see figure 4.6).

Changing the values of a and b corresponds to moving the position of the central source over the entire surface and at the same time shifting the saddle points along the edges. To be precise, the position of the fixed points are given terms of (η, θ) coordinates as

$$\begin{aligned} P_C &= \left(\arccos\left(\frac{3a}{a+2b+2}\right), \arccos\left(\frac{1+2a+4b}{3}\right)\right) \\ P_{0-1} &= \left(\arccos\left(a\right), 0\right) \\ P_{1-2} &= \left(\pi, \arccos\left(b\right)\right) \\ P_{2-0} &= \left(0, \arccos\left(a+b\right)\right). \end{aligned} \tag{4.17}$$

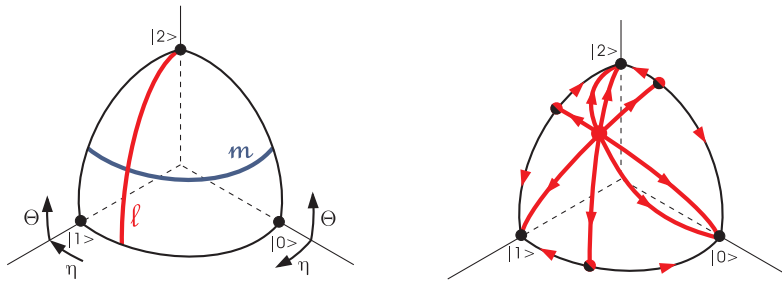

Figure 4.6: Left: the quarter of a sphere on which the three-state time evolution can be depicted. The line m is a line of constant θ while l has constant η. Right: the generic flow pattern for the flow defined by equations (4.16).

Here P_C is the central source and P_{i-j} is the saddle point on the edge connecting $|i\rangle$ with $|j\rangle$. Clearly the flow pattern for the three state superposition fulfills the first two requirements for being considered as a collapse process. The stable points (the sinks) in the flow represent precisely the three possible wavefunctions that do not involve a superposition over gravitationally distinct states, and that are therefore acceptable as possible outcomes of a quantum measurement. The time involved in getting to such a stable state is again governed by the ratio between gravitational and kinetic energy. The microscopic superpositions will thus be able to avoid collapse for a very long time, while macroscopic superpositions are doomed to collapse within moments after their creation.

4.2.1 Born's Rule

The only thing left to do is to choose the function f in such a way that repeated application of the measurement model (4.16) will yield Born's rule. As before the introduction of some random variable cannot be avoided, and again we will try and use the one random variable that quantum mechanics automatically gives us: the total phase of the wavefunction.

While writing down an Ansatz for f we should keep in mind that the three-state time evolution must reduce to the two-state time evolution which we found before in the case that the initial state happens to be on one of the edges of configuration space. This in fact implies that the saddle points on the edges must move along the edges for varying χ just like the seperatrix moved along the meridian on the two-state Bloch sphere. In addition we ought to demand that the collection of all possible flow patterns posses a 3-fold rotational symmetry in the sense that for every flow pattern in the collection there must be two more flow patterns which coincide with the original one if the vertices are interchanged in a cyclic fashion. In the end there is just one possible choice for the function f (or equivalently, for a and b) that

satisfies all of these conditions and depends only on one random variable χ. This choice is given by

$$\begin{aligned} a &= \begin{cases} -1+\frac{3\chi}{2\pi} & \text{if } \chi < \frac{4\pi}{3} \\ 5-\frac{3\chi}{\pi} & \text{if } \chi \geq \frac{4\pi}{3} \end{cases} \\ b &= \begin{cases} 1-\frac{3\chi}{\pi} & \text{if } \chi < \frac{2\pi}{3} \\ -2+\frac{3\chi}{2\pi} & \text{if } \chi \geq \frac{2\pi}{3} \end{cases} . \end{aligned} \tag{4.18}$$

This choice for a and b implies that as a function of χ the central source moves all around the perimeter of configuration space, while the saddle points move up and down their respective edges, as depicted in figure 4.7.

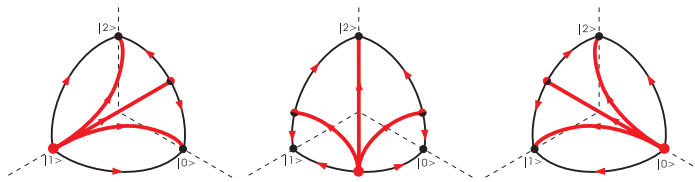

Figure 4.7: Part of the flow diagrams that are encountered as χ moves from 0 to 2π in equations (4.18).

This way we are certain that Born's rule will hold on the edges of configuration space, just like it did in the two-state superposition scenario. Whether or not it holds away from the edges is difficult to prove analytically in this case because an equation for the flow lines connecting the central source to the saddle points is not easily found. Numerically however it is rather straightforward to just do the simulated collapse many times and compare the result with the expected result of Born's rule.

As it turns out the proposed dynamics, including the definitions (4.18), do not agree with Born's rule. The difference is shown in figure 4.8. To fix the mismatch one could try other ways to define f. We could look for a different scheme in which f satisfies all necessary conditions but differs from (4.18); we could introduce a dependence of f on η or θ; or we could introduce additional random variables. We find that none of these approaches seems to work. Even the simulated solution in which we force the central source to be at a random position in configuration space for every new experiment does not yield the desired result (see figure 4.9). Moreover, the introduction of more random variables would be a rather undesirable element in the theory, because they should physically emerge from some fluctuating field for whose existence there is no experimental indication.

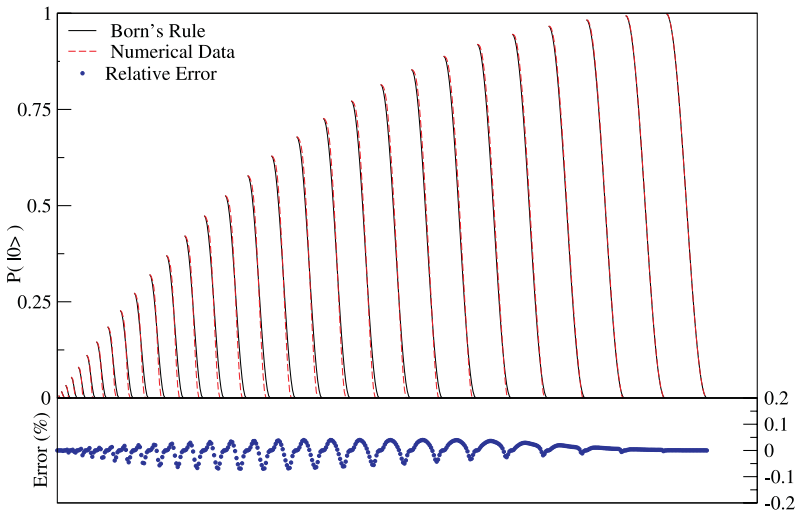

Figure 4.8: The probability for finding outcome $|0\rangle$ using the measurement scheme defined by equations (4.18). The horizontal axis consists of points in the (η, θ)-plane. Starting from $\theta = \pi$ we traverse all values of η and then move on to a lower value of θ. Iterating this procedure we display the data for all points considered sequentially on the horizontal axis. Each point in the upper part of the plot then represents the probability for ending up at $|0\rangle$, starting from some initial point (η, θ), and averaged over many values of χ (the different lines thus represent lines of constant initial θ and differing initial η). The lower plot shows the difference between the probabilities found in our model and the ones defined by Born's rule.

4.3 The Requirement of Statistics

The results discussed in this chapter clearly show that the Schrödinger-Newton equation (4.1) which was proposed by Penrose as a replacement for the quantum mechanical Hamiltonian [29] can hardly serve as a description of the dynamics of wavefunction collapse. On the other hand, a slight modification of the equation, i.e. making the gravitational potential energy appear as an imaginary term, causes the associated dynamics to show at least two of the three characteristics necessary for being considered as a possible model for quantum collapse. The modified equation causes the system to evolve toward states which are not superposed over gravitationally different positions, and thus selects the correct Pointer basis for the quantum system to collapse into. On top of this the equation naturally provides a reason for the observed difference between microscopic and macroscopic objects. Microscopic systems have a very small gravitational potential energy as compared

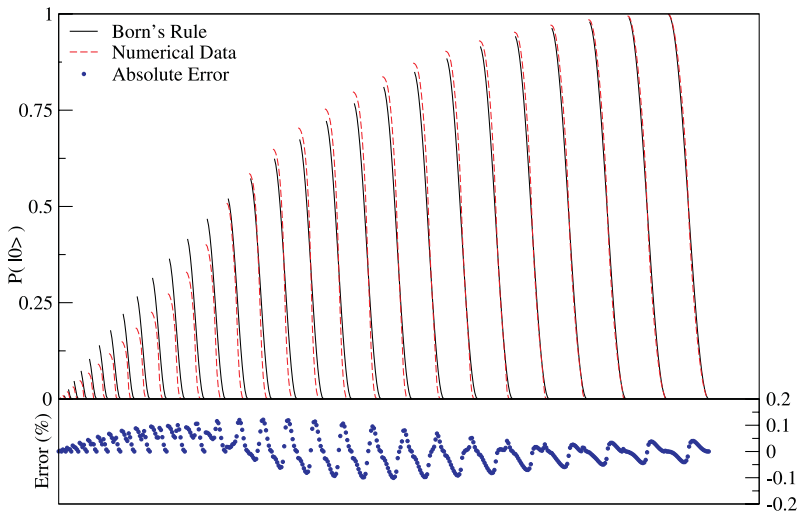

Figure 4.9: A probability plot like figure 4.8, but now for the measurement scheme in which we force the centre of the flow to be in a completely random position for each value of χ.

to their internal quantum mechanical potential and kinetic energy. The collapse process will therefore be so slow that it cannot be noticed on human timescales. On the other hand the gravitational term will dominate in the dynamics of macroscopic superposition states, and these will thus collapse before their existence can be noticed.

If the wavefunction is a sum of only two distinct states then the addition of a random variable into the dynamics rather straightforwardly leads to the desired statistics for the outcomes of measurements. As a physical source for the random variable the total phase of the wavefunction could be considered. However, as soon as the wavefunction represents a superposition over more then two states, it immediately becomes impossible to force the dynamics of the collapse model to agree with Born's rule using only one random variable. Even apart from the fact that there is no physical ground for introducing them, more than one random variable does not automatically solve the problem. At least the obvious choices of how to implement them into the theory do not yield the desired outcome.

In the end the Schrödinger-Newton equation, even in its modified forms, is thus still not fit as a complete description of the dynamical collapse process of quantum superpositions, because it seems to be impossible to make it agree with Born's rule under all circumstances.

Chapter 5

Conclusions and Outlook

The unitary time evolution dictated by quantum mechanics must break down if we do an experiment involving the interaction between a microscopic system and a macroscopic measurement device [39]. This crucial point has been recognized and emphasized by many different physicists ever since the first formulations of quantum mechanics emerged. The popular assertion that decoherence could serve as a substitute for a truly non-unitary process does not sufficiently explain the experiments on single particles, most notable of which is the Young's slits experiment with single electrons [30, 31, 35].

5.1 Penrose's Idea

It is also clear that there is a serious challenge in trying to unite quantum mechanics with the theory of general relativity. This has lead Penrose to the suggestion that gravity might introduce an instability into quantum mechanical superposition states which could perhaps be used as an explanation of the collapse process [26,27]. In this part of the thesis we have seen that the idea of gravity introducing a finite lifetime for quantum superposition should have measurable implications in principle. The practical experiments that are necessary to confirm this influence of gravity however, are out of reach of the present day experimental possibilities [28].

If gravity does cause the elusive quantum collapse process, then there should also be a dynamical description of the collapse which combines the gravitational influence with the quantum mechanical effect. As a first try for such a dynamical model we have studied the Schrödinger-Newton equation proposed by Penrose [29]. This equation, in its original form, turns out not to collapse quantum superposition states. With a slight modification we introduced collapse dynamics so that the equation singles out the correct states to collapse into. With this modification we are able to explain the difference in collapse time between microscopic

and macroscopic superpositions. We also found a simple case in which the dynamics reproduces Born's rule, but we did not find a way to generalise that result. Because of the inability to comply with Born's rule under all circumstances, the Schrödinger-Newton equation, even in its modified forms, is still not a complete model for quantum collapse.

5.2 Combining Ideas

Although the attempted combination of gravity and quantum mechanics did not immediately result in the resolution of the quantum measurement problem, it did give us some insight into the possibilities for such a description. In future research we should definitely keep on looking for possible implications of gravity's influence on quantum mechanics in different experimental setups. Perhaps with the advance of both theoretical and experimental work in that direction we could at some point measure the gravitationally induced lifetime of a quantum superposition.

At the same time we should also keep on looking for a dynamical description of the quantum collapse process. At this point an approach based on gravity seems to be an unlikely candidate for such a description, but perhaps we can combine the lessons of this part of the thesis with those of the previous part. It might very well be that quantum collapse is really a symmetry breaking effect in which an infinitesimally small non-unitary field is still able to cause the collapse of a quantum superposition as long as the involved number of particles is close to the thermodynamic limit. One could for example study the time evolution generated by

$$G = H + iB\,\langle X\rangle\,, \tag{5.1}$$

where H is a quantum Hamiltonian which can spontaneously break some continuous symmetry, X is the operator measuring the associated order parameter, and B the field conjugate to the order parameter. If the time evolution G reduces quantum superpositions to pointer states instantaneously in the limit $\lim_{B\to 0}\lim_{N\to\infty}$, then it could be seen as a description of 'spontaneous collapse'.

This setup naturally provides a distinction between the microscopic and the macroscopic world. It also provides a natural way of introducing some randomness because the orientation of X can be chosen randomly, and independently of the symmetry breaking field in H itself. Whether this randomness is enough to lead to Born's rule, and even whether G can select the right set of pointer states in the first place, remains to be investigated.

Part V

Epilogue

Chapter 1

Summary

Quantum Mechanics is arguably the must successful physical theory of the last century. Using quantum mechanics we can explain physical phenomena all the way from the behavior of elemental particles to the bulk properties of macroscopic objects [13, 62]. Despite this apparent triumph the theory still is seen by many people as a mysterious theory, shrouded in clouds of unexplainable effects. All of these feelings of unease eventually turn out to be based on the simple fact that although the world around us is supposed to be built up out of quantum mechanical building blocks, the classical world itself does not seem to follow the rules of quantum mechanics.

In this thesis I have discussed both some examples of how Quantum Mechanics influences the properties of the Big World, and an idea of how quantum mechanics could eventually be forced to break down

1.1 Quantum Mechanics in the Big World

As an example of the necessity to use quantum mechanics in order to be able to describe bulk material properties, I have chosen to take a closer look at the titanium pyroxene compound $NaTiSi_2O_6$ [19, 20]. Experimentally it has been shown that this material undergoes a magnetic transition at 210 K [21]. At the same temperature there is also evidence that something happens to the crystal structure of the material: the phonon properties undergo a sudden change and X-ray diffraction experiments show that some form of dimerization must occur. Soon after these experimental results were published it was already suggested that the interplay between the orbital and magnetic degrees of freedom of the titanium atoms could explain the coupled magnetic and structural transitions [22]. Numerical simulations however showed that the orbitals might be severely restricted by the surrounding

crystal field, which would strongly suppress the possibility of a coupled transition to occur [71–73].

In our study of the material we have used three different theoretical approaches to show that the orbital-assisted Peierls transition could occur in $NaTiSi_2O_6$, despite the presence of a sizable crystal field [19]. The orbital-assisted Peierls transition is a transition in which the spins on the one dimensional zig-zag chains of titanium atoms start to pair up and form magnetic singlet states precisely at the temperature at which the orbital degrees of freedom start to uniformly align. The transition is shown to be driven by combined quantum fluctuations of the orbital and the spin sector. Using our results we are able to explain all of the observed effects in the material, and we can distill a prediction for the actual size of the crystal field splitting in $NaTiSi_2O_6$ [19, 20].

We have thus shown that the novel orbital-assisted Peierls transition is not only still a feasible scenario for the titanium pyroxene compound, but in fact the only way in which all of the available experimental and numerical data can be combined and explained. This also shows that indeed the quantum mechanical properties of the constituent particles (the orbital and spin degrees of freedom and their quantum fluctuations) are a necessary ingredient to explain the bulk thermodynamical properties of the macroscopic material. It is therefore one of the many, many ways in which Quantum Mechanics manifests itself in the Big World.

1.2 Quantum Mechanics of the Big World

Having firmly established that quantum mechanics is the correct way to describe microscopic particles, and having seen that the quantum properties of their constituent particles dictate the behavior of macroscopic materials in the Big World, one may begin to wonder why our everyday world does not look *more* quantum mechanical. One of the defining properties of quantum mechanics is the extremely powerful role of symmetry. If space is homogeneous and isotropic, then a quantum object in that space can see no reason to value one place over another, and thus it will spread out into a superposition state that covers all the equivalent points in space. Extending this type of reasoning to the world around us, it could be argued that because a classical object (say a chair) is made entirely out of quantum mechanical building blocks, the chair itself should obey the basic laws of the quantum theory as well. Thus a chair in a homogeneous room should spread out all over the available empty space. Clearly this does not happen in reality.

The way out of this paradoxical situation is the process of spontaneous symmetry breaking [51]. It can be shown that the symmetric wavefunction of a body becomes increasingly unstable as the number of constituent particles grows. The chair with its wavefunction spread out all over the room is therefore extremely unstable, and even only an infinitesimally small symmetry breaking field will suffice to

localize it [124]. Thus the very fact that the chair seems to be classical and can avoid the power that quantum mechanics gives to symmetry, is really a quantum effect.

The implication of this way of spontaneously breaking a continuous symmetry is that there is a remnant of the quantum origin left over in all classical objects. This remnant, the so called thin spectrum, consists of a set of eigenstates which are extremely close to the groundstate. Such a dense set of low lying states can in principle be very dangerous to the coherence of qubits [24]. We have shown that the symmetry breaking in crystals and antiferromagnets indeed gives rise to a decoherence effect if these systems are used as qubits. The resulting decoherence time turns out to be a universal timescale that is completely independent of the details of the underlying microscopic model [23, 25].

It is often thought that because Elitzur's theorem forbids the spontaneous breaking of local gauge [107] symmetry, the superconducting state should not be characterized by a spontaneously broken symmetry. We have shown that in fact a superconductor has a spontaneously broken *global* symmetry in its classically realized state. The breaking of this total phase symmetry again requires the existence of a thin spectrum in superconductors. The decoherence time associated with the thin spectrum of superconducting qubits coincides with the universal timescale that we found before for antiferromagnets and crystals. The expected decoherence time for the superconducting Cooper box qubits that are used in contemporary experiments however, is still well above the decoherence time that is caused by the usual thermal environment of the qubits [79, 83].

With the advance of technology and the improvements of the thermal isolation of superconducting qubits it is well possible that the decoherence effects caused by the thin spectrum will be observable in the foreseeable future. The demonstration of this type of decoherence would also be a clear demonstration of the quantum mechanical behavior of an object which we would normally call classical. It is thus a way to probe the Quantum Mechanics of the Big World itself.

1.3 Quantum Mechanics or the Big World

Even though quantum mechanics reduces itself to classical physics in the thermodynamic limit by the process of spontaneous symmetry breaking, there is still a need for an additional process that can reduce macroscopic superpositions to the more usual states which we see in the everyday world. This quantum collapse process is an absolutely necessary addition to quantum mechanics because the unitarity of the quantum theory clearly contradicts the experimental observations during the act of measurement. Spontaneous symmetry breaking cannot cure this problem [25], and neither can the popular invocation of decoherence [18].

There have been many proposals for what physical phenomenon can cause the onset of the quantum collapse process [15, 52–60]. None of these have yet resulted

in a measurable prediction that could validate or falsify the theory. There is however one recent idea due to Roger Penrose who suggested that general relativity could cause spatial quantum superpositions to become unstable [26, 27]. Based on some very general arguments, Penrose showed that this gravitationally induced instability should manifest itself in a maximum lifetime for these superposition states that is of the order of the inverse gravitational self energy of the difference between the superposed mass distributions [26]. The typical collapse time thus calculated turns out to be extremely large for all quantum mechanical systems that have been studied experimentally, and extremely small for all macroscopic objects in physical experiments. The mass size at which the collapse process would take place within a measurable time has not been targeted by any experiments yet [27, 28].

As an example of a system which could in principle have a measurable collapse time according to Penrose's idea, we have studied the flux qubit. In this setup there is a superposition of a supercurrent which flows both clockwise and counterclockwise [78, 80, 81]. After taking into account the additional condition that the entire flow must collapse as soon as one of its constituent parts decides to collapse, we found that the collapse time for this particular setup would come into the measurable range only for some rather extreme specifications of the device. It is not inherently impossible to measure the gravitationally induced collapse this way, but it will be a tough experimental challenge to do so.

Apart form the issue of whether or not the gravitationally induced collapse can take place within a measurable time, we are also faced by the remaining question of what exact mechanism will direct the quantum collapse process. In his proposal Penrose has suggested that the so called Schrödinger-Newton equation could be used to find the stable states into which quantum superpositions can collapse [29]. If we take this equation for the total energy at face value and try to use it as a generator for the time evolution of a macroscopic superposition, then we have shown that it could never lead to collapse. With some slight modifications however, the dynamics can lead to the reduction of macroscopic superposition states to localized, classical states while leaving microscopic superpositions intact for all observable times. Unfortunately the theory cannot reproduce Born's rule which predicts the statistics of the possible outcomes of measurement. It therefore seems impossible to use the Schrödinger-Newton equation as a model for the quantum collapse process.

Despite this setback the study of the dynamics involved does suggest that perhaps it is possible to come up with a way to combine the story of spontaneous symmetry breaking with that of quantum collapse. Using the insights gained in this study of the subjects it may be possible to construct a process in which some unitarity-breaking field could lead to the spontaneous collapse of quantum states in the thermodynamic limit. This spontaneous collapse process is thus envisaged as the ultimate umpire in the choice between Quantum Mechanics or the Big World.

Appendices

A: The Relation between Decoherence and the Quantum Measurement Problem

Having seen the interaction between the Lieb-Mattis antiferromagnet and a two spin singlet, and the subsequent decoherence, one could be tempted to claim that what we found is a description of a quantum measurement process. Indeed we started out with a macroscopic, symmetry broken, classical state (the antiferromagnet) and coupled it to a microscopic spin state. The classical mixed state that we end up with at times $t > t_{\text{spon}}$ seemed to consist only of states with either zero or two magnons, since the off-diagonal matrix elements which mix the two states had disappeared. It should be noted however, that this is not enough to constitute a description of quantum measurement. If we consider the coupling of a single two-spin singlet to the antiferromagnet, then the calculations imply that the resulting state is a macroscopic superposition of zero and two magnon states, which in fact remains coherent forever. The apparent reduction to a classical mixture of states is due to the fact that we choose to trace away a certain portion of the available Hilbert space (i.e., the thin spectrum). This leads to decoherence. If we were to wait long enough, the unitarity of quantum mechanical time evolution guarantees that after a time t_{rec} the original quantum superposition of zero and two magnons shows up again. Since t_{rec} turns out to be a very long time, one could be tempted to make the case that for all practical purposes our description gives the same result as a true measurement process would give. This is not so. It should always be kept in mind that decoherence of states, as we have here, is very different from a projection of states. Projections are non-unitary. A single quantum measurement is a projection of the wave function. The statistical interpretation of quantum mechanics of course circumvents this problem: ensembles of our decohered states and ensembles of measured states have exactly the same density matrix. However, if one aims to describe a single measurement then decoherence cannot explain the projection of states that is seen to take place experimentally.

B: The Thermodynamic Weight of Thin Spectrum States

It is easy to show that the contribution of the thin spectrum of the symmetric N-spin Lieb-Mattis Hamiltonian to the free energy density is proportional to $\frac{\ln N}{N}$ and thus vanishing in the thermodynamic limit. The energy of a state with total spin S is $E_{\text{thin}} = JS(S+1)/N$ and its degeneracy is $2S+1$, so that the contribution of the thin states to the partition function is

$$\begin{aligned} Z_{\text{thin}} &= \sum_{S=0}^{N} (2S+1)\, e^{-\beta E_{\text{thin}}} \\ &\approx \int_0^N (2S+1)\, e^{-\frac{\beta J}{N} S(S+1)} dS \approx \frac{N}{\beta J}, \end{aligned} \tag{B-1}$$

in the limit of large N. Therefore its total contribution to the free energy is $F_{\text{thin}} = -T \ln Z_{\text{thin}} \propto -\ln N$ and for large N its contribution to the free energy per spin –and the free energy density– is proportional to $\frac{\ln N}{N}$.

C: The Orderparameter in the Symmetry Broken State

Consider the symmetry broken Lieb-Mattis Hamiltonian:

$$H = \frac{2J}{N} \mathbf{S}_A \cdot \mathbf{S}_B - B\left(S_A^z - S_B^z\right). \tag{C-1}$$

If the number of spins N is large, then the eigenfunctions $|n\rangle$ of this Hamiltonian are to a very good approximation given by the eigenfunctions of (half of) a harmonic oscillator:

$$\begin{aligned} |n\rangle &= \sum_S u_S^n |S\rangle \\ &= \sum_S \sqrt{\frac{\sqrt{\omega}}{\sqrt{\pi} 2^{n-1} n!}} e^{-\frac{1}{2}\omega S^2} H_n\left(\sqrt{\omega} S\right) |S\rangle, \end{aligned} \tag{C-2}$$

where $|S\rangle$ are the total spin eigenstates, H_n are the Hermite polynomials, ω equals $\frac{2}{N}\sqrt{\frac{J}{B}}$, and n can only be an odd integer number. Using this exact expression to calculate the ground state expectation value of the order parameter, we find:

$$\begin{aligned} \left\langle S_A^z - S_B^z \right\rangle &= \sum_{S,S'} u_S^1 u_{S'}^1 \left\langle S' \right| S_A^z - S_B^z \left| S \right\rangle \\ &= 2 \sum_S u_S^1 u_{S-1}^1 \sqrt{\frac{\left((N/2+1)^2 - S^2\right) S^2}{4S^2 - 1}}. \end{aligned} \tag{C-3}$$

The shape of the function u_S^1 guarantees that $S \ll N$, so that for large N the expectation value is approximately given by:

$$\begin{aligned} & \frac{N}{2}\int_1^\infty \sqrt{\frac{16}{\pi}}\omega^{3/2} S e^{-\frac{1}{2}\omega S^2}\,(S-1)\,e^{-\frac{1}{2}\omega(S-1)^2} dS \\ = \;& \frac{N}{2}\left[e^{-\frac{1}{4}\omega}\left(1-\frac{1}{2}\omega\right)\left(1-\mathrm{erf}\left(\sqrt{\frac{\omega}{4}}\right)\right)+\sqrt{\frac{\omega}{4}}e^{-\frac{1}{2}\omega}\right] \\ = \;& \frac{N}{2}e^{-\sqrt{\frac{J}{B}}\frac{1}{2N}}+O(1), \end{aligned} \tag{C-4}$$

which reduces to the classically expected order parameter in the thermodynamic limit. Note that in this expression it is immediately clear that the limit of vanishing symmetry breaking field does not commute with the limit of infinitely many spins: they form a singular limit.

D: Sublattice Spin Matrix Elements

By expressing the matrix elements of all components of the spin operators $\mathbf{S}_A$ and $\mathbf{S}_B$ in terms of Clebsch-Gordon coefficients, one can evaluate them by performing the appropriate summations. The resulting matrix elements are:

$$\begin{aligned} & \left\langle S'_A S'_B S' M' \left| S_A^{\pm} \right| S_A S_B S M \right\rangle = \\ & \delta_{S'_A,S_A}\delta_{S'_B,S_B}\delta_{M',M\pm1}\cdot \\ & \Bigg[\mp\delta_{S',S+1}\sqrt{\frac{\left(S'^2-(S_A-S_B)^2\right)\left((S_A+S_B+1)^2-S'^2\right)(S'\pm M)(S'\pm M+1)}{4\left(4S'^2-1\right)S'^2}} \\ & +\delta_{S',S}\frac{((S_A-S_B)(S_A+S_B+1)+S(S+1))\sqrt{(S\pm M+1)(S\mp M)}}{2S(S+1)} \\ & \pm\delta_{S',S-1}\sqrt{\frac{\left(S^2-(S_A-S_B)^2\right)\left((S_A+S_B+1)^2-S^2\right)(S\mp M)(S\mp M-1)}{4\left(4S^2-1\right)S^2}}\Bigg] \end{aligned} \tag{D-1}$$

$$\begin{aligned} & \left\langle S'_A S'_B S' M' \left| S_A^{z} \right| S_A S_B S M \right\rangle = \\ & \delta_{S'_A,S_A}\delta_{S'_B,S_B}\delta_{M',M}\Bigg[\delta_{S',S+1}\sqrt{\frac{\left(S'^2-(S_A-S_B)^2\right)\left((S_A+S_B+1)^2-S'^2\right)\left(S'^2-M^2\right)}{4\left(4S'^2-1\right)S'^2}} \\ & +\;\delta_{S',S}\frac{((S_A-S_B)(S_A+S_B+1)+S(S+1))M}{2S(S+1)} \\ & +\delta_{S',S-1}\sqrt{\frac{\left(S^2-(S_A-S_B)^2\right)\left((S_A+S_B+1)^2-S^2\right)\left(S^2-M^2\right)}{4\left(4S^2-1\right)S^2}}\Bigg] \end{aligned} \tag{D-2}$$

$$\begin{aligned}&\left\langle S'_A S'_B S' M' \left| S_B^{\pm} \right| S_A S_B S M \right\rangle = \\ &-\left\langle S'_A S'_B S' M' \left| S_A^{\pm} \right| S_A S_B S M \right\rangle + \delta_{S',S} \sqrt{(S \pm M + 1)\,(S \mp M)}\end{aligned} \tag{D-3}$$

$$\begin{aligned}&\left\langle S'_A S'_B S' M' \left| S_B^{z} \right| S_A S_B S M \right\rangle = \\ &-\left\langle S'_A S'_B S' M' \left| S_A^{z} \right| S_A S_B S M \right\rangle + M \delta_{S',S}.\end{aligned} \tag{D-4}$$

E: The Bogoliubov Transformation

We have used a Bogoliubov transformation to diagonalize bosonic bilinear Hamiltonians of the form

$$H = \sum_k A_k b_k^\dagger b_k + \frac{B_k}{2}\left(b_k b_{-k} + b_k^\dagger b_{-k}^\dagger\right), \tag{E-1}$$

where $A_{-k} = A_k$ and $B_{-k} = B_k$. The relevant transformed bosons $\beta_k^\dagger$ are defined through

$$\begin{aligned}b_k^\dagger &= \cosh(u_k)\beta_{-k}^\dagger - \sinh(u_k)\beta_k, \\ b_{-k} &= \cosh(u_k)\beta_k - \sinh(u_k)\beta_{-k}^\dagger.\end{aligned} \tag{E-2}$$

The parameters u_k obey $u_k = u_{-k}$ and are chosen such that the Hamiltonian reduces to diagonal form. This implies that

$$\begin{aligned}\cosh(2u_k) &= \frac{A_k}{\sqrt{A_k^2 - B_k^2}}, \\ \sinh(2u_k) &= \frac{B_k}{\sqrt{A_k^2 - B_k^2}} \quad \text{and} \\ H &= \sum_k \sqrt{A_k^2 - B_k^2}\left(\beta_k^\dagger \beta_k + \frac{1}{2}\right) - \frac{1}{2}A_k.\end{aligned} \tag{E-3}$$

We can also use the exact same definition of u_k to diagonalize the Hamiltonian

$$H = \sum_k A_k\left(a_k^\dagger a_k + b_k^\dagger b_k\right) + B_k\left(a_k b_{-k} + a_k^\dagger b_{-k}^\dagger\right). \tag{E-4}$$

In that case the transformed bosons and Hamiltonian are given by

$$\begin{aligned} a_k^\dagger &= \cosh(u_k)\beta_{-k}^\dagger - \sinh(u_k)\alpha_k, \\ b_k^\dagger &= \cosh(u_k)\alpha_{-k}^\dagger - \sinh(u_k)\beta_k \text{ and} \\ H &= \sum_k \sqrt{A_k^2 - B_k^2}\left(\alpha_k^\dagger\alpha_k + \beta_k^\dagger\beta_k + 1\right) - A_k. \end{aligned} \tag{E-5}$$

F: The Metric of an Infinite Plane

Because we have been discussing a possible effect of general relativity on a quantum superposition of infinite planes, one might be interested in the metric which describes such an infinite plane.

In analogy with the construction of the Schwarzschild metric [136, 137], we can construct the metric for this case by demanding that a freely falling observer will measure an equation of motion for himself that coincides with the expected Newtonian dynamics for the mass distribution of the infinite plane $\rho = \rho_0\delta(x)$. As an Ansatz, let's consider the Schwarzschild-like metric given through

$$ds^2 = \gamma\,|x|\,dt^2 - \frac{1}{\gamma\,|x|}dx^2 - dy^2 - dz^2. \tag{F-1}$$

Here we have used $c = 1$ and γ is some constant with dimension m^{-1}, which will be fixed later on. From this definition of ds^2 we can immediately deduce both the metric $g_{\mu\nu}$ and the Lagrangian L. The geodesics in turn are then given by the equation [137]

$$\frac{d}{d\sigma}\left(\frac{\partial L}{\partial \dot{x}^\mu}\right) - \frac{\partial L}{\partial x^\mu} = 0, \tag{F-2}$$

where σ is an affine parameter along the geodesic. Solving these equations for the null-geodesics yields the light ray paths

$$\gamma t = \pm\ln(|x|) + t_0, \tag{F-3}$$

while solving them for the world lines of an inertial observer yields

$$\begin{aligned} x &= \mathrm{sgn}(x)\frac{A}{\gamma}\cosh^{-2}\left(\gamma\,(t - t_0)\,/2\right) \\ &= -\mathrm{sgn}(x)\frac{\gamma}{4}\sigma^2 + B\sigma - \frac{\mathrm{sgn}(x)}{\gamma}\left(B^2 - A^2\right). \end{aligned} \tag{F-4}$$

Here A, B and t_0 are constants that can be adjusted to meet the appropriate initial conditions. A schematic depiction of some of these worldlines is shown in figure 1.1.

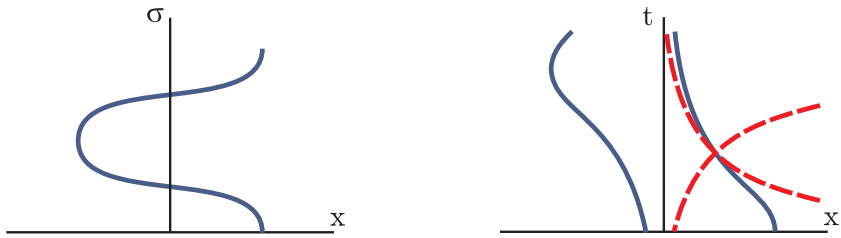

Figure 1.1: Left: the worldline followed by an inertial observer, as measured with its own eigentime σ. Right: The worldlines of inertial objects, as seen from a fixed position and using the coordinate time t. The dashed lines form the worldlines of light rays as seen by the same observer. The crossing incoming and outgoing light ray define a light cone in this spacetime.

To pin down the actual value of γ we can compare the equation of motion of an inertial observer with the one in standard Newtonian dynamics. The force exerted on a test mass m by an infinite plane in Newton's theory can be found by using Poisson's equation on the mass distribution. The resulting force is $F = -\mathrm{sgn}(x)2\pi G m \rho_0$. This should coincide with the acceleration experienced by the free-falling observer multiplied my its mass

$$\begin{aligned} F &= m\ddot{x} = -\mathrm{sgn}(x)\gamma/2 \\ &\Rightarrow \gamma \equiv 4\pi G\rho_0. \end{aligned} \tag{F-5}$$

Reincluding the speed of light, $\gamma \equiv 4\pi G\rho_0/c^2$.

From here on it is easy to construct a conformal map which allows us to draw the Penrose diagram of the spacetime associated with an infinite sheet [136]. We can even analytically extent the diagram beyond $x = 0$ if we assume for a moment that it would be possible to travel through the sheet of mass (see figure 1.2). Taking a closer look at the geodesics and the Penrose diagram, it becomes clear that the sheet $x = 0$ really corresponds to a singular sheet in spacetime. For a free-falling observer it seems as if he is always in a perfectly harmless oscillation around the singular sheet, but for an outside observer the infalling mass seems never to actually reach the singularity. It is in a sense like a Schwarzschild black hole with its horizon exactly at the singularity. The sheet-like singularity however is a naked singularity since one can always escape it if sufficient acceleration is applied. In fact the singularity is very much like a conical singularity in the sense that its influence extents all the way to $y, z \to \pm\infty$, while the curvature tensor $R^{\mu}{}_{\nu\rho\sigma}$ is identically zero everywhere. This absence of curvature incidentally also implies that the tidal tensor is zero everywhere, so that no ill effects will be experienced by an extended object anywhere along its geodesic path.

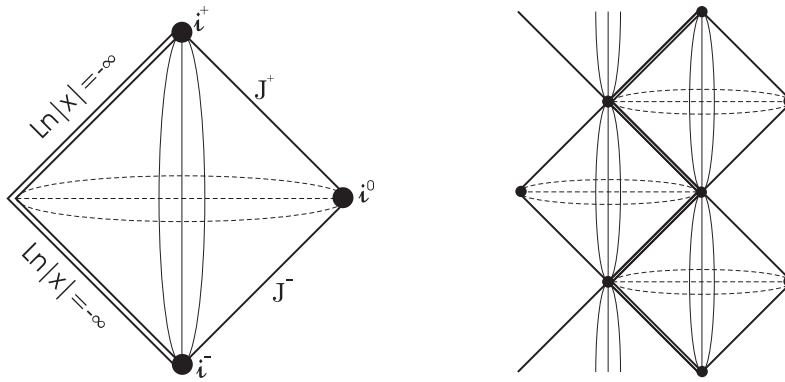

Figure 1.2: Left: the Penrose diagram for the metric given by (F-1). Right: the maximal analytic extension of the Penrose diagram.

In conclusion, the metric of an infinite plane seems to represent a conical, naked singularity in an otherwise perfectly flat spacetime.

Bibliography

[1] A. Einstein, in a letter to Heinrich Zangger, may 20, 1912.

[2] L. de Broglie, Comptes Rendus Acad. Sci. Paris **183**, 447 (1926).

[3] L. de Broglie, Comptes Rendus Acad. Sci. Paris **184**, 273 (1927).

[4] E. Schrödinger, Ann. Phys. **83**, 956 (1927).

[5] D. Bohm, Phys. Rev. **85**, 166 (1952).

[6] N. Bohr, Die Naturwissenschaften **18**, 73 (1929).

[7] N. Bohr, Nature **136**, 1025 (1935).

[8] W. Heisenberg, *The Physical Principles of the Quantum Theory*, Dover, New York, 1930, C. Eckhart trans.

[9] M. Jammer, *The Philosophy of Quantum Mechanics*, J. Wiley, New York, 1974.

[10] M. Jammer, *The Conceptual Development of Quantum Mechanics*, McGraw-Hill, New York, 1966.

[11] R. Feynman, *The Character of Physical Law*, MIT Press, Boston, 1965.

[12] J. Cramer, Rev. Mod. Phys. **58**, 647 (1986).

[13] A. Zeilinger, On the interpretation and philosophical foundation of quantum mechanics, in *'Vastakohtien todellisuus', Festschrift for*, edited by K. Laukikainen and U. Ketvel, Helsinki University Press, Helsinki, 1996.

[14] H. Everett, Rev. Mod. Phys. **29**, 454 (1957).

[15] D. Bohm and J. Bub, Rev. Mod. Phys. **38**, 453 (1966).

[16] L. Ballentine, Rev. Mod. Phys. **42**, 358 (1970).

[17] N. Mermin, Phys. Today **May**, 10 (2004).

[18] S. L. Adler, Stud. Hist. Phil. Mod. Phys. **34**, 135 (2003).

[19] J. van Wezel and J. van den Brink, J. Magn. Magn. Mater. **290-291**, 318 (2005).

[20] J. van Wezel and J. van den Brink, AIP Conf. Proc. **846**, 285 (2005).

[21] M. Isobe, E. Ninomya, A. Vasil'ev, and Y. Ueda, J. Phys. Soc. Japan **71**, 1423 (2002).

[22] M. Konstantinović et al., Phys. Rev. B **69**, 020409 (2004).

[23] J. van Wezel, J. van den Brink, and J. Zaanen, Phys. Rev. Lett. **94**, 230401 (2005).

[24] A. Caldeira and A. Leggett, Ann. Phys. **149**, 374 (1983).

[25] J. van Wezel, J. Zaanen, and J. van den Brink, Phys. Rev. B **74**, 094430 (2006).

[26] R. Penrose, Gen. Rel. Grav. **28**, 581 (1996).

[27] R. Penrose, Phil. Trans. R. Soc. Lond. A **356**, 1927 (1998).

[28] W. Marshall, C. Simon, R. Penrose, and D. Bouwmeester, Phys. Rev. Lett. **91**, 130401 (2003).

[29] I. Moroz, R. Penrose, and P. Tod, Class. Quant. Grav. **15**, 2733 (1998).

[30] T. Young, Phil. Trans. R. Soc. Lond. **94**, 1 (1804).

[31] M. Shamos, *Great Experiments in Physics*, Holt Reinhart and Winston, New York, 1959, Contains a reprint of Young's original article.

[32] C. Jönsson, Z. Phys. **161**, 454 (1961).

[33] C. Jönsson, Am. J. Phys. **42**, 4 (1974).

[34] P. Merli, G. Missiroli, and G. Pozzi, Am. J. Phys. **44**, 306 (1976).

[35] A. Tonomura, J. Endo, T. Matsuda, T. Kawasaki, and H. Ezawa, Am. J. Phys. **57**, 117 (1989).

[36] M. Arndt et al., Nature **401**, 680 (1999).

[37] Y. Kim, R. Yu, S. Kulik, Y. Shih, and M. Scully, Phys. Rev. Lett. **84**, 1 (2000).

[38] M. Born, Z. Phys. **40**, 167 (1926).

[39] J. von Neumann, *Mathematical foundations of quantum mechanics*, Princeton University Press, Princeton, 1955.

[40] N. van Kampen, Physica A **153**, 97 (1957).

[41] N. Mott, Cont. Phys. **5**, 401 (1964).

[42] R. Balian, Am. J. Phys. **57**, 1019 (1989).

[43] A. E. Allahverdian, R. Balian, and T. M. Nieuwenhuizen, Europhys. Lett. **61**, 452 (2003).

[44] C. Sun, Phys. Rev. A **48**, 898 (1993).

[45] S. Liu and C. Sun, Phys. Lett. A **198**, 371 (1995).

[46] J. Wheeler, Rev. Mod. Phys. **29**, 463 (1957).

[47] B. deWitt, Phys. Today **Sep.**, 30 (1970).

[48] M. Tegmark, Fortschr. Phys. **46**, 855 (1998).

[49] M. Tegmark and J. Wheeler, Sci. Am. **Feb.** (2001), Also available as: quant-ph/0101077.

[50] J. Zaanen, *The Classical Condensates: from crystals to Fermi-liquids*, Leiden University, Leiden, 1996.

[51] P. Anderson, Science **177**, 393 (1972).

[52] P. Pearle, Phys. Rev. D **13**, 857 (1976).

[53] P. Pearle, Int. J. Theor. Phys. **18**, 489 (1979).

[54] P. Pearle, Phys. Rev. Lett. **53**, 1775 (1984).

[55] P. Pearle, Phys. Rev. D **33**, 2240 (1986).

[56] N. Gisin, Phys. Rev. Lett. **52**, 1657 (1984).

[57] N. Gisin, Phys. Rev. Lett. **53**, 1776 (1984).

[58] G. Ghirardi, R. Grassi, and A. Rimini, Phys. Rev. A **42**, 1057 (1990).

[59] L. Diósi, Phys. Rev. A **40**, 1165 (1989).

[60] F. Károlyházy, Nuovo Cimento **A42**, 390 (1966).

[61] P. Dirac, *The Principles of Quantum Mechanics*, Clarendon Press, Oxford, 1958.

[62] J. Sakurai and S. Tuan, *Modern Quantum Mechanics*, Benjamin/Cummings, Menlo Park Calif., 1985.

[63] P. Anderson, *Basic Notions of Condensed Matter Physics*, Perseus Books, 1997.

[64] N. Ashcroft and N. Mermin, *Solid State Physics*, Holt, Rinehart and Winston, New York, 1976.

[65] J. Zaanen, G. Sawatzky, and J. Allen, Phys. Rev. Lett. **55**, 418 (1985).

[66] K. Kugel and D. Khomskii, Sov. Phys. Usp. **25**, 231 (1982).

[67] I. Bersuker, *Electronic structure and properties of transition metal compounds : introduction to the theory*, Wiley, New York, 1996.

[68] J. van den Brink, G. Khaliullin, and D. Khomskii, Orbital effects in manganites, in *Colossal Magnetoresistive Manganites*, edited by T. Chatterji, Kluwer Academic Publishers, Dordrecht, 2004.

[69] J. van den Brink and D. Khomskii, Phys. Rev. Lett. **82**, 1016 (1999).

[70] J. van Wezel and J. van den Brink, Europhys. Lett. **75**, 957 (2006).

[71] T. Hikihara and Y. Motome, Phys. Rev. B **70**, 214404 (2004).

[72] S. Bersier and M. Konstantinović, Private communications, to be Published (2005).

[73] Z. Popović, Ž.V. Šljivančanin, and F. Vukajlović, Phys. Rev. Lett. **93**, 036401 (2004).

[74] P. Anderson, Phys. Rev. **86**, 694 (1952).

[75] P. Anderson, Phys. Rev. **112**, 1900 (1958).

[76] P. Anderson, Phys. Rev. **130**, 439 (1963).

[77] C. Kaiser and I. Peschel, J. Phys. A **22**, 4257 (1989).

[78] J. Mooij et al., Science **285**, 1036 (1999).

[79] Y. Nakamura, Y. A. Pashkin, and J. S. Tsai, Nature **398**, 786 (1999).

[80] C. van der Wal et al., Science **290**, 773 (2000).

[81] I. Chiorescu, Y. Nakamura, C. Harmans, , and J. Mooij, Science **299**, 1869 (2003).

[82] V. Bouchiat, D. Vion, P. Joyez, D. Esteve, and M. Devoret, Physica Scripta **T76**, 165 (1998).

[83] Y. Nakamura, Y. A. Pashkin, T. Yamamoto, and J. S. Tsai, Phys. Rev. Lett. **88**, 047901 (1999).

[84] D. Vion et al., Science **296**, 886 (2002).

[85] J. Friedman, M. Sarachik, J. Tejada, and R. Ziolo, Phys. Rev. Lett. **76**, 3830 (1996).

[86] D. Awschalom, J. Smyth, G. Grinstein, D. DiVincenzo, and D. Loss, Phys. Rev. Lett. **68**, 3092 (1992).

[87] L. Susskind, Phys. Rev. D **20**, 2619 (1979).

[88] E. Cremmer et al., Nucl. Phys. B **147**, 105 (1979).

[89] S. Coleman, *Apects of Symmetry*, Cambridge University Press, Cambridge, 1985, See, for instance, Chapter 5.

[90] C. Leung, S. Love, and W. Bardeen, Nucl. Phys. B **273**, 649 (1986).

[91] V. Kostelecký and S. Samuel, Phys. Rev. D **39**, 683 (1989).

[92] C. Yannouleas and U. Landman, Phys. Rev. Lett. **82**, 5325 (1999).

[93] T. Kaplan, W. von der Linden, and P. Horsch, Phys. Rev. B **42**, 4663 (1990).

[94] K. Blum, *Density Matrix Theory and Applications*, Plenum Press, New York, 1937.

[95] U. Fano, Rev. Mod. Phys. **29**, 74 (1957).

[96] J. Goldstone, A. Salam, and S. Weinberg, Phys. Rev. **127**, 965 (1962).

[97] E. Lieb and D. Mattis, J. Math. Phys. **3**, 749 (1962).

[98] B. Bernu, C. Lhuillier, and L. Pierre, Phys. Rev. Lett. **69**, 2590 (1992).

[99] B. Bernu, P. Lecheminant, C. Lhuillier, and L. Pierre, Phys. Rev. B **50**, 10048 (1994).

[100] L. Capriotti, Int. J. Mod. Phys. B **15**, 1799 (2000).

[101] H. Neuberger and T. Ziman, Phys. Rev. B **39**, 2608 (1989).

[102] D. S. Fisher, Phys. Rev. B **39**, 11783 (1989).

[103] M. Gross, E. Sánchez-Velasco, and E. D. Siggia, Phys. Rev. B **40**, 11328 (1989).

[104] R. Kubo, Phys. Rev. **87**, 568 (1952).

[105] A. Auerbach, *Interacting Electrons and Quantum Magnetism*, Springer-Verlag, New York, 1994.

[106] D. Mattis, *The theory of magnetism I: thermodynamics and statistical mechanics*, Springer-Verlag, Berlin, 1988.

[107] S. Elitzur, Phys. Rev. D **12**, 3978 (1975).

[108] T. Hansson, V. Oganesyan, and S. Sondhi, Ann. Phys. **313**, 497 (2004).

[109] M. Tinkham, *Introduction to Superconductivity*, McGraw-Hill inc., New York, 1996.

[110] E. Šimánek, Phys. Rev. B **22**, 459 (1979).

[111] K. Efetov, Sov. Phys. JETP **51**, 1015 (1980).

[112] R. Bradley and S. Doniach, Phys. Rev. B **30**, 1138 (1984).

[113] M. Fisher and G. Grinstein, Phys. Rev. Lett. **60**, 208 (1988).

[114] M. Wallin, E. Sørensen, S. Girvin, and A. Young, Phys. Rev. B **49**, 12115 (1994).

[115] S. Sondhi, S. Girvin, J. Carini, and D. Shahar, Rev. Mod. Phys. **69**, 315 (1997).

[116] L. Ioffe et al., Nature **415**, 503 (2002).

[117] A. van Oudenaarden and J. Mooij, Phys. Rev. Lett. **76**, 4947 (1996).

[118] R. Micnas, J. Ranninger, and S. Robaszkiewicz, Rev. Mod. Phys. **62**, 113 (1990).

[119] P. Nozières and S. Schmitt-Rink, J. Low Temp. Phys. **59**, 195 (1985).

[120] P. Higgs, Phys. Lett. **12**, 132 (1964).

[121] P. Higgs, Phys. Rev. Lett. **13**, 508 (1964).

[122] Y. Makhlin, G. Schön, and A. Shnirman, Rev. Mod. Phys. **73**, 357 (2001).

[123] I. Siddiqi et al., Phys. Rev. B **73**, 054510 (2006).

[124] J. van Wezel, J. Zaanen, and J. van den Brink, ArXiv: Physics , 0609177 (2006), Submitted to AM. J. Phys.

[125] H. Zeh, Found. Phys. **1**, 69 (1970).

[126] W. Zurek, Phys. Rev. D **26**, 1862 (1982).

[127] E. Joos and H. Zeh, Z. Phys. B **59**, 223 (1985).

[128] W. Zurek, Phys. Today **44**, 36 (1991).

[129] J. Lebowitz, Phys. Today **Sep.**, 33 (1993).

[130] W. Zurek, Phys. Rev. D **24**, 1516 (1981).

[131] J. Christian, Phys. Rev. Lett. **95**, 160403 (2005).

[132] R. Feynman, Int. J. Theor. Phys. **21**, 467 (1982).

[133] P. Shor, Algorithms for quantum computation: discrete logarithms andfactoring, in *Foundations of Computer Science, 1994 Proceedings., 35th Annual Symposium on Foundations of Computer Science*, edited by S. Goldwasser, page 124, IEEE Computer Society Press, 1995.

[134] C. van der Wal, F. Wilhelm, C. Harmans, and J. Mooij, Euro. Phys. J. B **31**, 111 (2003).

[135] C. Ross, *Differential Equations*, Springer, New York, 1995.

[136] S. Hawking and G. Ellis, *The Large Scale Structure of Spacetime*, Cambridge University Press, Cambridge, 1973.

[137] J. Martin, *General Relativity, a first course for physicists*, Prentice Hall, New York, 1995.

Index

Nederlandse Samenvatting

De Quantum Mechanica is mogelijkerwijs de meest succesvolle natuurkundige theorie van de vorige eeuw. Met behulp van de quantum mechanica kunnen we natuurkundige verschijnselen verklaren die variëren van het gedrag van de elementaire deeltjes tot de eigenschappen van macroscopische objecten [13, 62]. Ondanks deze triomf, wordt de quantum mechanica door veel mensen nog steeds gezien als een mysterieuze theorie, die gehuld wordt in een mist van onverklaarbare verschijnselen. Al deze onrustige gevoelens blijken uiteindelijk gestoeld te zijn op de eenvoudige waarneming dat ondanks het feit dat de wereld om ons heen opgebouwd is uit quantum mechanische bouwstenen, diezelfde klassieke wereld om ons heen de regels van de quantum mechanica niet lijkt te volgen.

In dit proefschrift heb ik enige voorbeelden laten zien van hoe de Quantum Mechanica invloed heeft op de eigenschappen van de Grote Wereld, en ik heb een een idee besproken over hoe de quantum theorie uiteindelijk zijn geldigheid zou kunnen verliezen.

Quantum Mechanica in de Grote Wereld

Als een voorbeeld van de onontkoombare noodzakelijkheid van het gebruik van de quantum mechanica in de beschrijving van alledaagse materiaaleigenschappen, heb ik het titanium pyroxeen $NaTiSi_2O_6$ nader bestudeerd [19, 20]. Het is experimenteel vastgesteld dat deze stof een magnetische fase overgang ondergaat bij 210 K [21]. Er is ook bewijs dat er bij precies dezelfde temperatuur iets gebeurd met de kristalstructuur van het materiaal: de phonon eigenschappen veranderen dan plotseling en uit Röntgen-diffractie experimenten blijkt dat er een vorm van dimerisatie optreedt. Al snel na de publicatie van deze resultaten werd geopperd dat het samenspel van de orbitale en magnetische vrijheidsgraden van de titanium atomen verantwoordelijk zou kunnen zijn voor de gekoppelde magnetische en structurele overgang [22]. Numerieke simulaties lieten echter zien dat de orbitalen ernstig beperkt zouden kunnen zijn in hun vrijheid door het omringende kristalveld. Die beperking zou de waarschijnlijkheid van een gekoppelde overgang aanzienlijk ver-

kleinen [71–73].

In onze studie van $NaTiSi_2O_6$ hebben we drie verschillende theoretische methoden gebruikt om aan te tonen dat de zogenaamde 'orbitaal-ondersteunde Peierls overgang' er wel degelijk kan plaatsvinden, ondanks de aanwezigheid van een aanzienlijk kristalveld [19]. De orbitaal-ondersteunde Peierls overgang is een fase overgang waarbij de spins in de één-dimensionale zigzag ketens van titanium atomen paren van magnetische singlet-toestanden beginnen te vormen bij precies die temperatuur waarbij de orbitaal vrijheidsgraden zich in een parallel patroon beginnen te ordenen. We hebben laten zien dat de gekoppelde overgang mogelijk wordt gemaakt door de gecombineerde quantum fluctuaties van zowel de spins als de orbitalen. Met behulp van onze resultaten kunnen we alle geobserveerde effecten in het materiaal verklaren, en we kunnen een voorspelling doen van de daadwerkelijke grootte van het kristalveld in $NaTiSi_2O_6$ [19,20].

We hebben dus gedemonstreerd dat de nieuwe orbitaal-ondersteunde Peierls overgang niet alleen nog altijd een mogelijke beschrijving vormt van het titanium pyroxeen, maar ook dat het in feite de enige manier is waarop alle beschikbare experimentele en numerieke observaties kunnen worden gecombineerd en verklaard. Dit houdt ook in dat de quantum mechanische eigenschappen van de elementaire deeltjes (de orbitaal en spin vrijheidsgraden en hun quantum fluctuaties) inderdaad een noodzakelijk ingrediënt zijn in de verklaring van de materiaaleigenschappen van het macroscopische materiaal. Het is daarmee één van de vele, vele manieren waarop de Quantum Mechanica zichzelf laat zien in de Grote Wereld.

Quantum Mechanica van de Grote Wereld

Omdat duidelijk is aangetoond dat de quantum mechanica de correcte theorie is om microscopische deeltjes te beschrijven, en nu we hebben gezien dat de quantum mechanische eigenschappen van de elementaire deeltjes het gedrag van macroscopische materialen in de Grote Wereld bepalen, zou men zich kunnen afvragen waarom onze dagelijkse wereld er niet méér quantum mechanisch uitziet. Eén van de meest essentiële eigenschappen van de quantum mechanica is de extreem krachtige rol van symmetrie in de theorie. Als de ruimte homogeen en isotroop is, dan kan een quantum mechanisch object in die ruimte geen enkele positie bevoordelen boven een andere, en dus zal het zich uitspreiden in een quantum superpositie die alle equivalente punten in de ruimte bestrijkt. Als we deze manier van redeneren doorvoeren op de wereld om ons heen, dan zou je kunnen denken dat omdat een bepaald klassiek object, bijvoorbeeld een stoel, geheel is opgebouwd uit quantum mechanische bouwstenen, de stoel zelf de wetten van de quantum mechanica ook zou moeten naleven. Een stoel in een homogene kamer zou zich dus moeten uitspreiden over alle beschikbare lege ruimte. Dit is overduidelijk niet wat er in werkelijkheid gebeurd.

De manier om aan deze paradoxale situatie te ontkomen, is het proces van spontane symmetrie breking [51]. Het is mogelijk om aan te tonen dat de symmetrische golffunctie van een quantum object instabieler wordt naarmate het aantal deeltjes waaruit het object is opgebouwd groter wordt. De stoel met zijn over de hele kamer uitgespreide golffunctie is dus extreem onstabiel, en zelfs een infinitesimaal klein symmetrie brekend veld is genoeg om hem te lokaliseren [124]. Zelfs het feit dat de stoel er klassiek uitziet en klaarblijkelijk de kracht van symmetrie in de quantum mechanica kan ontlopen, is dus eigenlijk een quantum mechanisch effect.

Deze manier van spontane symmetrie breking impliceert het bestaan in alle klassieke objecten van een overblijfsel van hun quantum mechanische oorsprong. Dit overblijfsel, het zogenaamde dunne spectrum, bestaat uit een verzameling eigentoestanden die allemaal dicht tegen de grondtoestand aanliggen. Zo'n dichte verzameling laag liggende toestanden kan in principe erg gevaarlijk zijn voor de coherentie van qubits [24]. Wij hebben laten zien dat de symmetrie breking in kristallen en antiferromagneten inderdaad leidt tot decoherentie als deze systemen gebruikt worden als qubits. De hieruit volgende decoherentietijd blijkt een universele tijdschaal te zijn, die compleet onafhankelijk is van de details van het onderliggende microscopische model [23, 25].

Er wordt vaak gedacht dat het verbod van Elitzur's theorie op het spontaan breken van een lokale ijk-symmetrie [107], impliceert dat de supergeleidende toestand niet gekenmerkt kan worden door een spontaan gebroken symmetrie. Wij hebben laten zien dat een supergeleider een spontaan gebroken *g*lobale symmetrie heeft in zijn klassieke toestand. Dit breken van de totale fase symmetrie vereist wederom het bestaan van een dun spectrum in supergeleiders. De decoherentietijd die het dunne spectrum induceert in supergeleidende qubits komt overeen met de universele tijdschaal die we gevonden hadden voor kristallen en antiferromagneten. De verwachte decoherentietijd voor de Cooperpaar-doos qubits die in hedendaagse experimenten gebruikt worden is echter nog altijd veel groter dan de decoherentietijd die veroorzaakt wordt door de thermische omgeving van het qubit [79, 83].

Met de huidige vooruitgang van de technologie en de verbetering van de thermische isolatie van supergeleidende qubits is het zeker niet onmogelijk dat de decoherentie effecten veroorzaakt door het dunne spectrum binnen afzienbare tijd zullen worden waargenomen. Het aantonen van dit soort decoherentie zou ook een duidelijke demonstratie inhouden van het quantum mechanische gedrag van een object dat we normaal gesproken als klassiek zouden beschouwen. Het is dus een manier om te kijken naar de Quantum Mechanica van de Grote Wereld zelf.

Quantum Mechanica of de Grote Wereld

Ondanks het feit dat quantum mechanica zichzelf tot klassieke fysica terugbrengt in de thermodynamische limiet door middel van spontane symmetrie breking, is het

nog altijd noodzakelijk ook een dynamisch mechanisme te vinden dat macroscopische superposities terug kan brengen tot de meer alledaagse toestanden die we in de wereld om ons heen zien. Dit quantum mechanische ineenstortings effect is een absoluut noodzakelijke toevoeging aan de quantum fysica omdat de unitariteit van de quantum theorie duidelijk niet in overeenstemming gebracht kan worden met de experimentele observaties die tijdens een meetproces gedaan worden. Spontane symmetrie breking noch het populaire beroep op decoherentie bieden hier enig soelaas [18, 25].

Er zijn vele voorstellen gedaan voor een kandidaat fysisch fenomeen om het quantum ineenstortings proces te verklaren [15, 52–60]. Geen van alle hebben zij tot nog toe geleid tot een toetsbare voorspelling die de theorie zou kunnen onderbouwen of ondermijnen. Er is echter een recent idee, geopperd door Roger Penrose, waarin gesuggereerd wordt dat de algemene relativiteitstheorie er voor zou kunnen zorgen dat quantum mechanische superposities in de ruimte onstabiel worden [26, 27]. Met een redenatie gebaseerd op hele algemene argumenten toont Penrose aan dat zo'n gravitationele instabiliteit zou leiden tot een maximum levensduur van een superpositie van de orde van de inverse van de gravitationele zelf-energie van het verschil tussen de gesuperponeerde massa distributies [26]. De typische ineenstortings tijd wordt op die manier enorm groot voor alle quantum mechanische systemen die experimenteel bestudeerd zijn, en enorm klein voor alle macroscopische objecten in natuurkundige experimenten. De typische massa die zou leiden tot een ineenstortings proces dat plaats vindt binnen een meetbare tijd blijkt echter nog nooit experimenteel te zijn onderzocht [27, 28].

Als een voorbeeld van een systeem dat in principe een meetbare ineenstortingstijd zou kunnen hebben volgens het idee van Penrose, hebben wij de flux qubit bestudeerd. In zo'n qubit is er een superstroom die zowel linksom als rechtsom door een supergeleidende ring stroomt [78, 80, 81]. Als we ook de extra conditie in ogenschouw nemen dat de gehele stroom moet instorten zodra een deel van de stroom besluit in te storten, vinden we een ineenstortingstijd die alleen binnen het meetbare domein blijkt te vallen voor nogal extravagante geometrische specificaties van de qubit. Het is niet inherent onmogelijk om op deze manier de gravitationele ineenstorting van de golffunctie te meten, maar het zal een flinke experimentele uitdaging zijn om het ook daadwerkelijk voor elkaar te krijgen.

Niet alleen de vraag of de gravitationele ineenstorting plaats kan vinden binnen een meetbare tijd, maar ook de vraag op welke manier die ineenstorting dan precies zal gebeuren behoeft nog een antwoord. In zijn voorstel suggereerde Penrose dat de zogenaamde Schrödinger-Newton vergelijking gebruikt zou kunnen worden om te bepalen in welke toestanden een quantum superpositie terecht zou kunnen komen [29]. Als we deze vergelijking letterlijk nemen en hem gebruiken als de generator van de tijdsevolutie van een macroscopische superpositie, dan hebben we laten zien dat dit nooit kan leiden tot een ineenstorting. Met een paar minimale aanpassingen echter, kan de dynamica er wel voor zorgen dat macroscopische su-

perposities gelokaliseerd worden, terwijl microscopische quantum toestanden gedurende alle observeerbare tijden intact blijven. Jammer genoeg kan de theorie niet Born's vuistregel reproduceren, die de statistiek van de mogelijke uitkomsten van een meting voorspelt. Het lijkt dan ook onmogelijk om de Schrödinger-Newton vergelijking te gebruiken als een model voor het quantum ineenstortings proces.

Ondanks deze tegenslag lijkt de studie van de dynamica wel te suggereren dat het wellicht mogelijk is om het verhaal van spontane symmetrie breking te combineren met dat van het ineenstortings proces. Gebruik makend van de inzichten die verkregen zijn gedurende dit onderzoek zouden we misschien een proces kunnen construeren waarin een unitariteit-brekend veld leidt tot de ineenstorting van quantum mechanische superposities in de thermodynamische limiet. Deze spontane ineenstorting zou dan de ultieme scheidsrechter zijn in de keuze tussen Quantum Mechanica of de Grote Wereld.

Curriculum Vitae

Personal Data

- **Full name:**
  Jasper van Wezel
- **Contact information:**
  email: vanwezel@ilorentz.org
  website: www.ilorentz.org/~vanwezel
- **Date and place of birth:**
  31-12-1979, The Hague, The Netherlands

Employment History

- **2003 - 2007:** PhD student in theoretical condensed matter physics, Leiden University, The Netherlands.
  thesis advisors: Jeroen van den Brink and Jan Zaanen.
- **2001 - 2002 and 1999 - 2000:** Tutor for High School Students, institute "Mentor", Leiden, The Netherlands.

Finished Education

- **2003:** Master's diploma in theoretical condensed matter physics (cum laude), Leiden University, The Netherlands.
  thesis advisor: Jan Zaanen.
- **2000:** Exchange program: Six months in the graduate school of Utah State University, Utah, USA.
- **1998:** US High School Diploma (cum laude), Sanford High School, Maine, USA.

- **1997:** Dutch VWO Diploma (cum laude), Dalton Scholengemeenschap, Den Haag, The Netherlands.

Teaching Experience

- **fall 2003 through spring 2007:** Online tutor for High School students, "pws-exact.leidenuniv.nl", Leiden, The Netherlands.
- **spring 2006:** Teaching assistant and tutor for the Statistical Physics class of Peter Denteneer, Leiden University, The Netherlands.
- **spring 2005 and spring 2004:** Teaching assistant and tutor for the Condensed Matter and Statistical Physics class of Jeroen van den Brink, Leiden University, The Netherlands.
- **spring 2003 and spring 2002:** Teaching assistant and tutor for the Condensed Matter Theory class of Jan Zaanen, Leiden University, The Netherlands.
- **2001/2002 and 1999/2000:** Tutor for High School Students, Institute "mentor", Leiden, The Netherlands.

Prizes and Distinctions

- Research was elected the physics "Discovery of the year" by the Physics department of Leiden University in 2005.
- "Onderwijsprijs Natuurkunde 2004/2005", Leiden University, Leiden, November 2005. (Awarded by the student population for best teaching in the Physics department in the year 2004/2005.)

List of Publications

Scientific Publications

- “Orbital-Peierls State in NaTiSi2O6”, Europhysics Letters, **75**, 957 (2006).
- "Relation between decoherence and spontaneous symmetry breaking in many-particle qubits", Phys. Rev. B **74**, 094430 (2006).
- “Orbital Driven Spin Ordering in the One Dimensional Chains of Titanium Pyroxene”, AIP Conf. Proc. **846**, 285 (2006).
- “An Intrinsic Limit to Quantum Coherence due to the Classical Nature of Measuring Machines”, Phys. Rev. Lett. **94**, 230401 (2005).
- “Orbital-Peierls Transition in the Spin Chains of $NaTiSi_2O_6$”, J. Magn. Magn. Mater. **290**, 318 (2005).

Preprints of Scientific Articles

- “Limit to manipulation of qubits due to spontaneous symmetry breaking”, quant-ph/0606058, to appear in JMMM.
- "Spontaneous Symmetry Breaking in Quantum Mechanics", physics/0609177 (2006), to appear in Am. J. Phys.

Popular Publications

- "De Kwantumcomputer heeft een Onverwacht Lek", Kennislink, July 29, 2005
- "Quantumbits verliezen spontaan quantuminformatie", NTvN, **9**, 293, 2005